# Investigations on Dielectric Properties of Biodegradable Oil Based Composite Insulation in High Voltage Equipment

Thesis Submitted by

***Biswajit Chakraborty***

***Doctor of Philosophy***
***(Engineering)***

**Electrical Engineering Department**
**Faculty Council of Engineering & Technology**
**Jadavpur University**
**Kolkata, India**

**2024**

**Jadavpur University**
**Kolkata – 700032, India**

**INDEX NO. 289/21/E**

1. **Title of the Thesis:**

   Investigations on Dielectric Properties of Biodegradable Oil Based Composite Insulation in High Voltage Equipment

2. **Name, Designation & Institution of the Supervisors:**

**Dr. Sovan Dalai**
Professor,
Electrical Engineering Department,
Jadavpur University

**Dr. Arpan Kumar Pradhan**
Assistant Professor,
Electrical Engineering Department,
Jadavpur University

## 3. List of Journal Publications:

- **B. Chakraborty**, K.Y. Raj, A.K. Pradhan, B. Chatterjee, S. Chakravorti and S. Dalai, "Investigation of Dielectric Properties of $TiO_2$ and $Al_2O_3$ nanofluids by Frequency Domain Spectroscopy at Different Temperatures", **Journal of Molecular Liquids Elsevier**, Vol. 330 No. 5, Page No. 1-9, 2021.
- **Biswajit Chakraborty**, Subhajit Maur, Arpan Kumar Pradhan, Biswendu Chatterjee, Sovan Dalai, "Investigations on dielectric characteristics of hybrid nanofluids through time and frequency domain spectroscopic measurement," **Journal of Molecular Liquids**, Elsevier, Vol. 366, 2022.
- **B. Chakraborty**, S. Maur, A. K. Pradhan, B. Chatterjee and S. Dalai, "Study of Nonlinearity, Activation Energy and Temperature Effect on $Al_2O_3$ and $TiO_2$ Nanoparticles-based Mixed Oil Characteristics by Dielectric Spectroscopy," **IEEE Transactions on Dielectrics and Electrical Insulation**, vol. 30, no. 3, pp. 997 - 1004, 2023, doi: 10.1109/TDEI.2023.3235862.
- **B. Chakraborty,** S. Maur, A. K. Pradhan, B. Chatterjee and S. Dalai, "Insight the Impact of TiO2 and Al2O3 Nanoparticles in Mineral, Vegetable Oil Based on AC Dielectric Properties—Conformity With Weibull Distribution," **IEEE Transactions on Plasma Science**, vol. 51, no. 10, pp. 3095-3102, Oct. 2023, doi: 10.1109/TPS.2023.3311910.
- **B. Chakraborty**, S. Maur, S. Biswas, A. K. Pradhan, B. Chatterjee and S. Dalai, "State-of-Art Sensing Method for Condition Assessment of Nanofluids by Relaxation Current," **IEEE Sensors Journal**, vol. 25, no. 6, pp. 10055-10062, doi: 10.1109/JSEN.2025.3538495.

## 4. List of Patents:

Nil

## 5. List of Presentations in National/International Conferences:

- **B. Chakraborty**, K. Y. Raj, N. Haque, B. Chatterjee and S. Dalai, "Studies on the effects of $Al_2O_3$ and $TiO_2$ Nano materials on Conduction Properties of Mineral oil and Natural Ester based fluid," *2018* ***IEEE Applied Signal Processing Conference (ASPCON)***, Kolkata, India, 2018, pp. 337-341, doi: 10.1109/ASPCON.2018.8748331.
- **B. Chakraborty**, A. Mondal, S. Maur, B. Chatterjee and S. Dalai, "Investigation on Activation Energy and Temperature Conductivity Dependency of Laboratory prepared Mixed Insulation Samples," ***2020 IEEE 1st International Conference for Convergence in Engineering (ICCE)***, Kolkata, India, 2020, pp. 205-209, doi: 10.1109/ICCE50343.2020.9290625.
- **B. Chakraborty**, S. Maur, A. K. Pradhan, S. Chatterjee, B. Chatterjee and S. Dalai, "Estimation of Paper Moisture within Vegetable Oil based Hybrid Nanofluid Impregnated Paper Using Capacitance Ratio," ***2022 IEEE 6th International Conference on Condition Assessment Techniques in Electrical Systems (CATCON)***, Durgapur, India, 2022, pp. 303-307, doi: 10.1109/CATCON56237.2022.10077639.
- S. K. Paul, **B. Chakraborty**, S. Maur, B. Chatterjee, S. Dalai and A. K. Pradhan, "Study of Nonlinearity in Dielectric Response Current of Vegetable Oil based Hybrid Nanofluids," ***2023 IEEE 20th India Council International Conference (INDICON)***, Hyderabad, India, 2023, pp. 270-274, doi: 10.1109/INDICON59947.2023.10440838.
- S. K. Paul, **B. Chakraborty**, S. Maur, B. Chatterjee, S. Dalai and A. K. Pradhan, "Moisture Content Estimation of Nanofluids using LFD of Real and Imaginary Parts of Complex Capacitance," ***2024 IEEE 3rd International Conference on Control, Instrumentation, Energy & Communication (CIEC)***, Kolkata, India, 2024, pp. 407-411, doi: 10.1109/CIEC59440.2024.10468230.

# Statement of Originality

I, **Biswajit Chakraborty** registered on **30th July, 2021** do hereby declare that this thesis entitled "***Investigations on Dielectric Properties of Biodegradable Oil Based Composite Insulation in HV Equipment***" contains literature survey and original research work done by the undersigned candidate as part of Doctoral studies.

All information in this thesis have been obtained and presented in accordance with existing academic rules and ethical conduct. I declare that, as required by these rules and conduct, I have fully cited and referred all materials and results that are not original to this work.

I also declare that I have checked this thesis as per the "Policy on Anti Plagiarism, Jadavpur University, 2019", and the level of similarity as checked by iThenticate software is **4** %.

Biswajit Chakraborty

(Signature of Candidate)

Date: 09/12/2024

Certified by Supervisors:
(Signature with date, seal)

1. 09/12/2024

Dr. Sovan Dalai
Professor
Electrical Engineering Department
Jadavpur University
Kolkata-700032

2. 09/12/2024

Dr. Arpan Kr. Pradhan
Assistant Professor,
Electrical Engineering Department
Jadavpur University
Kolkata-700032

# Certificate from the Supervisors

This is to certify that the thesis entitled "***Investigations on Dielectric Properties of Biodegradable Oil Based Composite Insulation in HV Equipment***" submitted by **Shri Biswajit Chakraborty**, who got his name registered on **30th July, 2021** for the award of Ph. D.(Engg.) degree of Jadavpur University is absolutely based upon his own work under the supervision of **Prof. Sovan Dalai and Dr. Arpan Kumar Pradhan** and that neither his thesis nor any part of the thesis has been submitted for any degree/diploma or any other academic award anywhere before.

09/12/2024

Signature of the Supervisor and date with Office Seal

Dr. Sovan Dalai
Professor
Electrical Engineering Department
Jadavpur University
Kolkata-700032

09/12/2024

Signature of the Supervisor and date with Office Seal

Dr. Arpan Kr. Pradhan
Assistant Professor,
Electrical Engineering Department
Jadavpur University
Kolkata-700032

# Acknowledgment

The author expresses his sincere appreciation and deep gratitude to his esteemed guide Prof. Sovan Dalai and Dr. Arpan Kumar Pradhan of Electrical Engineering Department, Jadavpur University for his invaluable guidance in carrying out the thesis work. This work has reached at this stage for their expertise, encouragement and valuable criticisms. The author also expresses his sincere gratitude towards his supervisors for granting the essential freedom for his work, while the close oversight from the mentor directed the work towards excellence.

The author expresses his deep sense of appreciation to the Head of the Department of Electrical Engineering, Jadavpur University for his kind accordance in providing necessary departmental facilities for implementation of this work. The author also acknowledges the financial support provided by DST, Government of India (Grant no EEQ/2016/00046) and AICTE through AICTE Doctoral Fellowship (ADF 2020-21).

It is the author's pleasure to acknowledge his respected teachers Prof. Biswendu Chatterjee, Prof. Sivaji Chakravorti, Prof. Debangshu Dey, and Prof. Kesab Bhattacharya for their advice and encouragement in completing the research work.

The author also wants to acknowledge contributions of Mr. Subhajit Maur and Dr. Nasirul Haque in the course of the research work.

The author is thankful to his colleagues Dr. Suhas Deb, Dr. Soumya Chatterjee, Mr. Rakesh Das, Mr. Sandipan Kumar Paul, Mr. K.Y. Raj, Mr. Sourav Biswas, Mr. Arijit Mondal, Mr. Soumyadeep Maity, Mr. Pradipta Ghosh, Dr. Arup Kumr Das and Dr. Kaushik Sit for providing support in various ways for carrying out the work.

The author would like to express his heart-felt gratitude to all his family members and relatives for their never-ending support and encouragement during the course of the thesis work.

The author also extends thanks to all the members of the High Tension Laboratory of Electrical Engineering Department, Jadavpur University for making it possible to work in a homely atmosphere. Last but not least, the author remains indebted to all the resources that he was fortunate to have during the work.

Biswajit Chakraborty

09/12/2024

*Dedicated to*
*My Parents and Teachers*

# Table of Contents

**Chapter 2**

**Development of Experimental Setup for Investigation of Biodegradable Insulation**

**Chapter 3**

**$TiO_2$ and $Al_2O_3$ Nanofluids: Insulation Properties Investigation by Dielectric Spectroscopy**



**Chapter 4**

**Hybrid Nanofluids: Dielectric Characteristics Investigations by Dielectric Spectroscopy**

**Chapter 5**

**Mixed Oil based Nanofluids: Dielectric Characteristics Investigations by Dielectric Spectroscopy**



**Chapter 6**

**Comparative Study on AC Breakdown Characteristics and AC Conductivity of Different Prepared Nanofluids**



**Chapter 7**

**Moisture Assessment of Nano-particles based Composite Insulation by Dielectric Spectroscopy**

# List of Figures

# List of Tables

# List of Abbreviations

| Abbreviations | Full-Form |
|---|---|
| ACBDV | AC Breakdown voltage |
| ARTP | Atom Transfers Radical Polymerization |
| CdSe | Cadmium Selenide |
| CNTs | Carbon Nanotubes |
| CQD | Carbon Quantum Dots |
| CVD | Chemical Vapor Deposition |
| DAR | Dielectric Absorption Ratio |
| DBM | Debye Model |
| DCBDV | DC Breakdown voltage |
| DDF | Dielectric Dissipation Factor |
| DFR | Dielectric Frequency Response |
| DGA | Dissolved Gas Analysis |
| DIRANA | Dielectric Response Analyser |
| DLS | Dynamic Light Scattering |
| DTAB | Dodecyl Trimethylammonium Bromide |
| FDS | Frequency Domain Spectroscopy |
| FDS | Frequency Domain Spectroscopy |
| HCTAB | Hexadecyltrimethylammonium Bromide |
| HTH | High Temperature Hydrocarbons |
| HV | High Voltage |
| IDAX | Insulation Diagnostic Analyser |
| IEC | International Electrotechnical Commission |
| IEEE | Institute of Electrical and Electronics Engineers |
| IFT | Interfacial Tension |

| Abbreviations | Full-Form |
|---|---|
| IR | Insulation Resistance |
| KFT | Karl Fischer Titration |
| LFD | Low Frequency Dispersion |
| MO | Mineral Oil |
| MWCNTs | Multi-Walled Carbon Nanotubes |
| NE | Natural Esters |
| NPs | Nanoparticles |
| PD | Partial Discharge |
| PD | Partial Discharge |
| PDC | Polarization and Depolarization Current |
| PDC | Polarization and Depolarization Current |
| PI | Polarization Index |
| PVP | Polyvinyl Pyrrolidone |
| RFD | Relaxation Frequency Distribution |
| RVM | Return Voltage Method |
| RVM | Recovery Voltage Measurement |
| SDS | Sodium Dodecyl Sulfate |
| SWCNTs | Single-Walled Carbon Nanotubes |
| VO | Vegetable Oil |
| ZnO | Zinc Oxide |
| ZnS | Zinc Sulfide |

# List of Mathematical Symbols

| Symbol | Meaning |
|---|---|
| $C$ | Capacitance |
| $D$ | Flux Density |
| $P$ | Polarization |
| $\chi$ | Electrical Susceptibility |
| $E$ | Electric Field Vector |
| $f$ | Frequency |
| $\delta(t-t_0)$ | Dirac-delta function |
| $J(t)$ | Total Current Density Function |
| $\sigma_0$ | DC Conductivity |
| $\varepsilon_0$ | Permittivity in Free Space |
| $C_0$ | Geometric Capacitance |
| $I_{pol}(t)$ | Polarization Current |
| $I_{depol}(t)$ | Depolarization Current |
| $r(t)$ | Dielectric Response Function |
| $C(\omega)$ | Frequency Dependent Complex Capacitance |
| $C''(\omega)$ | Imaginary Part of Complex Capacitance |
| $C'(\omega)$ | Real Part of Complex Capacitance |
| $tan\delta$ | Dielectric Dissipation Factor |
| $Eg$ | Activation Energy |
| $\Delta C'$ | Change in Real Capacitance |
| $I_{cond}$ | Conduction Current |
| $t$ | Temperature in °C |
| $T$ | Temperature in Kelvin |
| $\varepsilon'$ | Real Part of Permittivity |

| | |
|---|---|
| $V_b$ | Measured Data of Breakdown Voltages |
| $\alpha$ | Scale Parameter |
| $\beta$ | Shape Parameter |
| $\sigma'$ | AC Conductivity |
| $C_0$ | Geometric Capacitance |
| $\lambda$ | Integrating Constant |
| $\tau$ | Relaxation Time Constant in Debye Model |
| $v$ | Relaxation Frequency |
| $r(v)$ | Distribution Density Function |
| $R_{T_1}$ | Geometric DC Resistance at Temperature $T_1$ |
| $\%_0pm$ | Percentage Moisture Content |
| $f_{p\_paper}$ | Relaxation Peak Frequency |
| $M_{oil}$ | Relaxation Peak for Oil |
| $M_{paper}$ | Relaxation Peak for Paper |
| $\Delta C''$ | LFD of Imaginary Capacitance |

# Chapter 1

## 1.1.Introduction

Transformers are one of the most important and expensive equipment associated with the power system network. Catastrophic failure of transformer interrupts the power flow to the consumer's end resulting subsequent loss specially in heavy industries. Being very expensive, it is utmost priority that transformer should operate reliably in the power system network. The life and reliable performance of the transformer is almost entirely determined by the condition of the insulating system. Transformers are classified in terms of their insulating systems i.e. oil filled, dry type and gas type. However, oil filled transformers are widely used in power transmission systems [1]. In the oil filled transformer, paper and pressboard with insulating oil are used as insulation. Cellulose, a homopolymer containing D-anhydroglucose units (AGU) joined by a C1–C4 glycosidic oxygen bond, is the primary component of paper and pressboard insulation [2]. Mineral oils continue to be the recommended option for insulation and cooling in liquid-filled transformers because of their affordability, superior dielectric qualities, and increased compatibility with cellulose materials. However, mineral oil suffers from high fire risk and low biodegradability. To eliminate such problem, researchers are working on vegetable oils to use as an alternative liquid insulation in power transformer. Vegetable oils have the advantage of higher fire resistance, which ensures the safety of the personnel and environment [3]. In addition, Natural Esters (NE) exhibit greater hygroscopicity than mineral oils due to their molecular structure's ester linkages, leading to approximately 20 times higher solubility at room temperature than minerals oil. In the late 1990s, FR3 and BIOTEMP were introduced to the market after preliminary research on the necessary insulation properties of NEs for retro-filling mineral oil-filled units over the past 20 years. However, current experience in using NEs for effective and reliable field applications is very limited. The main result of these studies is that ester oils are more resistant to paper pulp degradation than mineral oil due to more hygroscopic nature [3]. Though usage of pure vegetable oils can eliminate the above problems, yet it has drawback like prone to moisture ingression etc. when used in high voltage equipment like power transformer. For the further enhancement of the dielectric properties, nanofluid was first coined by Choi and Eastman at Argonne National Laboratory in 1995 [4]. It has been reported that the dispersion of nanoparticles within vegetable as well as mineral oils improve the oil characteristics [1]. Therefore, there are

extensive research works going on all over the globe regarding the usage of nanoparticles-based oil in power transformer. Nanofluids basically consist of nanoparticles of size less than 100 nm dispersed in the base oil [4]. Based on the conducting behavior of the nanoparticles, three different types of nanoparticles, i.e. a conducting nanoparticle of iron oxide (Fe3O4), a semi-conducting nanoparticle of titanium dioxide (TiO2) and a non-conducting nanoparticle aluminium oxide (Al2O3) can be dispersed within the base oil (like transformer oil) [5]. However, there is currently insufficient experience about the nanofluids as a mineral oil substitute for dependable and reasonable field applications.

Degradation of insulations is also growing concern for the transformer life. Several factors are responsible for the degradation of liquid insulations such as temperature which is considered as the most evident factors in the existence of dissolved oxygen and metal catalyst which govern the rate of oxidative degradation of oil [6-10]. Therefore, grasping thermo-oxidative deprivation of the next generation insulating oils is still insufficient to produce a clear idea for correlating how their physicochemical traits change to how much their cooling and insulating qualities deteriorate. Based on statistical data on transformer failures, the considerable percentage of failure statistics is represented by winding failure brought on by insulation system flaws [11, 12]. Transformer failures caused by poor insulation are frequently catastrophic and come with high direct and indirect expenses, such as those associated with replacement or repair as well as lost revenue from unplanned outages. For the transformer insulation system to remain in excellent condition, sufficient maintenance is also necessary. Utilities are forced by a competitive and independent energy market to modify their maintenance policies from a time-based approach to condition and reliability-based. In such a scenario, evaluating a transformer insulation system using reliable techniques is the fundamental need of contemporary power system operation to reduce the likelihood of malfunctions and prevent the forced shutdown of strategically significant units. A number of well-established chemical, physical, and electrical methods have been developed throughout the years for assessing the state of mineral oil impregnated paper insulation systems. The most popular techniques to evaluate the quality of mineral oil in use are measurements of breakdown voltage, viscosity, acidity value, colour, interfacial tension and Dielectric Dissipation Factor (DDF). Mineral oil and ester insulating oil have very distinct chemical structures [13]. Esters, both synthetic and natural, undergo hydrolysis degradation to produce acids. Short chain acids, which are more reactive and dangerous, are mainly produced in synthetic esters. Long chain fatty acids made by NEs are less reactive than those found in synthetic esters. As vegetable oil aging byproducts are less

carbonaceous, decay products dissolve more readily in NE, causing a quick color shift in NE insulating oils [14]. Another insulation degrading factor i.e. moisture poses a risk to an insulation system in a number of ways, including quickening the aging process of paper insulation, lowering the permissible hot spot temperature, making PD inception more significant when the moisture content of solid insulation exceeds 3% and weakening the insulation system's dielectric strength [15, 16]. Therefore, in order to improve the longevity and safety of transformers in operation through corrective maintenance activities, it is imperative to properly measure the moisture content in a transformer insulating system using a dependable technique. Thus, throughout decades, transformer insulation systems' general condition and moisture content have been assessed using dielectric response measuring techniques. Return Voltage Method (RVM), Polarization and Depolarization Current (PDC) and Frequency Domain Spectroscopy (FDS) are three of the most popular methods for measuring dielectric response [17-19]. Furthermore, these techniques enable to distinguish between the impacts of solid insulation's moisture content and oil condition on a transformer insulation system's dielectric response. A transformer insulation system's dielectric response behavior is influenced by a number of elements, including temperature, oil conductivity and moisture etc. To minimize the aforementioned research gap, the primary work represented in this thesis have been conducted to investigate the dielectric characteristics of the next generation dielectrics i.e. Mineral oil and NE based nanofluids and ageing state of the oil-paper considering moisture content have been estimated.

## 1.2.Overview on Transformer Insulation

The transformer used before 1887, mainly possess dry type insulation and small in size. In 1887, Elihu Thomson filed a patent for the application of mineral oil in transformers for the intention to distribute heat from the transformer's core and extend the lifespan of the equipment [20]. Between the timeframe of 1890 and 1990, petroleum-based oils were used as dielectric liquids in transformer due to their insulating strength and high heat transfer capability [21]. On the other hand, paraffinic oils typically have elevated pour points because of their high paraffin wax content, making them unsuitable for power distribution equipment operating in cold conditions. Moreover, the viscosity of these oils increases because of the formation of sludge as a result of oxidation which is not soluble. High-viscosity oils decreased heat transfer efficiency resulting overheating. Later on, transformer oil made from naphthenic was introduced to address the challenges previously mentioned

[22]. Even though naphthenic oils are more prone to oxidation than paraffinic oils, the oxidized substances are still soluble, leading to a decrease in viscosity. Naphthenic oils have a decreased pour point, allowing them to stay fluid in transformer systems even at low temperatures. Nevertheless, the issue with using transformer oil derived from naphthenic compounds is its tendency to catch fire easily. Askarels, which are synthetic chlorinated aromatic hydrocarbons, were utilized as insulating oils to improve fire resistance. The initial transformer to use askarel was in 1932 and was in use until the 1970s when it was found to be not environment friendly [23]. Later, silicone oils were introduced as an alternative to chlorine-based oils due to their excellent electrical insulation, anti-oxidation properties, higher flash point, low-flammability fluids and high Si-O bond energy, and excellent thermal stability [21]. It has been used for more than 20 years [24]. Another way to improve insulation and flash point was to combine high temperature hydrocarbons (HTH) with silicone fluids [21]. On that time, oils based on chlorofluorocarbons with good electrical insulation and non-flammability was also used commercially. However, it was suffered with a low boiling point and tends to evaporate at operating temperatures. In 1978, isopropyl biphenyl hydrocarbons, consisting of propylated biphenyl isomers, were used for electrical insulation for relatively lower flammability than other commercial fluids. In 1980, Liquid dielectrics based on tetrachlorethylene were introduced commercially (WECOSOL$^{TM}$) [25]. WECOSOL$^{TM}$ has a low viscosity and excellent heat dissipation properties. It was used alone or mixed with transformer mineral oil to improve lubrication at lower costs [26]. However, its electrical insulating properties are relatively low compared to mineral oil which was a threat to safe operation. Among the various oils, silicone oil, HTH fluids, chlorofluorocarbon liquid substances like fluorescein, and isopropyl biphenylene hydrocarbon fluid have excellent electrical insulation properties. Despite its excellent heat resistance, the properties of silicone oil are not entirely satisfactory.

To enhance the insulation and thermal performance, Natural ester-based liquid dielectrics have been significantly utilized over the last 25 years. In 1990, Diana *et al.* discovered that the breakdown characteristics of esters were similar to mineral insulating oils [27]. David Sundin also noted that the reduction in breakdown voltage with repeated breakdowns of polyester is gradual, and the reclamation procedures are identical to those for mineral oil [28]. In 1998, Oommen *et al.* [29] verified that esters are considered low class flammable liquids because of their elevated fire and flash points. In 1999, McShane *et al.* [30] found that ester-based dielectric fluids can increase the thermal stability for transformers after conducting accelerated life tests.

Rapp *et al.* [31] studied ester temperature performance and found that ester-based fluids have a high solidification temperature i.e. the freezing and melting of esters does not impact their dielectric or physical properties, making esters suitable substitutes for mineral oils at all operating temperatures. In 2002, Gockenbach *et al.* [32] studied the dielectric characteristics of esters versus mineral oil and endorsed esters for use in transformers. In 2005, Thomas stated that transformers containing ester are less likely to pose a danger and can be placed in locations further away from water bodies, as well as in sensitive structures such as schools and hospitals [33]. In 2008, the IEEE Standards for Acceptance and Maintenance Procedures for the use of Esters as Transformer Insulating Fluids were published [34]. In 2009, Smith *et al.* [35] monitored an ester-filled transformer for three years and reported a successful experience. In 2010, a CIGRE working group studied the requirements and experience of the performance of ester-based dielectric fluids [36].

## 1.3.Flashcard of reliable transformer oil's properties

In this section the basic characteristics of mineral and vegetable oil has been compared in Table 1.1 [37-38].

Table 1.1 Comparison between mineral & vegetable oil on different primary characteristics

| **Properties** | **Standard** | **Mineral oil** | **Vegetable oil** |
|---|---|---|---|
| Source | | Petroleum Crude oil | Crops, Sunflower beans, soya beans etc. |
| Principal Components | | Complex mixture of hydrocarbons | Plant based natural ester |
| Total acidity (mg KOH/g) | IEC 62021-3 | 1.2 | < 0.6 |
| Visual Examination | ASTM D 1524 | Clear and bright | Clear and bright |
| Colour | ASTM D 1520 | Pale Yellow | Light Green |
| Interfacial Tension (dyne/cm) | ASTM D 971 | 38 | 25-30 |
| Fire Safety Class (according to fire point & calorific value) | IEC | O1 | K2 |
| Flash Point (°C) | ISO 2592 | ≥135 | Min. 250 |
| Fire Point (°C) | ISO 2719 | Limit 170 | Limit 300 |
| Calorific Value (MJ/kg) | ISO 1928 | 46 | 37.5 |

| | | | |
|---|---|---|---|
| Biodegradability at 28 days | Method OECD 301 F | <10% | >94% |
| Pour Point (°C) | ISO 3016 | -40 | -10 |
| Breakdown Voltage (kV) | IEC 60156 | >30 | >35 |
| Viscosity (cSt) at 40°C | IEC – ISO 3104 | <12 | <50 |
| Relative Permittivity at 20°C | IEC 60247 | 2.2 | 3.1 |
| Specific Heat (J/kgK) at 20°C | ASTM E1269 | 1860 | 1883 |
| Thermal Conductivity (W/mK) | ASTM C1696 –20 | 0.126 | 0.1644 |
| Power Factor at 25°C | | 0.02 | 0.08 |
| Dielectric Dissipation Factor at 90°C | IEC 60247 | ≤ 0.005 | ≤ 0.05 |
| Moisture equilibrium between oil & paper | | Moisture tends to remain in paper | Moisture tends to remain in oil owing to its higher hydrophilicity |
| DC Resistivity at 20°C (Ω-m) | IEC 60247 | $4.36 \times 10^{11}$ | $4.16 \times 10^{9}$ |
| PDIV for 50 mm gap, 100 Pc (kV) | IEC 61294 | 38.2 | 34 |

## 1.4.Factors for the Degradation of Insulating Oils

### 1.4.1.1.Contamination

Mineral oil is made by refining crude oil. So, it contains fractions of sulfur compounds, such as sulfides and carbon hydride. It is well known fact that this sulfide's oxidants, sulfoxides and sulfones, lead to a strong electrostatic charging of the insulating oil [39, 40]. The properties of insulating oils are also thought to be influenced by degradation products (organic acids, alcohols, ketones, and esters) having electrically polarized structures like hydroxyl and carboxyl groups. Sulfur-free corrosion processes have also been linked to the presence of metals (mostly copper) in mineral oils that do not include corrosive sulfur-based chemicals. The dielectric dissipation factor (*tan δ*) rises and the interfacial tension (IFT) decreases when copper is present in oil, which deteriorates the oil's insulating properties. Moreover, the oxidative breakdown of insulating oils could be accelerated by dissolved

copper. Additionally, studies have shown how metals have an oxidative role in the oxidative deterioration of vehicle oils [41]. Mineral oil, paper samples (cellulose and Aramid), and metallic catalysts (each 3 g/L of zinc, copper, aluminum, and iron of cuts) were aged for 1000 hours at 105°C in sealed container.

#### 1.4.1.2.Overheating

When transformers are in operation, core and coil losses produce a substantial amount of internal heat that, if not released, can accelerate the aging of the transformer's non-metallic components and reduce the insulation system's lifespan. As long as there are no additional thermal or dielectric flaws, properly constructed transformers can endure up to 55 years or longer, according to IEC 60076-2 [42]. The development of gas bubbles (dissolved in the oil) is invariably linked to thermal and electrical defects in power transformers, raising the possibility of partial discharge initiation. The most thermally vulnerable material is cellulose, which degrades quickly at temperatures beyond 90°C [43]. For instance, cellulose pressboards have a 10-year lifespan at 110°C [44]. In addition to loadings, ageing is also highly dependent on the type of paper, the composition of the pulp, the levels of moisture and oxygen in the pulp, and the acidity of the oil [45–51]. Electric fields may hasten aging by increasing the amount of acid products from oil degradation that precipitate onto paper surfaces [50].

#### 1.4.1.3.Stress

Transformer insulation is exposed to a variety of stresses which expedite the ageing of the insulation [45–51]. Due to the service environment and the four-dimensional problems i.e. electrical, thermal, and mechanical stresses. Water, acids, and other compounds that are somewhat polarizable and ionizable are formed which are harmful to the transformer insulation [45–51].

#### 1.4.1.4.Oxidation

The insulating liquid is exposed to oxygen, water, and rising temperatures during its life cycle. It will ultimately result in oxidation, the chemical reaction of oxygen and unstable hydrocarbons due to its interaction with the windings, tank, the core and copper metals. This reaction is catalyzed by heat and moisture and is accelerated by mechanical, electrical, and

copper/aluminum strains. Sludge and organic acid are produced by the oxidative reaction, and these materials will eventually obstruct the coil and core's ability to cool. Therefore, the tensile strength of the insulating paper will deteriorate chemically due to the acid build-up. It has been reported that, hydrogen is produced during the decomposition of oil in the presence of oxygen at comparatively low temperatures [52]. Again, the presence of copper, which encourages the oxidation of the oil and so favorably accumulates the oxygen, somewhat mitigates the harmful effects of oxygen on the paper [50].

### 1.4.1.5.Moisture

The weight of the moisture divided by the weight of the dry, oil-free paper is the standard formula used to quantify the moisture concentration in paper as a percentage. The maximum moisture content of paper for reliable operation is roughly 3%–4% for transformers with voltages not exceeding 120 kV, and 2% for EHV transformers [53].

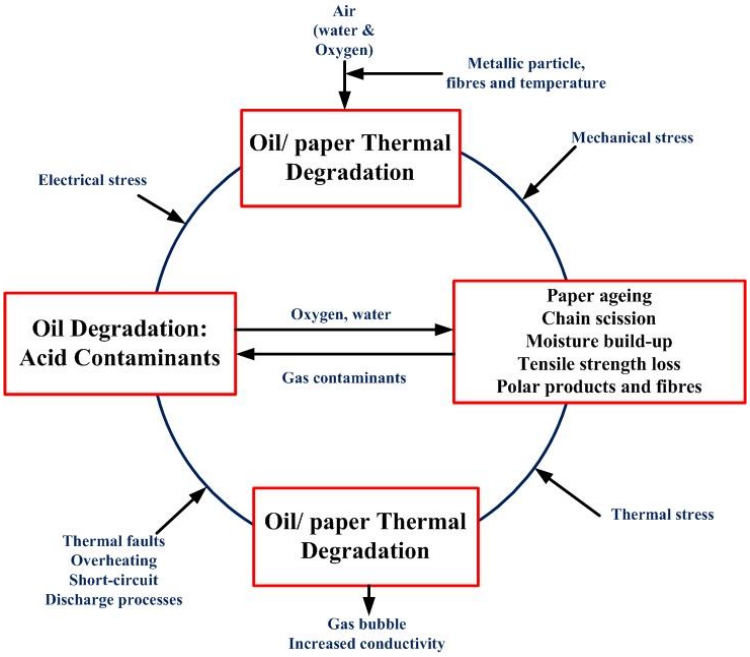


Fig. 1.1. Deterioration mechanism of Oil-paper insulation.

There are four different states of water in paper: vapor, ingested free water, free water in capillaries and maybe adsorbed to surfaces. Compared to the oil, the moisture content of the paper can be substantially higher. For instance, 223 kg of water can be found in a 150 MVA 400 kV transformer containing almost 7 tons of paper [54]. Improper handling during storage or transportation, may also contribute to a rise in moisture content [53]. Water has an impact on the insulation's conductivity, which raises the dissipation factor [55]. As a transformer ages while in service, the oil inside of it gets more and more contaminated. Particulate matter from the thermal, oxidative, or electrical deterioration of solid or oil-based insulation, fibers, gas, moisture, etc. are examples of contaminants. Since, water is a byproduct of deterioration, the paper insulation's moisture content will accelerate aging. Previous research [56, 57, 58] showed that the amount of water in the paper directly correlated with the pace of breakdown. Fig. 1.1 provides an overview of the mechanisms causing deterioration and failure [47].

## 1.5.Application of Nanotechnology in Transformer Insulating Oil

For the establishment of an enhanced dielectric liquid than mineral and vegetable oil the following properties like better dielectric strength, efficient cooling, lower dielectric losses, lower electrical conductivity, high fire resistance, biodegradability, high thermal conductivity etc. must be possessed. Therefore, there are extensive research works going on all over the globe regarding the application of nanotechnology in high voltage engineering. It is to be stated here that, initially micron sized particles were chosen for dispersion in the oil for improving thermal properties [59]. However, it fails to improve dielectric properties. After 1990s, based on the current advancements in nanotechnology, nanodielectric has drawn a lot of attention in this field [59]. Therefore, in this section, a detailed discussion about the classification, preparation, properties, issue of stability and their enhancement procedure, applications and challenges of the nanofluids has been stated.

### *1.5.1.Classification of Nanoparticles*

The nanomaterials have been primarily classified into organic and inorganic categories [59-60]. Graphite, fullerenes, carbon nanotubes (CNTs), single-walled carbon nanotubes (SWCNTs), multi-walled carbon nanotubes

(MWCNTs), and nanofibers are examples of organic nanomaterials. Carbon-based nanoparticles are the majority of available organic nanomaterials [61]. On the other hand, inorganic nanomaterials are defined as those based on metals and metal oxides, such as aluminum, zinc, copper, iron, aluminum oxide, iron oxide, and titanium oxide [62]. Inorganic nanomaterials are also classified as metalloid nanomaterials, which includes quantum dots like cadmium selenide (CdSe), zinc sulfide (ZnS), ZnO (zinc oxide) and so on [63, 64]. The chart in Fig. 1.2 includes a novel type of nanoparticles called hybrid nanomaterials. Combining organic and inorganic nanomaterials by synthesis techniques such atom transfers radical polymerization (ARTP), chemical vapor deposition (CVD) and electrospinning, results in hybrid nanomaterials [65, 66]. Therefore, the nanoparticles have been dispersed in different fluids to prepare nanofluids as depicted in Fig. 1.2.

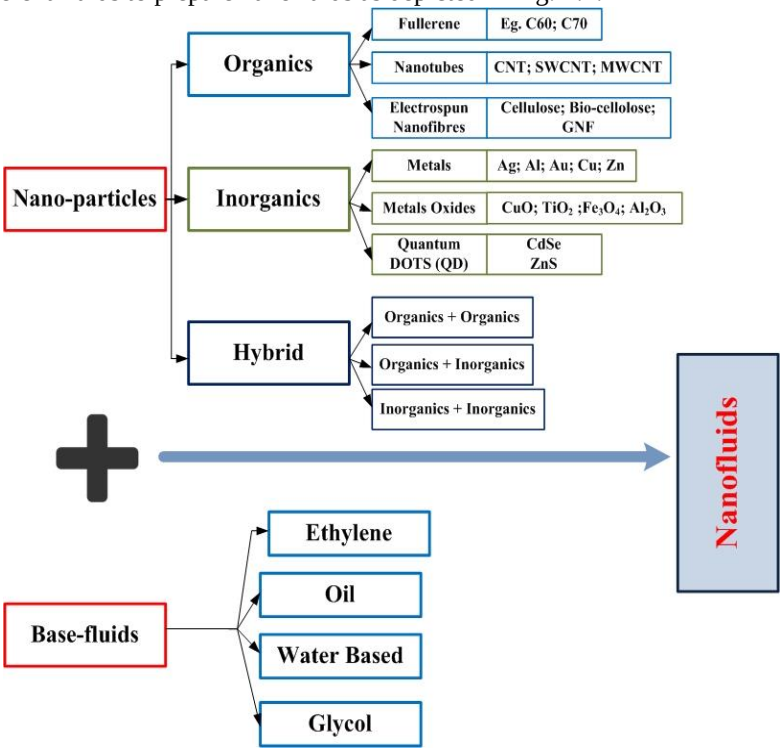


Fig. 1.2. Types of nanoparticles & fluids for preparing nanofluids.

## *1.5.2.Preparation of Nanofluids*

The first step in perusing nanofluids experimentally is their preparation. The single-step and two-step preparation procedure are the two main ways to prepare nanofluids.

### 1.5.2.1. Single-step preparation process

The one-step synthesis of nanofluids is indicated by the single-step preparation technique. A number of one-step techniques have been developed for the preparation of nanofluids [67-70]. A direct evaporation technique with a single stage i.e. VEROS, vacuum evaporation onto a running oil substrate, was coined by Akoh *et al*. [67]. However, separating nanoparticles from fluids proved to be challenging. Cu vapor is directly condensed into nanoparticles by contact with flowing low vapor-pressure ethylene glycol in a modified VEROS process which was pioneered by Eastman *et al*. [68]. One benefit of the one-step synthesis approach is the reduction of nanoparticle aggregation. The main issue, though, is that this kind of operation can only use fluids with low vapor pressure [70].

### 1.5.2.2. Two-step preparation process

The synthesis of nanofluids is often accomplished by a two-step preparation procedure that combines base fluids with commercially available nano-powders derived from various mechanical, physical, and chemical processes, including grinding, milling, and sol-gel and vapor phase techniques [71-76]. To combine nano-powders with base fluids, an ultrasonic sonicator or greater shear mixing equipment is typically utilized. To reduce particle agglomeration, stirring and ultrasonication must be used often. A two-step procedure was utilized by Eastman *et al*. [68], Lee *et al*. [71], and Wang *et al*. [72] to create alumina nanofluids. Using the similar technique, Murshed *et al*. [73] created a $TiO_2$-water nanosuspension. According to several literatures, preparing nanofluids with oxide nanoparticles is a much better idea than one with metallic nanoparticles, and a two-step approach is ideal for this [76]. The strong van der Walls force between the nanoparticles in the powders makes stability a major problem that is intrinsic to this process. Despite these drawbacks, this method is still widely used as the most cost-effective way to produce nanofluids. Fig. 1.3 depicts different nanofluids preparation procedures.

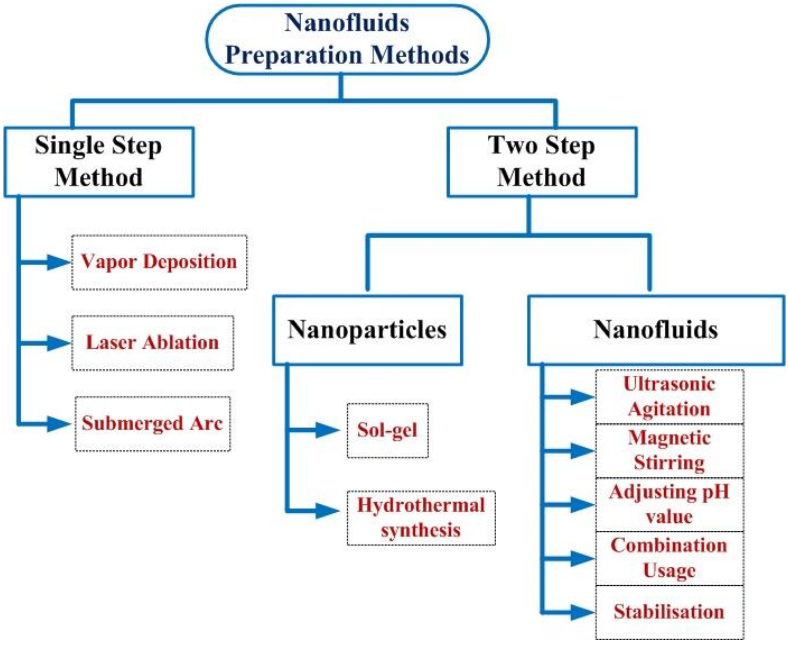


Fig. 1.3. Methods for preparing nanofluids.

### 1.5.2.3. Other methods

Other than these two processes, there exist other literatures that present various methodologies. Aqueous organic phase transfer was employed by Feng *et al*. [77] to create gold, silver, and platinum nanoparticles. Another method for preparing $Fe_3O_4$ nanofluids with kerosene through the grafting of oleic acid onto the $Fe_3O_4$ surface has been reported in [78]. Wei *et al*. set up a continuous flow microfluidic microreactor to create copper nanofluids [79]. Changes in concentration, flow rate, and additives can effectively modify the microstructure and characteristics of nanofluids. Furthermore, using ultrasonic and microwave irradiation, a unique precursor transformation process can be used to generate an aqueous CuO nanofluid [80]. Ammonium citrate is used to stop nanoparticles from growing and aggregating, which produces a stable CuO aqueous nanofluid that has a greater thermal conductivity than nanofluids made using other dispersion techniques [80].

## *1.5.3.Properties of Nanofluids*

### 1.5.3.1.Electrical Properties

For the enhancement of the electrical properties of the liquid dielectric, Nanoparticles are dispersed in the base oil to achieve better resistivity, dissipation factor, AC and DC breakdown voltage (AC BDV and DC BDV), partial discharge (PD), and relative permittivity ($\varepsilon_r$). Researches revealed that mineral oil with 0.01 wt% of alumina nanofluids show higher $\varepsilon_r$, and lower *tan* $\delta$. From [81], it can be stated that, by dispersing nanoparticle, $\varepsilon_r$ of the base oil can be enhanced which further ensure uniformity of electric field within the dielectric which leads to lower electrostatic charging. Dielectric strength of an insulating medium reveals the maximum voltage (breakdown voltage) that it can tolerate. Therefore, high BDV is ideal for materials used as insulation. For different insulation systems, different BDV test configurations (needle-sphere [82], sphere-sphere [83], needle-plate [84], and plate-plate [85] can be utilized. The results of [86, 87] show that, 0.0005 weight percent of MWCNT increased the BDV of transformer oil by approximately 490.6% and 49.5% lightning impulse, whereas a 90% Weibull distribution showed an improvement of 156% and 1.9% in BDV and lightning impulse, respectively. The authors of [88] looked into the impacts of three distinct nanoparticles i.e. $Fe_3O_4$, $TiO_2$, and $Al_2O_3$ on the AC BDV of palm fatty acid ester for the fluid insulation system. Oil samples based on $Fe_3O_4$ NPs produced the best AC BDV results, improving the results by almost 43%. Again, the impact of distributing ZnO on AC BDV of mineral TO was taken into consideration by the authors of [89]. The oil with the highest dielectric strength contained 0.0057 weight percent ZnO. In spite of the low concentration of nanofiller approximately 0.05 weight percent, the authors of [90] discovered that the AC BDV of maize oil was vividly increased when NPs (insulative or semiconductive) were treated with carbon quantum dots (CQD). Numerous studies have been done on the discharge phenomena of transformer oil in the presence of nanoparticles [91]. The effects of $TiO_2$ on reducing discharge in mineral TO were investigated in [92]. When associated to the base oil, the produced nanofluid with 0.0061 weight percent $TiO_2$ and 0.1 weight percent CTAB as a surfactant had the highest corona incept voltage. The nano-insulation system's resistance to the partial discharge (PD) is an important factor that desires to be taken into account [93]. When there is high pressure on a small fraction of insulation

which leads to breaks down of insulation and the area between conductors does not isolate, which results in PD [94]. The researchers discovered that when the NPs fraction dispersion ranged from 0 to 1 weight percent. DC flashover voltage dropped, and it increased when the NPs fraction was between 1 and 5 weight percent.

### 1.5.3.2.Thermal Properties

Pour point, flashpoint, viscosity, interfacial tension (IFT), thermal conductivity, hotspot temperature and top oil temperature have been studied in the presence of nanoparticles. According to [95], many nanoparticles have very high thermal conductivity like $Al_2O_3$ with 38-42 $W \cdot m^{-1} \cdot K^{-1}$, ZnO with 60 $W \cdot m^{-1} \cdot K^{-1}$ and AlN with 150–220 $W \cdot m^{-1} \cdot K^{-1}$. Flash point is an important factor to decide the point of fire hazard of the transformer which should be high for insulation [96]. The fire point is particularly important since, it establishes the temperature at which oil may catch fire [97]. To increase the flash and fire points, the authors of [98] $TiO_2$ nanoparticles have been dispersed in synthetic ester oil. By adding 0.05 weight percent of $TiO_2$, the flash and fire points were enhanced by 4.72% and 8.5%, respectively, while the thermal conductivity enhanced by 8.3% and 5.5% for 25°C and 80°C, respectively. Pour point and viscosity are two important thermal properties of insulations. Pour point stands for the lowest temperature at which oil begins to flow. Oil ceases transferring heat below this threshold, which is regarded as interfering with the cooling cycle. The fluid flow's resistance is inversely related to temperature, is known as viscosity. Insulating oil's viscosity should be as low as feasible to reduce resistance to the heat flow of oil [99]. The viscosity of oil will rise when NPs are dispersed. As a result, the ideal amount of nanoparticle is needed to balance viscosity with other characteristics [100]. By adding 0.05 weight percent of $ZrO_2$ and 3.8% of $TiO_2$, respectively, the viscosity increased by 21.9% and 33.1%, and the flashpoint was enhanced by 2.5% and 3.8% when 0.01 weight percent of $ZrO_2$ and $TiO_2$ was added. Top oil is the median between the temperature of the oil in the tank and the temperature of the oil at the tank outlet and hotspots are the areas inside the transformer that are not cooled by convection. Using nanoparticles these parameters can be reduced [101]. The effects of adding $Fe_3O_4$ to mineral oil were examined electrically and thermally in [101] which revealed that nanofluids have far lower hot spot and oil top temperatures than base oil without altering the dielectric characteristics of the base oil. IFT i.e. a marker of the attracting forces between oil and water molecules, should be high for pure oil [102]. The capacity of a material to transfer heat is known as its thermal conductivity.

An insulating system's generated heat must be released. Metal, by nature, conducts heat far more effectively than liquids. Consequently, thermal conductivity is increased when metal nanoparticles are added to a fluid [103]. The authors of [104] focused on adding varying amounts of $TiO_2$ and BT to mineral oil in order to increase its thermal conductivity. In mineral TO, the addition of 0.01 weight percent $TiO_2$ and 0.005 weight percent BT increased heat conductivity by 33% and BDV by 45%. According to [105], at 45 °C, NF with Eh-BN increased thermal conductivity by approximately 37.87% with 0.01 weight percent of nanoparticles added, but $TiO_2$ only demonstrated a 3.07% boost. The addition of BN to mineral oil in [106] greatly increased the thermal conductivity and made it possible for the heat produced to disperse proportionately with the mass fraction growth from 0.01 to 0.1 wt%. The effects of $Fe_3O_4$ and BT on the thermal conductivity of mineral oil were examined by the authors of [107]. The findings demonstrated that adding $Fe_3O_4$ improved the BDV and improved thermal conductivity with the increment of BN concentration this is due to the fact that, $Fe_3O_4$ has good electrical qualities and BT has good thermal properties. Temperature increases lead to an increase in thermal conductivity, which is correlated with Brownian motion [108]. In addition to the rapid motion of the fluid's molecules, the scattered particles in the fluid that are created by their collisions move randomly which is known as the Brownian motion of NPs. The reduction of NP aggregation and sedimentation can be attributed to the Brownian motion, as it increases the number of particle collisions caused by the absorption of kinetic energy [109].

### 1.5.3.3.Chemical, Mechanical and Rheological Properties

Various chemical, mechanical and rheological characteristics of insulating oils, including sheer rate, moisture, acidity, pH effect, mechanical strength and magnetic field should be taken into contemplation for choosing an insulating oil. It should be mentioned here that, the size and structure of NPs, suitable surfactant type have impact on stability [110]. Various properties like dynamic viscosity depends on several environmental factors like temperature etc. which should be considered during experiments [111]. Furthermore, the viscosity of various base fluids varies and can be affected in distinct ways by temperature changes. Examining the stability of oil-impregnated insulating paper is crucial since the cellulose paper that gets into connection with the mineral oil produces various hazardous byproducts, such as oxides, peroxides, and sludges. The chemical, mechanical, and electrical qualities of cellulose paper are impacted by these contaminants [112]. The authors of [113] looked for ways to enhance the pressboards mechanical

capabilities in transformers. While researchers employed nano-fibrillated cellulose instead of other forms of paper for the study, they discovered a considerable improvement in the tensile strength of insulating pressboard. Both AC BDV and DC BDV were enhanced by the obtained nanocellulose [113]. A study on adding 0.01 weight percent of Eh-BN to mineral oil in order to improve the electro-mechanical stability of kraft paper was conducted in [114]. The resulting NF improved mechanical stability throughout a range of thermal aging times in the lab and decreased the early polymerization of kraft paper in mineral oil. One way to achieve a stable NF is to regulate the fluid's pH level to prevent particle agglomeration and the sedimentation process by creating repulsive forces [115]. The electrical charge density on the surfaces of the NPs that affect fluid stability is correlated with the pH level. However, as documented in the literature, there is a relationship between Zeta potential and pH level [116, 117]. The behavior of the NF, which is Newtonian or non-Newtonian fluid, presents another stability concern. The primary factors influencing this attribute are the kind of NPs and the base fluid. The connection between the shear stress and the shear rate [118] can be used to estimate it. The fluid is Newtonian if the apparent viscosity, or the relationship, is linear. If not, non-Newtonian fluid is indicated by a non-linear relation or shear rate-dependent viscosity [119]. In [120], three NPs ($Al_2O_3$, $TiO_2$, and $SiO_2$) were added in varying quantities to study the heat transmission of mineral oil. The linear relationship between the shear rate and the shear stress indicated that the NFs behaved like Newtonian fluids and the addition of 0.001 weight percent $SiO_2$ showed the best improvement in heat transmission. The heat transmission of mineral oil when MWCNT was dispersed was examined and found to be enhanced which ensure the Newtonian behavior for different nanofluids [121]. Another crucial matter is to examining how moisture affects the electrical characteristics of insulating systems with various nanoparticles [122]. Moisture can cause breakdown by warping the electrical field. $TiO_2$ nanoparticles have the ability to absorb moisture which leads to lessen electric field distortion and stop start decomposition. As a result, oil containing nanoparticles might be stated to be more resistant than base oil to moisture deterioration [123]. The Karl Fischer titration is typically used to determine the amount of dissolved water present in insulating oil [124]. On the other hand, acidity influences both insulating paper and the oil’s BDV strength [125]. Acidity is associated with both moisture and dissolved gases. Excessive acidity in nanofluids can therefore result in excessive oxidation and inadequate stability [126]. So, to extend the life of the insulation system, a low acid number is necessary to minimize metal corrosion and electrical conduction [127]. The oxidation and aging of the insulating system in the

presence of nanoparticles can be predicted based on several studies in the literature about moisture and acidity. Researchers found in [128] that dispersing $Fe_3O_4$ to transformer oil enhanced the amount of soluble water present, particularly when NP content was increased. But nanofluid's BDV is superior to base oil. It was revealed that, fullerene C60 was found to slow down the oxidation and aging processes. The inclusion of nanomagnetic particles to create an insulating fluid as a magnetic nanofluids has drawn significant consideration from researchers to prepare stable nanofluids [129]. Additionally, magnetic nanoparticles can improve the dielectric qualities of certain insulating fluid [130]. In order to obtain NPs with appropriate magnetic characteristics and create stable insulating fluids, it is crucial to investigate the magnetic properties (such as high saturation magnetization and high magnetic permeability) of various metal NPs [131]. The majority of the targeted magnetic nanoparticles (NPs) are iron oxides, such as hematite, magnetite, and maghemite [132], as well as ferrites with the formula $MFe_2O_4$, where M can be any metal precursor, such as Fe, Co, Cu, Ni, Zn, Mg, Mn, Ba, Au, Ag, and Cu, or any oxide, such as $Al_2O_3$ and CuO, carbide (SiC and TiC), and nitride (AlN and SiN) [133]. These magnetic nanoparticles can enhance the PD resistance of the base oil [134]. However, larger size of magnetic nanoparticles might increase the internal local electric field and cause a breakdown [135].

From the above discussion, it can be stated that, using nanoparticles the properties of the base oil can be enhanced. However, nanofluids that are prone to coagulation may lose their ability to transport heat [115]. As a result, research into stability is a necessary topic that can change the thermophysical characteristics of nanofluids for use in applications. It is also critical to examine the variables that affect the stability of these suspensions.

## *1.5.4.Stability of Nanofluids*

This section includes an overview of the stability mechanisms pertaining to nanofluids, as well as approaches for improving stability.

### 1.5.4.1. Stability evaluation methods for nanofluids

#### *1.5.4.1.1. Zeta potential analysis*

The potential difference between the stationary fluid layer attached to the particle and the dispersion medium is known as the zeta potential. The degree

of repulsion between neighboring, similarly charged particles in dispersion is indicated by the zeta potential. Therefore, colloids with low zeta potentials tend to flocculate or coagulate, whereas those with high zeta potentials (positive or negative) are electrically stabilized. It is considered that nanofluids with zeta potentials between 40 and 60 mV exhibit good stability. Zeta potential analysis was employed by Kim *et al*. [136] to determine the stability for Au nanofluids. The zeta potential of alumina-water based nanofluids was determined by Zhu *et al*. [137] at various pH levels and SDBS concentrations. To calculate the attractive and repulsive potentials, the DLVO theory (coined by Derjaguin, Landau, Verwey, and Overbeek in 1940) was used.

#### *1.5.4.1.2. Sedimentation method*

The simplest technique for evaluating nanofluids' stability is sedimentation [138]. To initiate the sedimentation of nanoparticles in the nanofluids, an external field is introduced. The stability of nanofluids is shown by the volume or weight of the sediment. If the supernatant particle concentration doesn't change over time, nanofluids are usually regarded as stable. Zhu *et al*. measured the stability of graphite suspension using the sedimentation method [139]. Utilizing a camera has shown to be an effective tool for taking sedimentation photos so that the stability of nanofluids may be observed [140]. The duration required to take pictures is correlated with the quality of the nanofluids during preparation to produce a stable nanofluids. Wei *et al*. took pictures of their samples 24 hours after they were prepared. The procedure for measuring the sedimentation of an alumina-water nanofluid was followed by Wang *et al*. [141].

#### *1.5.4.1.3. Centrifugation method*

The sedimentation process takes a lot of time since it necessitates extended observation. Therefore, the centrifugation method was created to assess stability. Sing *et al*. [142] assessed the stability of a silver nanofluid made by decreasing $AgNO_3$ and using PVP (polyvinylpyrrolidone) as the stabilizer using the centrifugation method. PVP's protective function, which slows down particle agglomeration through steric action, was discovered to contribute to the exceptional stability of silver nanofluids.

#### *1.54.1.4. Spectral analysis method*

Examining the spectrum with a UV-vis spectrophotometer is an advanced method for assessing the stability of nanofluids. The benefit of UV-vis spectroscopy over other techniques is that it provides quantitative findings that match the concentration of nanofluids. The stability of MWNT nanofluids was examined by Hwang *et al*. [143] through the measurement of MWNT's UV-vis absorption at various sedimentation times. The stability evaluation procedure can be conducted by combining the three methods mentioned above. For instance, Li *et al*. [144] conducted sedimentation photography, absorbency and zeta potential examination for copper nanofluids at various concentrations, pH levels, and dispersion kinds.

#### *1.5.4.1.5. 3ωMethod*

This approach allows for the evaluation of suspension stability while taking into account the increase in thermal conductivity brought on by the sedimentation of nanoparticles throughout a broad range of nanoparticle volume fractions [145]. According to [146], this technique can be used to verify the stability of nanofluids.

#### *1.5.4.1.6. Electron Microscopy and Light Scattering Methods*

Two common ways to observe particle aggregation are light scattering techniques and electron microscopy, which measure the particle size distribution. The term "electron micrograph" refers to the digital image of nanoparticles that is captured using very high-resolution microscopes like TEM and SEM [147, 148]. If the microstructure of the nanofluids is not altered during preparation, cryogenic electron microscopy can also be employed for the same objective [149]. Complex nanosuspensions can also be studied using the light scattering approach using Dynamic Light Scattering methods.

### 1.5.4.2. Stability Enhancement Procedures

#### *1.5.4.2.1. Addition of Surfactants*

Usually, dispersants or surfactants are used to stabilize the nanofluids. When surfactants are added, the surface tension of the base fluids is lowered and particle immersion is increased. Chemical substances applied to

nanoparticles with the purpose of decreasing liquid surface tension and increasing particle immersion are known as surfactants. Numerous researches discuss the addition of surfactant to nanoparticles in order to prevent rapid sedimentation; in each given situation, though, the particle should receive an adequate amount of surfactant. Various surfactant types have been used in studies for various sorts of nanofluids. Gum Arabic [150], Hexadecyltrimethylammonium bromide (HCTAB) [151], Sodium dodecyl sulfate (SDS) [152], Salt and oleic acid [153], Dodecyl trimethylammonium bromide (DTAB) [154], and Polyvinylpyrrolidone (PVP) [155] are a few significant surfactants. It should be mentioned that this method is not suitable for use with high-temperature nanofluids due to the possibility of damaging the link between the surfactant and nanoparticle. Surfactants may also prevent heat transfer and cause foaming during heating. Moreover, surfactants may improve the heat resistance between base fluids and nanoparticles, which could reduce the increase of thermal conductivity [157].

#### *1.5.4.2.2. Surface modification techniques*

The surfactant-free approach is discussed in this section. Long-term stability of nanofluids can be achieved by injecting functional nanoparticles into the basic fluids. These types of alteration approaches come in many forms. For instance, in the initial nanoparticle solutions, Yang *et al*. [157] grafted silanes directly onto the surface of silica nanoparticles. One unique characteristic of the nanofluids was that, following a pool boiling operation, no deposition layer developed on the heated surface. The addition of hydroxyl groups to the surface of carbon nanotubes (CNTs) can enhance their stability [158]. Diamond nanoparticles' surface can be altered by plasma treatment to enhance their water-soluble dispersion characteristics [159].

#### *1.5.4.2.3. pH control of nanofluids*

As nanofluid's electro-kinetic characteristics directly affect its stability, altering its pH can make it more stable because of strong repulsive forces. For instance, a straightforward acid treatment could result in CNT stability in water [160]. According to [160], different pH values for $Al_2O_3$ nanofluid, Lee *et al*. [141] observe a decrease or increase in agglomeration in response to pH changes. In addition, it should be mentioned that every sample has a different ideal pH value. For example, alumina, copper, and graphite dissolved in water have ideal pH values of approximately 8, 9.5, and 2, respectively [159].

#### *1.5.4.2.4. Ultrasonic agitation*

Agglomeration may happen after the nanofluids are prepared, which increases the downward body force and causes the nanoparticles to settle quickly. Manson *et al*.'s investigation [161] involved two distinct nanofluids: silver-silicon oil and carbon black-water. Using this method, particle clusters have been broken up using high cavitation energy or ultrasonic agitation.

### 1.5.4.3. Stability Mechanisms

Particle aggregation can cause problems with stability, which is the most important factor to study. The combination of the attraction and repulsive interactions between particles causes nanoparticles to aggregate. When attractive forces outweigh repulsive ones, particles group together to form clusters. Therefore, stability may be ensured and particle aggregation can be avoided by increasing repulsive forces over attractive forces. Two strategies are available for enhancement: electrostatic stabilization and steric stabilization. A brief discussion of these two mechanisms is given here.

#### *1.5.4.3.1. Electrostatic stabilization*

One important source of kinetic stability is the presence of an electric charge on particle surfaces. Ions adsorb to the electrophilic metal surface to cause electrostatic stabilization. A Columbic repulsion force develops between the nanoclusters as a result of adsorption, which produces an electrical double or multilayer. However, the application of electrostatic stabilization is restricted as it is sensitive to pH.

#### *1.5.4.3.2. Steric stabilization*

By adhering (grafting or chemisorbing) macromolecules such polymers or surfactants to the particle surfaces, stem cell stability of nanoparticles is achieved. Large adsorbents that provide a steric barrier to keep particles from getting too near to one another are what cause the stabilization. For instance, PVP's protective function in preventing nanoparticle aggregation due to the steric effect is responsible for the stability of graphite nanofluids [139].

### 1.5.5. Advantages of Nanofluids [162-163]

i. High specific surface area, which increases the surface area available for heat transmission between fluids and particles.
ii. Particles moving mostly in a Brownian motion with high dispersion stability.
iii. Less pumping power needed to obtain the same intensity of heat transfer as compared to pure liquid.
iv. Less particle clogging than with traditional slurries, which encourages system downsizing.
v. Modifiable qualities that can be tailored to various applications by changing the particle concentration, such as surface wettability and thermal conductivity.

### 1.5.6. Limitations of Nanofluids [162-166]

i. The manufacture of nanoparticles is highly expensive due to the need of complex technology.

ii. In the absence of surfactant, there is an issue of nanofluid stability.
iii. The fluid's density and viscosity raise the pumping power and pressure drop, respectively. Compared to the basic fluid, the density and viscosity of the nanofluid are substantially higher. Consequently, the pressure drop and pumping power of the nanofluid are greater than those of the base fluid.

iv. The specific heat of a nanofluid is less than that of a basic fluid.

v. Nanoparticles are thought to be far more harmful than micron-sized particles because of their extremely reactive nature. The nanosized particles can readily enter into the nasal canal, which may cause serious health problems. For human lungs, iron oxide is thought to be disastrous. According to [165], alumina nanoparticles are somewhat harmful, while ZnO nanoparticles are very poisonous.

vi. The worldwide guidelines express concerns about nanoparticles and the risks they pose to occupational health and safety (OHS). Nanoparticles have the potential to seriously harm the ecology when they penetrate the atmosphere, soil, and water during the production, transportation, and processing stages.

### *1.5.7. Applications of Nanofluids*

Numerous industries, including the automotive, medicinal and energy sectors, use nanofluids. Coolants, nanofluids in heat exchangers, cancer treatment, solar cells, solar absorption, energy storage, nanodrugs, and automotive braking and shock absorbers are a few examples of specific applications. The function of nanofluids in various applications represented in the Fig. 1.4 [167].

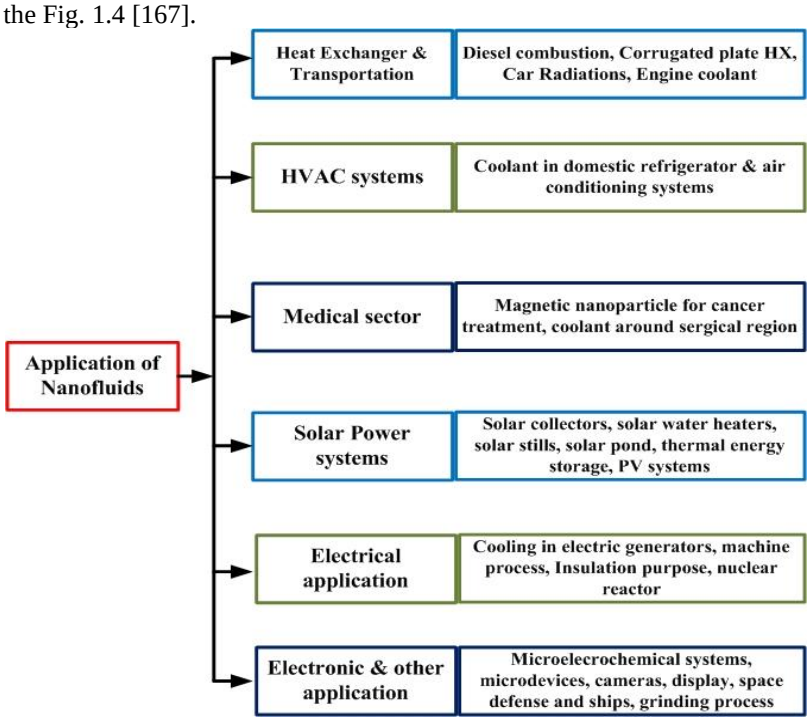


Fig. 1.4. Various field for application of nanofluids.

### *1.5.8. Challenges in Implementation of Nanofluids as Transformer Insulating Oil*

Before the practical application of nanofluids as transformer insulating oil, there are a number of problems and difficulties related to nanofluids that need to be resolved. The primary problems are (i) inconsistencies in the results outcome from the experimental data and between the results and predictions

of the theoretical model; (ii) inadequate characterization of the nano suspensions; and (iii) ignorance of the intricate physical processes underlying the unusual behavior of nanofluids [168]. The preparation of nanofluids comes with a number of economical and technological difficulties. The primary technical challenge lies in achieving a uniform suspension of nanoparticles, mostly because of the strong Van der Waals interactions that force the particles to constantly agglomerate [168-169]. The practical applications of nanofluids heavily depend on their stability. The features of the base fluid and suspended particles, such as their chemical structures and shape, have a significant impact on the stability of the nanofluid [170]. Aggregation and sedimentation are hence two processes that are essential to the stability of nanofluid. In the study of CuO–ethylene glycol nanofluid, Kwak *et al*. [171] found that significant increases in thermal conductivity in relation to particle concentration are only possible when particle concentration is below the dilute limit. This is because, according to rheological properties, the volume fraction at the dilute limit is 0.002, which is significantly smaller than the value based on the shape of individual particles as a result of particle aggregation. By tracking the changes in particle size and distribution over time, the aggregation of particles is observed. Since only tens to hundreds of particles are measured out of a large number of particles, the SEM and TEM are useful tools for observing nanoparticles in nanofluids but are insufficient for statistical analysis. In order to verify the particle size over a larger sample size, the DLS (Dynamic Light Scattering) method was used to measure the particle size. Particles in suspension smaller than tens of micrometers move randomly via Brownian motion in the presence of heat. The Stokes–Einstein equation describes the variation in particle movement speed as a function of particle size. Larger particles move more slowly, while smaller particles move quicker [172]. High production costs, unusually high thermal conductivity, high viscosity, low specific heat, and higher-pressure drop-in comparison to the base fluid are the other major issues with nanofluids. Overcoming these obstacles will make the effective commercialization of nanofluids possible and lead to significant advancements in a wide range of applications.

## 1.6. Background on Composite Oil-paper Insulation

Cotton fabric covered in paper or broiled in oil served as the first insulation for transformers. In the 1920s, the cellulose-oil composite

insulation of kraft paper-insulating oil first arose as a result of an increase in transformer voltage class [173-175]. In addition to being utilized more frequently in transformers, synthetic materials were first created in the 1950s. Excellent performance is also exhibited by the composite insulating paper composed of synthetic and cellulose materials. It has been demonstrated that, in comparison to pure cellulose paper, composite paper made of cellulose paper and polymer film has superior dielectric characteristics [176]. The primary raw material used to make cellulose-rich insulating paper is the plant. Coniferous wood from the Pinaceae family has long fibers and a high cellulose content which makes it a popular material for making insulating paper [177]. Natural cellulose insulating paper has reduced production costs and is more affordable and environmentally friendly than composite insulating paper such as Nomex insulating paper. The insulating paper created from natural cellulose has the advantages of great mechanical strength and easy size control because of its long length. The cellulose insulating paper works well with transformers and has outstanding electrical performance. Sufficiently dried cellulose has a resistivity of about 1018 Ω/cm and a dielectric strength of about 250 kV/mm, which is higher than most dielectrics [178]. The primary insulating materials between winding turns and wire cakes are insulating paper and insulating cushion block, which also serve as isolation and support elements. In addition, strong mechanical qualities are needed because the insulating paper is wound on the copper conductor. Even though cellulose insulating paper has numerous benefits, over time, as transformers operate, it ages due to a variety of factors like temperature, electric field, moisture, oxygen and so on, and its performance will irrevocably change. The degree of polymerization decreases together with the breakdown of cellulose and several aging products are created throughout this process. The service life of transformers will decrease when the cellulose insulating paper begins to gradually lose its mechanical and electrical properties. Till date, there has been little progress in the creation of pure cellulose insulating paper.

## 1.7. Condition Monitoring of Oil Immersed Transformer Insulation

Transformer health mainly depends on the condition of the insulation used in it which is a major concern for every power sectors. According to the health of insulation, condition-based maintenance has been considered. To check the health of the transformer insulation a number of tests are being performed as presented in Fig. 1.5 [179].

## *1.7.1.Thermal Methods*

It is a known fact that the purpose of the oil used in transformers is to perform both the tasks of insulation and cooling. Therefore, in this context, the physical and thermal properties of the fluid become instrumental in the development of nanofluids synthesized for the function of ensuring electrical insulation. Some of the physical and thermal parameters are thereby been discussed herein.

### 1.7.1.1.Thermal conductivity

Thermal conductivity is the trait of a material by the virtue by which it conducts heat. The fluids required for the transformer should act as a heat transfer medium. Hence, thermal conductivity is an important factor for enhancing the heat transfer capability of a transformer fluid. It is, therefore, utmost necessary for the oil to hold high thermal conductivity which decides the course for the selection of the materials as transformer liquids. The thermal conductivity can be measured by heat flow meters according to ASTM C1696 – 20 [37-38].

### 1.7.1.2.Flammability

Flammability of the transformer oil is a hazardous and an intricate safety issue. Hence, a few parameters like the flash Point and fire Point have, thus, been defined in the context of flammability of a transformer oil [182-183]. The lowest temperature at which a volatile fluid's surface releases enough vapors to create an ignitable combination in air is known as the fluid's flash point. The temperature at which vapors ignite and continue to burn is known as the fire point. It is the minimum temperature at which a fire will start in the sample. One of the finest quality indicators to assess the likelihood of a fire danger is flash point. To measure the Flash Point and Fire Point, ISO 2592 and ISO 2719 has been followed [37-38].

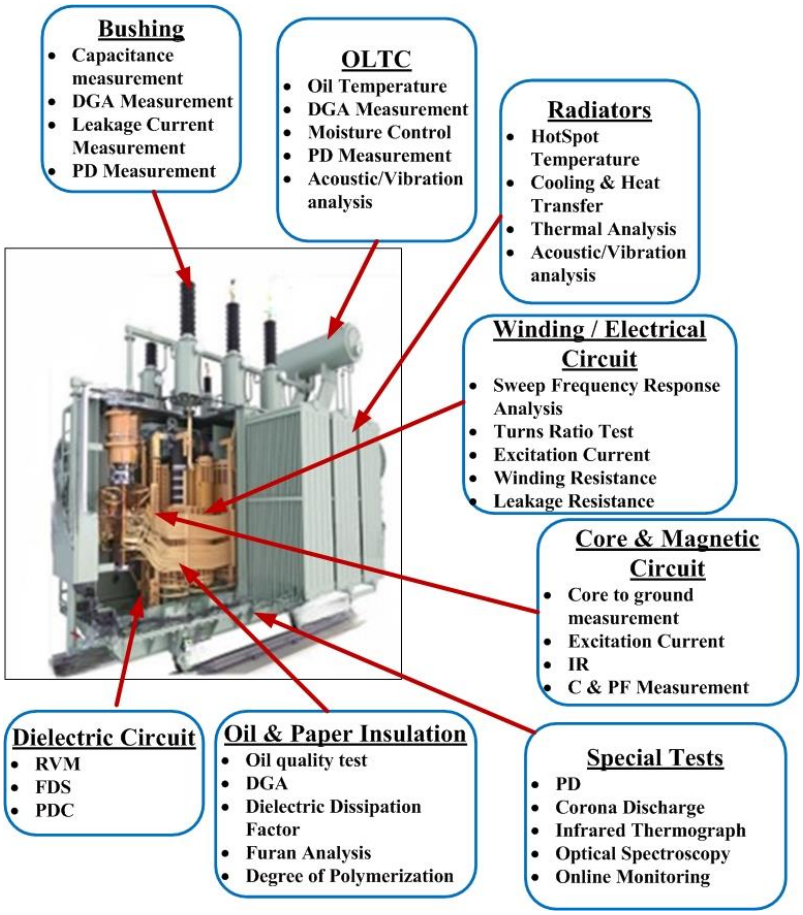


Fig. 1.5. Condition monitoring methods for insulation used in different parts in Transformer [179].

## *1.7.2.Chemical Based Techniques*

A number of chemical-based diagnostic methods have been employed for many years to evaluate the state of transformer paper and oil insulation.

#### 1.7.2.1.Karl Fischer Titration (KFT) method

This method is the most often used chemical-based methods to assess the level of moisture content in insulation as per the procedure outlined in IEC Std. 60814 [37-38].

#### 1.7.2.2.Interfacial Tension (IFT) and colour

The molecular attractive force at the interface between water and oil which do not mix, is measured by interfacial tension, or IFT. IFT is a helpful metric to detect the existence of polar impurities that are soluble and originate from solid insulators and oil degradation products. A high IFT is typically seen in new, quality oil. Contaminants from oil oxidation do reduce the IFT.

One of the main indicators of the level of deterioration and potential contamination of oil during usage is its colour. When expressing colour changes, a numerical value based on international colour standards (ASTM D1500) is typically utilized.

#### 1.7.2.3.Dissolved Gas Analysis (DGA)

Irregular conditions in an oil-filled transformer like insulation overheating, arcing, pump failure, and overloading, produce intense heat that produces low-molecular combustible gases, such as hydrogen ($H_2$), methane ($CH_4$), acetylene ($C_2H_2$), methylene ($C_2H_4$), ethane ($C_2H_6$), carbon monoxide (CO), and incombustible gases, such as carbon dioxide ($CO_2$). For identifying early defects and characterizing the aging of insulation, dissolved gas analysis (DGA) can be performed according to the procedure described in IEC 60567 [37-38].

#### 1.7.2.4. Furfural Analysis

When a class of heterocyclic compounds is broken down by cellulose paper insulation used in electrical equipment, 2-furfural aldehyde (2-FAL), 2-acetylfuran (2-ACF), 2-furoic acid, 5-methyl-2-furfural (5-MEF), 2-furfurylalcohol (2-FOL), and 5-hydroxymethyl-2-furfural (5-HMF), are produced. The furfural analysis according to IEC Std. 61198, can be used to determine these chemicals, which are partially dissolved in oil medium based on High-Performance Liquid Chromatography (HPLC).

#### 1.7.2.5.Neutralization Number

For oil insulation, a rise in the neutralization number primarily indicates the oil's degree of deterioration in an oxidizing environment. Acceptable maximum neutralization numbers are 0.2 mg KOH/g [175] and 0.3 mg KOH/g [103] for in-service mineral and NE oils of voltage class less than 69 kV, respectively.

#### 1.7.2.6.Viscosity

Viscosity measurement can help to investigate the binding effect of the nanoparticles with the base oil. Estimation of viscosity of oil insulations have been conducted through employing different viscometer.

Additionally, some of the literature has cited the use of thermogravimetry analysis, gel permeation chromatography (GPC) for molecular weight measurement, and FTIR spectroscopy for cellulose paper insulation [184-185].

However, in these thermal and chemical methods, the difficulty of obtaining insulation samples from an operational transformer hinders the practical application of these paper-based approaches. Therefore, modern researches have primarily focused on the condition monitoring of the transformer insulation based on electrical methods.

### *1.7.3.Electrical Methods*

Breakdown voltage (BDV), partial discharge (PD) measurements, insulation resistance (IR), dielectric absorption ratio (DAR), polarization index (PI), power frequency loss factor (DDF), polarization and depolarization current (PDC), recovery voltage measurement (RVM), and frequency domain spectroscopy (FDS) are typical electrical-based traditional diagnostic tools that have been used to assess the quality of oil-paper insulation in transformers both individually and collectively [186–187].

#### 1.6.3.1. Power Frequency Breakdown Voltage Measurements

The most widely used method to evaluate insulating oil quality is BDV at power frequency. It essentially gauges the oil's resistance to electrical strains. When impurities such water, cellulosic fiber, dirt and conductive particles are present in the liquid insulation, breakdown voltage of the insulation has been affected. ASTM Std. D1816-4 and IEC Std. 60156 specify the standard test protocol for determining the breakdown voltage of liquid insulations derived

from petroleum, different electrode types, electrode spacing, voltage ramp rates, stir durations between tests and sample sizes. IEEE Std. C57.147-2008 advises a longer rest period before analyzing the BDV of ester oil in order to allow air bubbles to remove because ester-based insulating oils have a higher viscosity than ordinary mineral oil [188].

#### 1.6.3.2. Overview of IR, DAR and PI measurements

One fundamental dielectric parameter that can be used to evaluate a transformer's insulation system is IR. This method involves applying a DC step voltage across the insulation under investigation and measuring the charging current over a one-minute period as presented in (1.1). This test is usually run on a regular basis, and a significant decline in IR over time suggests that the insulation needs to be under maintenance. The dielectric parameters for DAR and PI, which are extensions of IR measurement, are computed using the IR values at 30 seconds, 1 minute, and 10 minutes as provided by (1.2) and (1.3). Three types of current flow through an insulating item under a DC step voltage are the charging current, the absorption current and the conduction current. It is believed that absorption current, which is the polarization current caused by molecule charge shifting in the insulator, will eventually decay to zero. As a result, DAR and PI should both have values higher than 1 [103]. DAR and PI values of well-maintained insulation are typically higher than 1.6 and 2, respectively [189].

$$IR = Insulation\ resistance\ at\ 1\min = \frac{Applied\ voltge}{Current\ at 1\min} \tag{1.1}$$

$$DAR = \frac{1\min\ insulation\ resistance\ reading}{30\sec\ insulation\ resistance\ reading} \tag{1.2}$$

$$PI = \frac{10\min\ insulation\ resistance\ reading}{1\min\ insulation\ resistance\ reading} \tag{1.3}$$

#### 1.6.3.3. Dielectric Dissipation Factor Measurement

For decades, transformer insulation status has been effectively evaluated using DDF, a dimensionless metric measured at power frequency [186, 189, 190]. A transformer's DDF primarily describes the insulation system's level of contamination and moisture. In field measurements, the test voltage is usually between 100 V and 10 kV AC. The majority of field experiments are carried out at rated voltage or up to 10 kV [190]. A current flows through an

insulator when an AC voltage is put across it. Capacitive and resistive currents make up the two main components of this current. DDF, referred to as *tanδ*, is essentially the resistive current to capacitive current ratio. When an insulation system is in good working order, the resistive current is pointedly less than the capacitive current. As a result, DDF is extremely minimal because the source voltage is almost 90 degrees lag the source current. DDF largely depends on temperature, therefore in order to accurately draw conclusions from DDF measurement findings, it is important to take measurement temperature into account. This is to be stated here that DDF is a dimensionless parameter that is independent of the insulation's geometrical properties. This is a single frequency test; hence the transformer's insulation state can only be evaluated to a limited extent. Furthermore, DDF lacks sufficient data to address the distinct impacts of solid and oil insulation. DDF at power frequency mostly describes the state of the oil insulation in older transformers. These shortcomings in the single frequency DDF measurement could cause the state of the transformer solid insulation to be interpreted incorrectly. The maximum allowable DDF of new NE-based insulating liquids, as per IEEE Std. C57.147-2008, is 0.002 at 25ºC using the test procedure outlined in ASTM D 924. At 90 ºC, that of newly developed synthetic ester insulating liquids is 0.03 [191]. The limiting value for DDF of both serviced aged mineral oil and NE insulating liquids at 25ºC is 0.005, following IEEE Std. C57.152-2013. However, for service-aged NE insulating oils at 25ºC, IEEE Std. C57.147-2008 proposes a temporary acceptable limitation value of 0.03.

#### 1.6.3.4. Dielectric response Measurement

For a vacuum insulated electrode arrangement, the flux density *D* is proportional to electric field vector *E*. If homogenous isotropic dielectric medium is used instead of vacuum, then polarization (*P*). *D* can be regarded as (1.4)

$$D = \varepsilon_0 E + P \text{ where } P = \chi \varepsilon_0 E \tag{1.4}$$

Here, $\chi$ is the electrical susceptibility of the material. If the electric field is generated by a time varying function, then polarization function can be written as (1.5).

$$P(t) = \chi(t) \varepsilon \ E(t) \tag{1.5}$$

Similarly, the electric flux density *D(t)* can be expressed as (1.6).

$$D(t) = \varepsilon_0 E(t) + P(t) = \varepsilon_0 (1 + \chi(t)) E(t) \tag{1.6}$$

The polarization process, *P(t)*, is comprised of the combined effect of all the polarization mechanisms. As all the polarization take a long time to settle and finally becomes static i.e. $P(t\rightarrow\infty) = P_s$. When a step voltage $V_{dc}$ is applied to dielectric medium the polarization vector *P(t)* maintains as monotonically increasing profile can be expressed as (1.7).

$$P(t) = (P_S - P_\infty)g(t - t_0) + P_\infty\delta(t - t_0) \tag{1.7}$$

Where $\delta(t\text{-}t_0)$ is dirac-delta function which is considered for the fast polarization processes and $g(t\text{-}t_0)$ is monotonically increasing function, is considered for the interfacial polarization process as shown in Fig. (1.6).

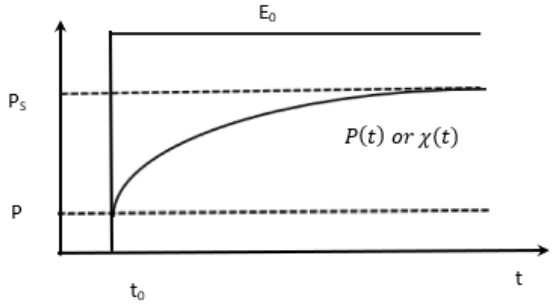


Fig. 1.6. Response for polarization process.

Where, $g(t - t_0) \geq 0$, $\frac{dg(t - t_0)}{dt} \geq 0$ for all $t_0 < t < \infty$

$g(t - t_0) = 0$ for all $t \leq t_0$; $g(t - t_0) = 1$ when $t \rightarrow \infty$

Using (1.8) the polarization vector *P(t)*, due to electric field at any time instant can be expressed by the following equation.

$$P(t) = \varepsilon_0[\chi_\infty + (\chi_S - \chi_\infty)g(t - t_0)]E(t) \tag{1.8}$$

Since, susceptibility is related to the permittivity of the dielectric medium so the polarization can be expressed as (1.9).

$$P(t) = \varepsilon_0[(\varepsilon_\infty - 1) + (\varepsilon_S - \varepsilon_\infty)g(t - t_0)]E(t) \tag{1.9}$$

In general, a material cannot polarize instantaneously in response to an applied field. The polarization is a convolution of the electric field at previous times with time dependent susceptibility. So, *P(t)* can be expressed by (1.10).

$$P(t) = \varepsilon_0(\varepsilon_\infty - 1)E(t) + \varepsilon_0 \int_{-\infty}^{t} f(t - \tau)E(\tau)d\tau \tag{1.10}$$

Where, *f(t)* is dielectric response function. It is monotonically decreasing function as presented in (1.11).

$$f(t-\tau) = (\varepsilon_S - \varepsilon_\infty)\frac{dg(t-\tau)}{dt} \tag{1.11}$$

Therefore, under an electric field *E(t)* total current density *J(t)* in the dielectric medium can be expressed as (1.12).

$$J(t) = \sigma_0 E(t) + \varepsilon_0 \varepsilon_\infty \frac{\partial E(t)}{\partial t} + \frac{\partial P(t)}{\partial (t)} \tag{1.12}$$

Where $\sigma_0$ is dc conductivity of the dielectric medium and $\varepsilon_0$ is the permittivity in free space. For a homogenous material, the total current through the dielectric medium can be written as (1.13).

$$i(t) = C_0[\frac{\sigma}{\varepsilon_0}U(t) + \varepsilon_r \frac{dU(t)}{dt} + \varepsilon_0 \frac{d}{dt}\int_0^t f(t-\tau)U(\tau)d\tau] \tag{1.13}$$

Where, $C_0$ is geometric capacitance. In the above equation first term is considered for the conductivity of the test sample and the other is owed to the different polarization processes occurring within the test sample. This equation is valid for a single as well as an arrangement of several dielectric materials in series or parallel. This dielectric spectroscopy can be classified into two categories named as time domain spectroscopy and frequency domain spectroscopy. The time domain dielectric diagnosis mainly includes Polarization and depolarization current (PDC) and Return Voltage (RV) Measurement methods. The frequency domain method is known as Frequency Domain Spectroscopy (FDS)

### 1.6.3.5. Polarization and Depolarization Currents measurements

This method captures the insulation's charging and discharging currents. One method to study the slow polarization processes in the time domain is to measure the polarization and depolarization currents (PDC) after a dc voltage step. Prior to the PDC measurement, the test object's dielectric memory needs to be purged. To accurately capture the tiny polarization current, the voltage source needs to be devoid of noise and ripple. The test setup for the PDC measuring method is displayed in Fig. 1.7. Applying a dc charging voltage of magnitude Uc to the test object over an extended period of time (for example, 10,000s) is the process. The polarization current $I_{pol}(t)$ through the test object is measured during this period. This current results from the polarization process being activated with varying time constants that correspond to various insulation materials and the conductivity of the object, which has been carefully discharged beforehand.

$$I_{pol}(t)=C_0V_{dc}[\frac{\sigma_0}{\varepsilon_0}+\varepsilon_\infty\delta(t)+f(t)] \quad (1.14)$$

The depolarization current (also known as the discharging or de-sorption current) $I_{depol}(t)$ in the opposite direction can then be measured without the conductivity's contribution by removing the voltage and short-circuiting the item at $t=tc$. If the current becomes stable or extremely low, the polarization current measurement can typically be halted. The abrupt drop in voltage Uc to zero is considered a negative voltage step at time $t=tc$ in accordance with the superposition principle. The dielectric response function $f(t)$ is proportional to the depolarization current if the test object is charged over an extended period of time such that $f(t+ tc)=0$.

$$I_{depol}(t)=-C_0V_{dc}[f(t)-f(t+t_c)] \quad \text{for } 0<t<\infty \quad (1.15)$$

Therefore, for long charging time $t_c$ the value of $f(t + t_c)$ is very low with respect to $f(t)$ and can be neglected. Hence the depolarization current equation can be rewritten as (1.16).

$$I_{depol}(t)=-C_0V_{dc}f(t) \quad \text{for } 0<t<\infty \quad (1.16)$$

The Fig. 1.8 shows the principle of polarization and depolarization current. The insulation between windings is charged by the dc voltage step $U_0$. A long charging time is required (10,000 s) in order to assess the interfacial polarization and paper condition. The initial time dependence of the polarization and depolarization currents (<100 s) is very sensitive to the conductivity of the oil while the moisture content of press board influences mainly the shape of the current at much longer time. Further, the dc conductivity can be from the PDC curves by subtracting the depolarization current from the polarization current at larger values of time. Therefore, the dc conductivity $\sigma_0$ can be expressed by (1.17).

$$\sigma_0=\frac{\varepsilon_0}{C_0V_{dc}}[I_{pol}(t)-I_{depol}(t)] \quad (1.17)$$

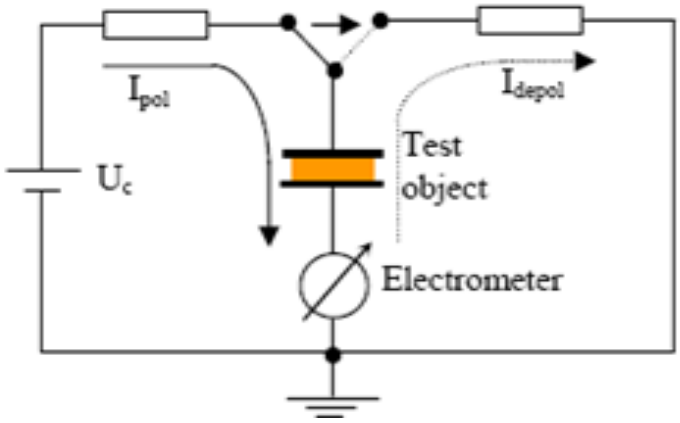


Fig. 1.7. Test arrangement for the PDC.

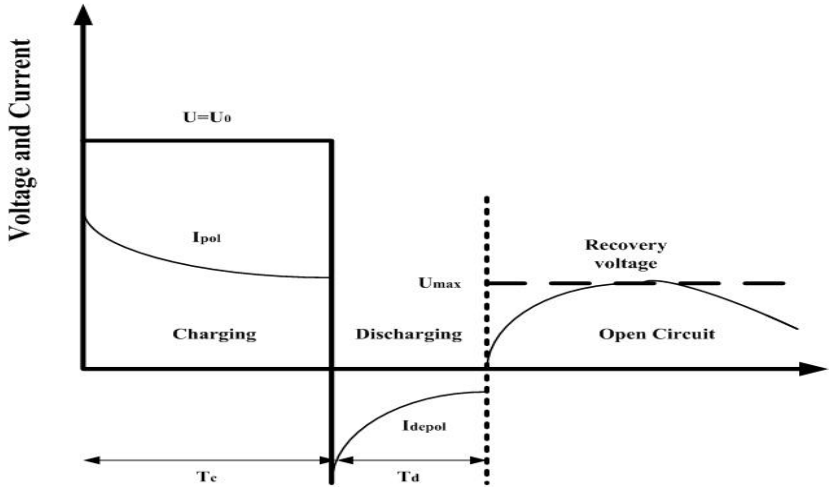


Fig. 1.8. Response for PDC and RVM of a dielectric.

### 1.6.3.6. Return Voltage Measurement

This approach involves applying a step voltage of $U_c$ across the totally discharged test object for a duration of $t_c$ seconds. Thereafter, the test object is short circuited for $t_d$ seconds, and step voltage is eliminated. After $t_d$ seconds, the discharging process is interrupted and a high impedance voltmeter is associated across the test object's terminals to perform Return

Voltage measurement. Activated polarization processes with varying time constants are relaxed to different degrees over the short-circuited time period ($t_d$). As a result, charge redistribution takes place in the system shortly after the voltmeter is attached, producing a voltage across the test object's terminals as shown in Fig. 1.8. The recovery voltage $U_r(t)$ that builds up across the test object's electrodes is presented in (1.18). If the insulation material's DC conductivity ($\sigma_0$), high frequency permittivity ($\varepsilon_\infty$), and dielectric response function $f(t)$ are known, Ur(t) can be analytically calculated using (1.18) [192].

$$\sigma U_r(t) + \varepsilon_0 \frac{dU_r(t)}{dx} + \varepsilon_0 U_0 \{f(t) - f(t - t_c)\} + \varepsilon_0 \frac{d}{dx} \int_{t_c+t_d}^{t} f(t-\tau) U_r(\tau) d\tau$$

$$= 0 \quad \in \text{for } t_c + t_d < t < \infty \qquad U_r(t = t_c + t_d) = 0 \tag{1.18}$$

### 1.6.3.7. Frequency Domain Spectroscopy Measurement

Dielectric response in the frequency domain is another alternative method to study the polarization phenomena. In this test, dielectric dissipation factor, power factor, complex permittivity, complex capacitance are measured as a function of frequency over a range of mHz to kHz. The dielectric is energized with sinusoidal voltages with variable frequencies and the response current is measured. The impedance is then calculated which helps in the evaluation of power factor, capacitance, dissipation factor, permittivity etc. The relationship between the applied voltage $V(\omega)$ and measured current $I(\omega)$ can be written as (1.19) [193].

$$I(\omega) = C_0 [\frac{\sigma_0}{\varepsilon_0} V(\omega) + j\omega\varepsilon_\infty V(\omega) + j\omega F(\omega) V(\omega)] \tag{1.19}$$

Here, $F(\omega)$ is the Fourier transform of the dielectric response function $f(t)$. $F(\omega)$ is actually related to the susceptibility of the dielectric media as represented in equation (1.20).

$$F(\omega) = \chi(\omega) = \chi'(\omega) - j\chi''(\omega) = \int_0^\infty f(t) \exp(-j\omega t) dt \tag{1.20}$$

Here, $\chi(\omega)$ represents the complex susceptibility of the dielectric sample. $\chi'(\omega)$ and $\chi''(\omega)$ is the real part and the imaginary part of the $\chi(\omega)$ respectively. Therefore, the resultant dielectric response current, $I(\omega)$ can be written as (1.21).

$$I(\omega) = j\omega[C'(\omega) - jC''(\omega)]V(\omega) \tag{1.21}$$

From the above equation, $C(\omega)$ is the frequency dependent complex capacitance of insulating medium. The frictional loss due to interactions among the dipoles under sinusoidal excitation, is represented by the imaginary part $C''(\omega)$. The energy storage in the dielectric medium during polarization is represented by the real part $C'(\omega)$.

The dielectric dissipation factor is defined as the ratio of energy loss to the energy storage in dielectric media, can be represented as (1.22).

$$\tan\delta(\omega) = \frac{\frac{\sigma_0}{\omega\varepsilon_0} + \chi''(\omega)}{\varepsilon_\infty + \chi'(\omega)} = \frac{C''(\omega)}{C'(\omega)} \tag{1.22}$$

Therefore, pure sinusoidal excitation over a wide frequency range (mHz – KHz) is applied to the insulation under test in order to investigate its dielectric behavior over the entire frequency range so that interactions among different dipolar groups can be estimated.

### 1.6.3.8. PDC and FDS Measurements as Transformers Condition Monitoring Method

The literature has extensively examined the usage of PDC response measurement for power transformer insulation condition monitoring [194–199]. PDC response in the initial time range (1000 s) polarization and depolarization currents are primarily influenced by the condition of paper insulation [198, 200, 201]. The solid and liquid insulation conditions uniquely define the overall form and size of a transformer's PDC response at various time ranges. The initial feature of the exponentially decreasing current between them is the interfacial polarization phenomena that forms at the contact between the oil and paper insulation. The insulation system's geometry has a significant impact on the interfacial polarization effect. Initially polarization and depolarization currents generally depend on the oil conductivity. Conversely, prolonged polarization and depolarization currents rise as a result of increased conductivity in the paper insulation. With age and moisture, the conductivity of both oil and paper insulation changes significantly. As a result, it offers details regarding the ageing and moisture content of oil and paper insulation. The conductivity of oil and paper insulation separately can be considered with the assumption of the proportion of paper insulation in a transformer's composite insulation system [202]. In order to explain the PDC response of linear dielectric materials, the well-known R-C equivalent circuit is used in the majority of PDC interpretation methodologies suggested for transformers [203, 204, 205, 206, 207]. In this instance, a sequence of Debye relaxation processes with various time

constants is used to characterize the dielectric polarization behavior of a transformer insulation system [205]. The PDC responses of paper and oil insulation with different R-C equivalent circuits were presented by T. Leibfried *et al*. [207]. After that, in order to represent the entire transformer insulation, an equivalent hierarchical circuit was created by taking into account the geometry of the insulation system as well as the R-C models of the oil and paper insulation. In this method, they suggest utilizing the R-C equivalent circuit characteristics of paper and oil insulation with known qualities to calculate the PDC response of a transformer. This can be compared to the observed response to determine the insulation system's state. According to Der Houhanessian *et al*. [204, 208], a transformer's insulation system is made up of multiple layers of paper and oil insulation. According to Saha *et al*. [205, 206], a transformer's insulation system is a "black box," and the PDC response of the entire system is represented by a single level R-C equivalent circuit. They interpret the physical behavior of the model parameters so that the paper insulation condition can be inferred from the magnitudes of R-C elements of the larger time constant branches, and the oil condition can be observed from the R-C values corresponding to the smaller time constant branches. Furthermore, lower initial polarization and depolarization currents result from the tendency of capacitance values to fall and R values of the smaller time constant branches to grow in high-quality insulating liquid. Conversely, the lower R values and higher C values of the smaller time constant branches indicate that the insulating oil is of poor quality. A comparable interpretation that makes use of the R-C characteristics of large time constant branches has been put forth to analyze the quality of paper insulation. This method's primary benefit over previous R-C equivalent circuit based PDC analysis techniques is its ability to clearly assess the state of both oil and paper insulation without requiring prior information of their respective arrangements.

According to a number of academic studies, ageing, moisture, and temperature all have a significant impact on the frequency domain dielectric response of oil-impregnated cellulose paper insulation by enhancing the polarization and conduction processes [209, 210]. As a result, a rise in both temperature and moisture leads the dielectric response to shift upward in frequency. Arrhenius equation can be used to characterize the frequency shift caused by a change in temperature. The dielectric response's degree of temperature dependence is indicated by the activation energy $E_a$ [211]. According to Chandima *et al*. [210], the activation energy of oil-impregnated paper insulation ranges from 0.8 to 1.1 eV and tends to rise with moisture. Koch *et al*. [209] propose an activation value of 0.9 eV to characterize the temperature dependency of cellulose material. The activation energy of

mineral oil is between 0.4 and 0.5 eV, and that of oil-impregnated paper is normally in the range of 0.9 to 1 eV, according to [212]. According to Saha *et al*. [213], real and imaginary permittivity increase with increasing moisture content, and this behavior is dependent on temperature and frequency measurements. The conductive action of oil is responsible for the dissipation factor's increase in the midfrequency range (10 -100 Hz. The peak caused by the interfacial polarization which is caused by the buildup of space charges at the oil-paper interface. The response of the composite system follows the dielectric characteristics of paper insulation at even lower frequencies. The moisture and ageing byproducts in the paper insulation have a noteworthy impact on the dielectric response in this frequency range [209, 186]. A method for determining moisture content has been presented in [209, 211]. It involves comparing the observed FDS of a transformer across a broad frequency range to a theoretically modeled dielectric response. The cylindrical insulation structure between a transformer's low and high voltage windings is represented mathematically by the X-Y model where X is the ratio calculated by adding together all of the barriers' thicknesses in the duct, dividing that total by the duct width [214]. Y is the ratio of the oil duct's perimeter length to the combined width of all spacers. X typically has a value between 20 and 50 percent, while Y typically has a value between 15 and 25 percent. This technique is used by the majority of commercially available FDS-based moisture diagnostic systems, such MDOS [214]. However, research on the FDS behavior for ester based insulating oil and the effects of temperature, moisture, and aging on this behavior is limited.

## 1.8.Scope of the Thesis

The primary objective of this thesis is to outline a comprehensive framework to reduce the research gap towards the applicability of the nanofluids based on mineral and biodegradable oil as a next generation liquid dielectric used for high voltage equipment. Moreover, the dielectric behavior of multi nanoparticles in a base oil or nanofluids based on mixed oil (mixing of two base oil) need more exploration. From the literature survey it can be inferred that, moisture is regarded as main culprit for the degradation of transformer insulation. Henceforth, the suitability of established electrical-based condition monitoring methods created for insulating systems of the future i.e. nanofluids based on mineral and biodegradable oil insulation is thoroughly studied. The framework of this thesis has been presented in Fig. (1.9).

**Chapter 2** provides the details of developed Experimental set-up for dielectric response measurement, DLS measurement, viscosity measurement of the prepared insulating samples.

**Chapter 3** presents the preparation of nanofluids considering two types of nanoparticles and two types of base oil. Thereafter, the physical & electrical based condition monitoring of the prepared nanofluids have been established. Interpretation of the corresponding results have also been analyzed duly.

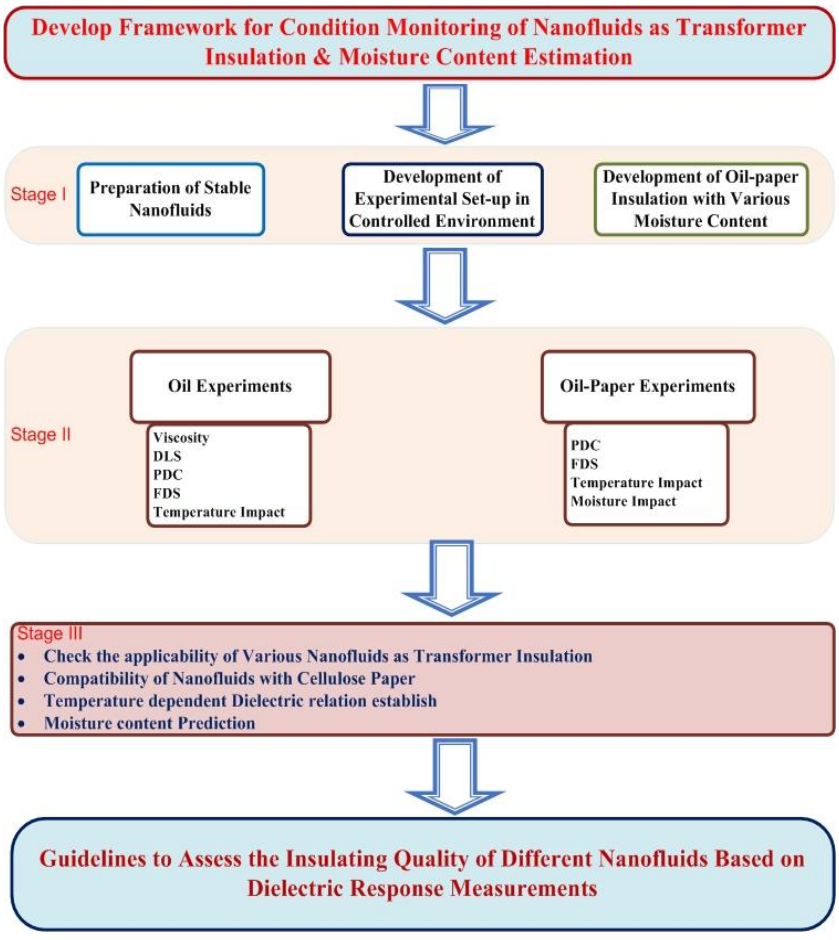


Fig. 1.9. Comprehensive framework of this thesis.

**Chapter 4** delivers the preparation of hybrid-nanofluids considering two types of nanoparticles in various ratios hence dispersed in either mineral or vegetable oil. Following that, the status of prepared hybrid nanofluids was monitored both physically and electrically. The associated results interpretation has also been thoroughly examined.

**Chapter 5** presents the overview of mixed oil. Mixed oils were prepared with mixing of two base oil i.e. mineral and vegetable oil in certain ratios. Moreover, nanofluids were prepared with those mixed oils After that, the prepared samples were subjected to electrical based measurement methods and analyses of the corresponding results have also been conducted.

**Chapter 6** delivers the comparative study of different prepared samples considering the breakdown voltage and ac conductivity which actually provides the information of the quality of those prepared insulating oils.

**Chapter 7** briefly discuss the compatibility of the prepared nanofluids with cellulose insulation. The impact of moisture has also been discussed based on dielectric relaxation current based approach.

**Chapter 8** enumerates the key conclusions and research findings from this thesis. In addition, recommendations for further research are provided.

## 1.9.Originality of the Thesis

*To the best of the author's knowledge, the current work has made the following original contributions:*

- Preparation of the stable nanofluids taking mineral oil or vegetable oil as base oil and compare their dielectric properties with mineral and vegetable oil.
- Development of an experimental set up to investigate dielectric parameters in Time and Frequency domain.
- Effect of the multi nano particles presence in base oil on the dielectric properties.
- Preparation of the stable mixed oil based nanofluids and check their applicability as transformer oil in terms of dielectric properties.
- Addressing the issue of temperature and moisture effect on nanofluids.

# Chapter 2

# Development of Experimental Setup for Investigation of Biodegradable Insulation

## 2.1 Introduction

This thesis primarily emphases on finding the next generation alternative liquid dielectric of mineral oil used as transformer insulation. For this purpose, the applicability of the prepared liquid insulation was ensured by conducting a series of experiments. Therefore, in this chapter, the experimental details have been presented which includes the selection of materials, various equipment like magnetic stirrer, ultrasonic sonicator, breakdown voltage measurement setup, dielectric response analyser (DIRANA), insulation diagnostic analyser (IDAX), heating oven, vacuum chamber etc. involved in the whole work. Besides, detailed discussion about experimental procedures like breakdown voltage measurement, viscosity measurement, polarization and depolarization current measurement, dynamic light scattering measurement have been presented in this chapter.

## 2.2 Equipment & Materials Used

### *2.2.1. Choice of Nanoparticles*

On the basis of electrical property i.e. conductivity, the nanoparticles are classified into conducting, semiconducting and insulating types. However, conducting nanoparticles have the tendency to agglomerate faster than other two types. Considering this fact, in this thesis, a semiconducting type nanomaterial and an insulating type nanomaterial were considered for the preparation of nanofluids by dispersing in mineral and vegetable oil. The two nanoparticles and two base oils used in the present work of this thesis have been presented in Fig. 2.1. The nanoparticles chosen for this work were as follows.

1. Semi-conducting nanoparticle: Titania- $TiO_2$ (Rutile) of diameter 20 nm.
2. Non-conducting nanoparticle: Alumina- $Al_2O_3$ (Alpha) of diameter (20-30) nm.

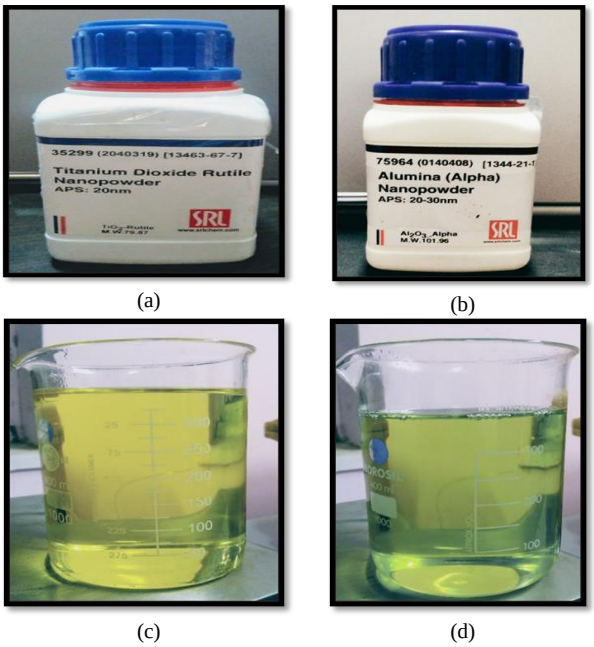


Fig. 2.1. materials user for preparing nanofluids: (a) $TiO_2$ (b) $Al_2O_3$ (c) mineral oil (MO) (d) vegetable oil (VO).

These two nanoparticles were chosen for preparing nanofluids for the reasons discussed in the following [215- 217].

i. **High thermal conductivity**: Both $TiO_2$ and $Al_2O_3$ nanoparticles have high thermal conductivity, which means they can efficiently transfer heat from the surrounding fluid to the nanoparticles, enhancing the overall thermal conductivity of the nanofluid. This is particularly important in transformer oil, as it helps to dissipate heat generated by the transformer's windings.

ii. **Stability and dispersion**: Titania and alumina nanoparticles are known for their excellent dispersion stability in transformer oil, which ensures that the nanoparticles do not settle or aggregate over time. This is crucial in transformer oil, as aggregation can lead to reduced thermal conductivity and even damage to the transformer.

iii. **Low viscosity**: The viscosity of the base oil does not increase to large extent with the addition of $TiO_2$ or $Al_2O_3$ nanoparticles comparing the other nanoparticles.

iv. **Corrosion inhibition**: Both $TiO_2$ and $Al_2O_3$ are known for their corrosion-inhibiting properties, which can help to protect the transformer's internal components (mainly metal conductor) from corrosion caused by moisture, salt, or other contaminants in the oil.

v. **Environmental benefits**: The use of nanofluids with $TiO_2$ or $Al_2O_3$ nanoparticles can also offer environmental benefits, such as reduced energy consumption, lower greenhouse gas emissions, and a longer lifespan for transformers.

vi. **Low cost**: Compared to other nanoparticle materials, $TiO_2$ and $Al_2O_3$ are relatively less expensive and widely available, making them a cost-effective choice for preparing nanofluids. The typical values of thermal and electrical characteristics of these nanoparticles have been presented in Table 2.1.

Table 2.1. Basic properties of nanoparticles [218]

| PARAMETERS | ALUMINA | TITANIA |
|---|---|---|
| **Density(g/cm$^3$)** | 3.96 | 4.2 |
| **Electrical Conductivity(S/m)** | $10^{-12}$ | $10^{-11}$ |
| **Relative Dielectric Constant** | 9.9 | 100 |
| **Relaxation Time Constant(s)** | 12.2 | 77 |
| **Thermal Conductivity(W/m.K)** | 30 | 7.6 |

Next aspect to be examined was the choice of carrier oils. The most obvious choice was the conventional petroleum based mineral oil used in the transformers owing to its excellent compatibility with the transformer and its electrical and dielectric properties. But in the recent times, the concern regarding environmental conservation has become a primary focus for utilities. The disposal of the oil is imminently challenging due to its non-biodegradable nature. As a result, several naturally obtained and synthetically procured oils are eventually desired by the power industry. These are expected to serve as potential alternatives to the conventional mineral oil primarily due to their biodegradable nature and several other enhanced attributes specific to the purpose of insulation in a transformer. One of such biodegradable alternatives is FR3 (a natural ester). Considering these facts, mineral oil and FR3 were considered for nanofluids preparation in this thesis.

### *2.2.2. Equipments Used*

Several equipment was employed in the preparation of the nanofluid samples as well as in the subsequent experimental procedures. The major equipments

have been, thereby, pictorially represented and their details have been elaborated in the following paragraph.

### 2.2.2.1. Magnetic Stirrer

A magnetic stirrer or magnetic mixer, as shown in Fig. 2.2, is a laboratory device that uses a spinning magnetic field to quickly spin a stir bar submerged in a liquid, churning it. Either a revolving magnet or a group of fixed electromagnets positioned underneath the liquid-filled vessel have produced the spinning field. In this application, the stir bar was rotated at 1200 rpm**.** It was employed for preliminary mixing the nanoparticles with the base liquid, prior to carrying out sonication. The magnetic stirrer just mechanically agitates the mixture for uniform mixing. Voltage rating of the stirrer is 220–240 volts at 50 Hz made by REMI.


Fig. 2.2. Magnetic Stirrer.

### 2.2.2.2 Ultrasonic Sonicator

The probe sonicator is a device used for generating waves of ultrasonic frequencies (20 kHz) through the probe as shown in Fig. 2.3. The mixture obtained from magnetic stirring, which when subjected to these ultrasonic waves result in generation of bonds between the nanoparticle and the base oil by means of dispersion. The stable and homogeneous suspensions which were prepared through probe sonication were used for further experimentation. The major functions of the probe sonicator were to provide uniform and stable dispersion in colloidal liquid, prevent the possibility of deagglomeration and reduction of particle size of the dispersing materials i.e. nanoparticles.


Fig. 2.3. Ultrasonic Probe Sonicator (Voltage rating 220V and Power rating 700 W).

### 2.2.2.3. Heating Oven

The heating oven, as shown in Fig. 2.4, maintains a controlled temperature in an isolated chamber by means of a thermostat. This oven not only used for conducting the experiments at various temperature but also prevent the stray capacitance during different measurement. The prepared samples were initially subjected to the heating oven for removal of moisture.

Fig. 2.4. Heating Oven (Voltage rating 220V, Temperature rise upto 100°C).

### 2.2.2.4. Vacuum Chamber

The vacuum chamber, shown in Fig. 2.5, ensured extremely low pressures close to that of vacuum. It is used for degasification process for the removal of dissolved gases from liquids, specifically the nanofluid in this work. This process was carried out in a specialised vacuum chamber. The principle being followed is *Henry's Law* which states that, the partial pressure of a liquid determines how much of a dissolved gas is present in it. Therefore, the dissolved gas becomes less soluble when a solution is put under lower pressure. The degasser, therefore, removes the dissolved gases from the nanofluid, which would otherwise form bubbles. Vacuum action is created with a help of a pump, which pulls out the air from the chamber, resulting in reduced pressure. In this work, degassing was performed at less than 1kPa pressure.

Fig. 2.5. Vacuum Chamber.

### 2.2.2.5. Particle Size Distribution Measurement

In order to study the uniformity of the nanoparticles throughout the base oil, the diameter distribution of the prepared samples was evaluated by Dynamic Light Scattering (Particle size analyser) instrument as shown in Fig. 2.6 whose particle size rating 0.2 to 1000 nm, having 785 nm laser light source. The typical variation of the nanoparticle's diameter should be within 100 nm in the base oil. This fact from the particle size distribution measurement

indicates that nano particles are uniformly dispersed within the base liquid dielectric.

Fig. 2.6. DLS instrument.

### 2.2.2.6. Oil Breakdown Test Kit

Breakdown voltage measurement setup (as shown in Fig. 2.7) was developed in the laboratory which consists of a test cell of 400 ml and spherical electrodes of 12.5 mm diameter moved apart by 2.5 mm [219]. AC breakdown voltages of oil were measured according to the IS 6792:2017 (similar to IEC 60156:2018) [219]. For this purpose, Next, the prepared sample was poured in the test cell and wait for 30 minutes to eliminate the possible air bubble during pouring. The voltage increment for the measurement was retained constant at 2kV/s. For each sample, 4 measurements were conducted and each measurement set was done on a new oil. The time gap between two consecutive measurement was kept at 5 minutes. The same measurement was repeated 4 times keeping a time gap of 30 minutes. This time delay was necessary for the self healing of the prepared samples. Total 16 measurements of each sample were performed and average value of those measurement was considered for analysis.

Fig. 2.7. Oil breakdown test kit.

### 2.2.2.7. Viscosity Measurement

For investigating the binding effect, the dynamic viscosity measurement of the prepared oil samples have been estimated through using Brookfield Viscometer (as shown by Fig. 2.8) Model DV2T (speed 0.1 - 200 rpm, ±1.0% of full scale range for viscosity accuracy, spindle LV01)

Fig. 2.8. Brookfield Viscometer for Viscosity measurement.

### 2.2.2.8. Dielectric Response Analyser

Dielectric Response Analyser (DIRANA), shown in Fig. 2.9. determine the state of dielectric response analysis-equipped high voltage insulation systems, such as those found in power transformers, cables, bushings, and generators. In the present work, it was used for polarization and depolarization Current (PDC) measurement in order to analyse the oil samples dielectric properties. Measurement voltage rating 200 Vpeak Maximum continuous output current rating 50 mApeak, measurement time within 1 hour 44 minutes.

Fig. 2.9. DIRANA model no. VEHP0072.

### 2.2.2.9. Insulation Diagnostic Analyzer

Insulation Diagnostic Analyzer, abbreviated as IDAX is a DFR (Dielectric Frequency Response) insulation diagnostic tool as shown in Fig. 2.10. DFR is the measurement of capacitance and losses (*tan* $\delta$ or PF) over a wide range of frequencies. The measured DFR curve is affected by the shape of the insulation, moisture, oil conductivity, and temperature. The model number of the one in the High-Tension Laboratory is IDAX-300 (manufactured by MEGGAR). It was employed to determine the prepared oil samples condition based on the frequency domain spectroscopy (FDS).


Fig. 2.10 IDAX 300.

### 2.2.2.10. Electrode Set-Up

A pair of Aluminum sheet of 16 cm × 4 cm separated by 1.79 mm is taken as an electrode as shown in the Fig. 2.11. For surface preparation of the electrode, Mechanical polishing has been adopted. For this purpose, Texmet pads have been used. After completing mechanical polishing, electrode has been rinsed with distilled water followed by few minutes of sonication in distilled water to remove unwanted particles. After sonication those electrodes were subjected to heat treatment for fully removal of moisture. Then those were dipped in the oil samples to conduct PDC and FDS measurement.

Fig. 2.11. Electrode set-up.

### 2.2.2.11. Transformer Insulation Prototype

Oil-paper samples emulating the transformer insulation (as presented in Fig. 2.12) were prepared in the laboratory for conducting the dielectric response measurement. For this purpose, kraft paper, pressboard and copper sheet were taken. The specifications of these samples have been provided in Table 2.2. Pressboard cylinders of 70 mm diameter were prepared on which a layer of unimpregnated kraft paper was wrapped. Over the unimpregnated kraft paper layer, a layer of copper foil was placed to form the low voltage winding of the traction transformer. Thereafter, two layers of unimpregnated kraft paper were wrapped over the copper foil. In between two layers of unimpregnated kraft paper, pressboard strips were placed which serve as oil ducts. Another layer of copper foil was wrapped to form the high voltage winding of the traction transformer. Lastly, a layer of unimpregnated kraft paper was placed to complete the test samples [27]. Then, the insulation prototypes were immersed in the base oils were kept at a constant pressure at 30°C for 72 hours to ensure proper impregnation process. Once the impregnation process was over, the impregnated samples were subjected to PDC and FDS measurement.

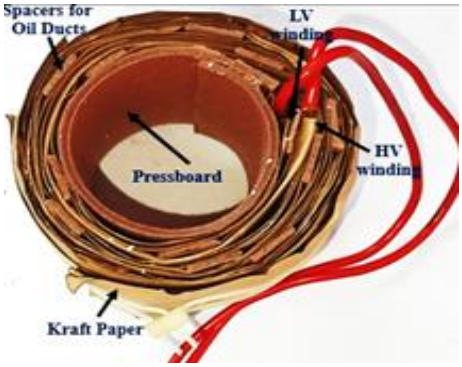


Fig. 2.12. Transformer insulation prototype.

Table 2.2. Basic properties of paper samples & Cu sheets

| | **Pressboard** | **Kraft-paper** | **Cu sheet** |
|---|---|---|---|
| **Length** | 55 cm | 55 cm | 55 cm |
| **Width** | 7 cm | 7 cm | 5 cm |
| **Thickness** | 2 mm | 0.12 mm (80 GSM) | 0.5 mm for low voltage<br>1 mm for high voltage |

## 2.2.3. Experimental Procedure

An experimental set-up was established in the laboratory to investigate the dielectric characteristics of the prepared nanofluids. The schematic diagram of the experimental set-up has been shown in Fig. 2.13. This experimental set-up mainly consists of AC voltage source, DIRANA™ (for PDC measurement) or IDAX 300 (for FDS measurement), Temperature control oven and data acquisition system. It should be mentioned here that, during the experiment, stray capacitance has been minimized by grounding the shielded oven where the prepared samples were placed.

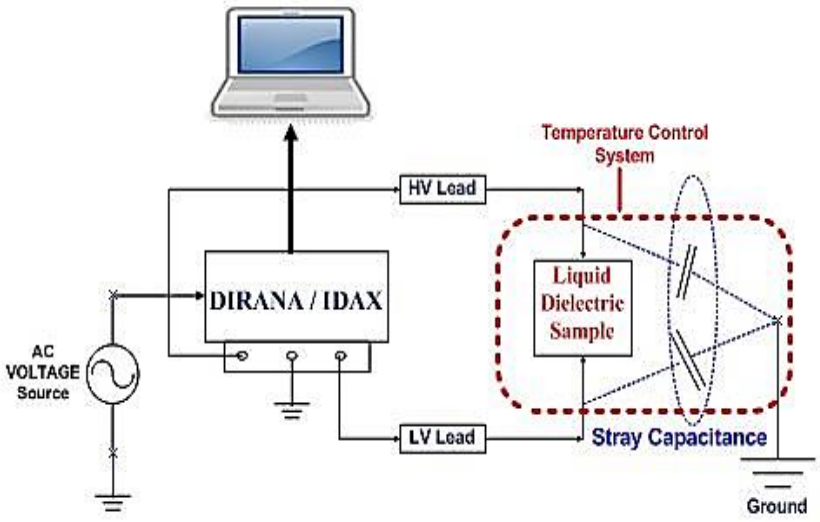


Fig. 2.13. Schematic of eexperimental set-up.

The PDC of the test samples were conducted under different voltage magnitude (50V, 100V, 150V, 180V and 200V) for nonlinearity study in conduction current whereas for FDS measurement, the voltage level was fixed at $140V_{rms}$. Both the measurements were conducted at different temperatures (25˚C, 40˚C, 50˚C, 60˚C, 70˚C and 80˚C) to have a clear idea about the temperature effect on their dielectric properties. Dielectric characteristics of the prepared samples were investigated through conducting PDC and FDS measurements employing DIRANA™ and IDAX 300, respectively. The developed experimental setup for PDC and FDS measurement have been presented in Fig. 2.14 and Fig. 2.15, respectively.


Fig. 2.14. PDC measurement of samples.


Fig. 2.15. Samples under FDS measurement.

## 2.3 Conclusions

This chapter has covered in brief the equipment and materials used in the search for a new type of insulation to replace mineral oil. These experimental procedures were followed by the electrical and chemical based methodologies for that insulation's quality assessment. Chapters 3 to 7 in this thesis have adhered to the scheme described in this chapter.

# Chapter 3

# $TiO_2$ and $Al_2O_3$ Nanofluids: Insulation Properties Investigation by Dielectric Spectroscopy

## 3.1. Introduction

From the detailed discussion about the oil insulation used over years for the transformer, it is essential for searching next generation enhanced dielectric liquid than mineral oil with the following properties like better dielectric strength, efficient cooling, lower dielectric losses, lower electrical conductivity, high fire resistance, biodegradability, high thermal conductivity etc. [220]. Therefore, there are extensive research works going on all over the globe regarding the usage of nanoparticles-based oil in power transformer. Though usage of nanofluids improves the electrical as well thermal properties [221], however, it has to withstand various stresses (like thermal, chemical, electrical etc.), which results in its degradation. The degradation of insulating material in transformer reduces its operating life span, which in turn results in its premature failure [1]. In order to prevent premature failure of transformer, the condition of transformer insulation should be monitored at regular intervals. The dielectric response analysis has become an important basis for assessing the insulation condition of transformer. This analysis is mainly categorized into ttime domain and frequency domain. polarization and depolarization ccurrent (PDC) and return voltage measurement (RVM) are two methods in time domain spectroscopy [222]. On the other hand, the condition assessment in frequency domain is known as frequency domain spectroscopy (FDS) or *tanδ* measurement [223, 224].

In this chapter, $TiO_2$ (titania) and $Al_2O_3$ (alumina) have been chosen for dispersing in mineral or vegetable oils to prepare nanofluids in the laboratory. Next, the prepared samples were subjected to viscosity, PDC and FDS measurements. In order to investigate the dielectric properties due to the presence of above-mentioned nanoparticles, a comparative study on the

experimentally obtained parameters has been done. Besides, the variation of parameters at various temperatures has been studied to investigate the effect of temperature on the nanoparticle based mineral and vegetable oils. Brief theory on the parameters obtained from PDC and FDS has been discussed in the next section.

## 3.2. Brief Theory on Activation Energy obtained from PDC

For investigation of the prepared dielectric samples, PDC measurement is conducted. From the measured polarization and depolarization current, an important parameter i.e. dc conductivity of different samples has been calculated using (3.1). Again, as discussed in Section 1.4, temperature is a dominating factor for the degradation of insulation. It is to be stated here that, polarization process in dielectric medium depends on the mobility of charge which further highly affected in different temperatures [225]. Moreover, it is revealed in [226] that, the time constant of the dipole changes with temperature which leads to the variation of the conductivity. The change in conductivity with the change in temperature is associated with the activation energy (*Eg*) and it is represented by (3.1). An estimation of activation energy of a dielectric specimen signifies the barrier potential that the trapped charges would need to possess in order to carry conduction in the dielectric material.

$$\sigma = Ae^{[-\frac{E_g}{KT}]} \tag{3.1}$$

Where, $E_g$ stands for the Activation Energy, *A*is a constant. *K* stands for the Boltzmann constant i.e. 1.38064852 × $10^{-23}$ $m^2$ kg $s^{-2}$ $K^{-1}$. The activation energy has been graphically figured out using the Arrhenius equation. Therefore, by taking log both side (3.1) can be written as (3.2).

$$\ln(\sigma) = \ln(A) - \frac{E_g}{KT} \tag{3.2}$$

It is quite clear that this equation resembles the equation of a straight line as in (3.3).

$$y = mx + c \tag{3.3}$$

Therefore, the graph for logarithm of conductivity versus the inverse of absolute temperature has been plotted to get the slope i.e. $E_g/K$. The regression technique was applied on the obtained curve. The value of activation energy was obtained by the product of the slope of the linear equation and the negative of the value of Boltzmann constant as presented in (3.4).

$$E_g = -K \times slope \tag{3.4}$$

From (3.4),the values of activation energy has been calculated in J. Then $E_g$ in eV can be obtained from $1eV = 1.6 \times 10^{-19}J$.

## 3.3. Brief Theory on Low Frequency Dispersion (LFD) obtained from FDS

For the evaluation of the dielectric properties of different prepared samples, FDS measurement is conducted. From the FDS measurement of oil, dielectric parameres like complex capacitance, *tanδ* can be evaluated as presented in (Chapter 1, Equation 1.21) and (Chapter 1, Equation 1.22), repectively. Therefore, it can be observed that the peak in the dielectric parameres like complex capacitance, *tanδ* etc. is occurred at low frequency [227]. Again, maximum dispersion of those parameters are observed to be within 100 Hz. Therefore, Low Frequency Dispersion (LFD) i.e. change in real capacitance (ΔC) at low frequency can be favorable parameter to indicate the condition of the liquid dielectrics and has been presented in (3.5).

$$\Delta C = C'_{1mHz} - C'_{100Hz} \tag{3.5}$$

At low frequency dielectric behaviour of oils depends on space charge polarisation. Ion conduction and peak of *tanδ* profile at low frequency indicate the space charge polarisation [227]. In that frequency range, due to space charge polarisation charge carriers near the electrode suface reduces which results in rise in capacitance but ac conductivity reduces [228]. Another fact can be noticed that with the increment in temperature in some cases *tanδ* profile reduces also at low frequency region. For this case change of real capacitance (ΔC) can be favorable parameter to indicate the condition of the liquid dielectrics. Akmal *et al* [227] have studied a correltaion between the increment of capacitance at low frequency and ageing condition of

insulating liquid. Then from the study in [229], ac conductivity(σ) can correlate with the low frequency dispersion (change of real capacitance (ΔC)) with the following expression (3.6).

$$\Delta C = A(T) \times \exp^{\frac{-b(T)}{\sigma}} \tag{3.6}$$

Where A, b are constant and depends on the temparature and electrode material. Therefore an investigation has been done for correlating the Low frequency dispersion characteristics and dielectric dissipation factor for different samples in section 3.4.5.

## 3.4. Preparation of Nanofluids & Experimental Procedures

In this work, nanofluids have been prepared by mixing up the nanoparticles with the base oil using the steps as depicted in Fig. 3.1. A beaker filled with 400ml of base fluid (mineral Oil/FR3) with 80 mg of surface modified using (5 ml of ethanol as dispersant and 2ml of oleic acid as surfactant) nanoparticles ($TiO_2$/$Al_2O_3$) was subjected to prepare a nanofluid concentration of 0.2g/l. Using a magnetic stirrer, mechanical agitation of nanoparticles was continued upto 45 minutes @ 1200 rpm. Next, the mixture was placed within an ultrasonic probe sonicator for sonication process and kept for 6 hours. During the sonication process, the sample was allowed to relax for 30 minutes after every 2 hours. After sonication process, it was observed that, few microbubbles were formed within the mixture. In order to remove these microbubbles, the mixture was heated at 50°C for 30 minutes in a controlled oven followed by vacuum in a chamber at less than 1kPa for about 2 hours. After that, the mixture was allowed to settle down for a period of 2 hours to reduce the thermal agitation of the nanofluids which is introduced during the ultrasonic sonication process. The nanofluids thus prepared were then used for experimental purpose. In the present work, FDS has been conducted within 24 hours after preparation of nanofluids to avoid significant agglomeration. According to variation of base oil and mixing particles, the nanofluids are categorized, although the preparation techniques remained the same. It should be mentioned here that, the diameter distribution of both types of nanofluids has been estimated through using DLS instrument [230]. The typical diameter size of both types of nanoparticles in the prepared nanofluid has been shown in the Fig. 3.2. It may

be observed from Fig. 3.2 that, the typical variation of nanoparticle diameter is from 40 nm to 80 nm.

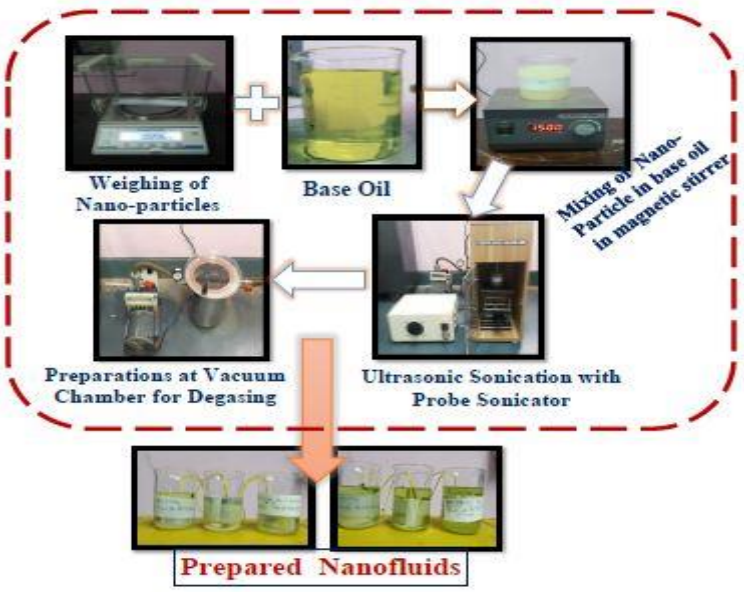


Fig. 3.1. Preparation of nanofluids.

Nonseparation of the constituent parts like nanoparticles of the composite liquid matrix may be ensured by reducing the possibility of the agglomeration of the nanoparticle in the liquid. This can be achieved by preparing the nanofluid in the presence of surfactant like oleic acid but using oleic acid the preparation may face difficulties in the sonication process. This difficulty can be overcome with the use of ethanol which performs as dispersant. So, uniform and stable nanofluid can be prepared with proper sonication and stirring time in addition of surfactant and dispersant [231]. After the preparation of stable hybrid nanofluids, the electrode setup was dipped into the samples for the dielectric experiments and viscosity measurement. Then, dielectric properties of the hybrid nanofluids were investigated through conducting PDC and FDS measurements employing DIRANA$^{TM}$ and IDAX 300, respectively (as shown in Fig. 2.14 and Fig. 2.15, respectively).

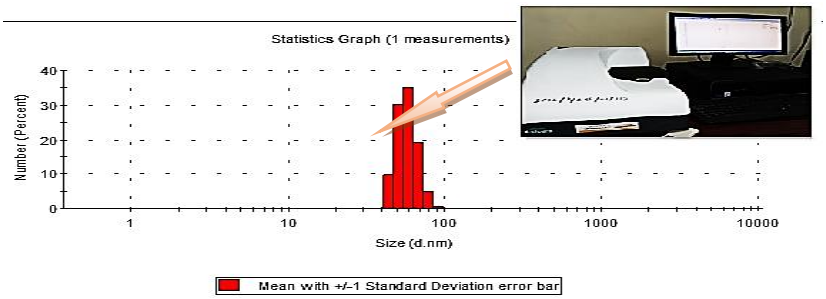


Fig. 3.2. Estimation of diameter distribution of nanoparticles in nanofluid through DLS instrument.

The PDC measurement was conducted on various voltage stages (50V, 100V, 150V, 180V and 200V) whereas the voltage magnitude for FDS measurement was fixed at $140V_{rms}$. Both the measurements were conducted at 25˚C, 50˚C, 60˚C, 70˚C and 80˚C to have a clear idea about the temperature effect on their dielectric properties.

## 3.5. Results & Discussion

### *3.5.1. Estimation of Viscosity*

Viscosity measurement can help to investigate the binding effect of the nanoparticles with the base oil. Table 3.1 shows the corresponding values of viscosity of the prepared samples.

Table 3.1. Results from Viscosity measurement of prepared dielectric samples at 25°C.

| Samples | Viscosity (cP) | Samples | Viscosity (cP) |
|---|---|---|---|
| MO | 13 | VO | 50 |
| MO+$TiO_2$ | 14.58 | VO+$TiO_2$ | 51.42 |
| MO+$Al_2O_3$ | 15.06 | VO+$Al_2O_3$ | 53.58 |

It may be observed from Table 3.1 that, viscosity has been increased by dispersing nanoparticles in the base liquid dielectric. The nanoparticles increase the surface area of interaction between the solid particles and base oil [232]. Another important observation i.e. hydrophilic nanoparticles form a thicker water-absorbing layer has been occurred in the nanofluids which further increase the viscosity of base oil. Although $TiO_2$ is more hydrophilic, its poor compatibility and higher aggregation tendency in non-polar oils may

lead to lower viscosity enhancement than $Al_2O_3$, which disperses better and interacts more uniformly with the oil medium [232].

### *3.5.2. DC Conductivity for different samples with varying temperature*

From the PDC measurement, polarization and depolariztion current for MO is shown in Fig. 3.3. Hence, the dc conductivity of each sample can be calculated by (Chapter 1, Equation 1.17). Calculated conductivity for different nanofluids (for mineral oil and vegetable oil base) at 25°C, 50°C, 60°C, 70°C and 80°C have been shown in Fig. 3.4a and 3.4b, respectively. From the Fig. 3.4a and 3.4b, it can be observed that, conductivity increases with temperature.

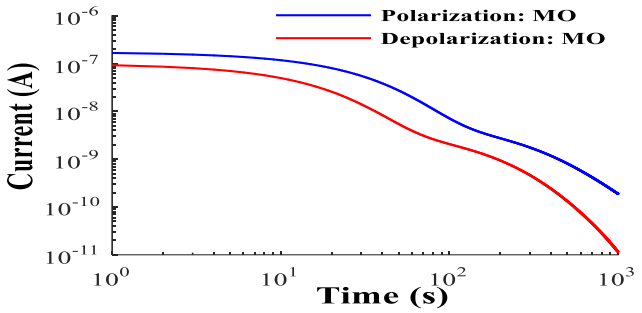


Fig. 3.3. Polarization and depolariztion current of mineral oil.

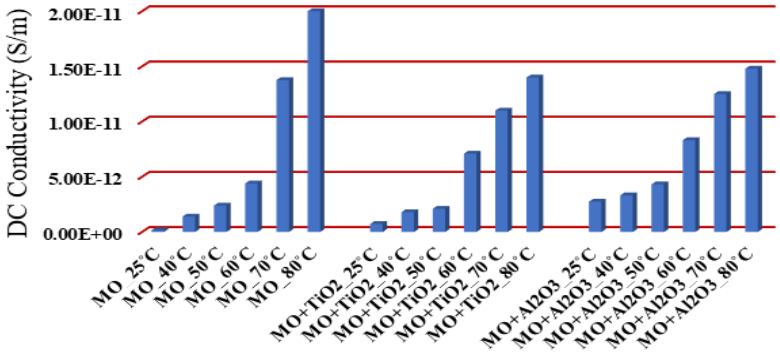


(a)

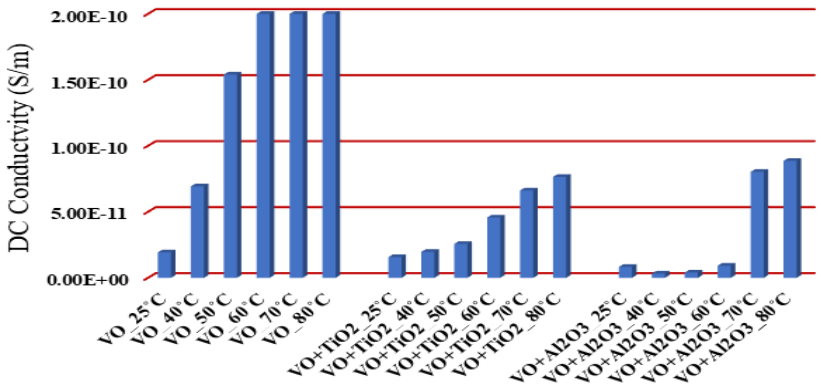


(b)

Fig. 3.4. Conductivity at different temperatures of (a) MO and its nanofluids and (b) VO and its nanofluids.

It is due to the fact that conduction current mainly is caused due to free charge present in the dielectric. Further, with increasing temperature, more number of free charge gain high thermal energy to enter into the conduction band which in turn increases the conductivity. Further, it has been observed that, at higher temperature, by dispersing nanoparticles, dc conductivity has been reduced for mineral as well as vegetable oil. Alumina based nanofluids exhibit enhanced dc conductivity among all prepared samples. This observation is due to the fact that, nanoparticles have the tendency to trap the electrons on the surface on it. This reduces the number of particles taking participate in the conduction i.e. conductivity reduces.

### *3.5.3. Estimation of Activation Energy*

Thereafter, to estimate activation energy, $ln(\sigma)$ has been plotted against inverse of temperature in Kelvin for different prepared samples as shown in Fig. 3.5. From the slope of the curve, activation energy has been estimated employing (3.4) and measured values have been shown in Table 3.2.

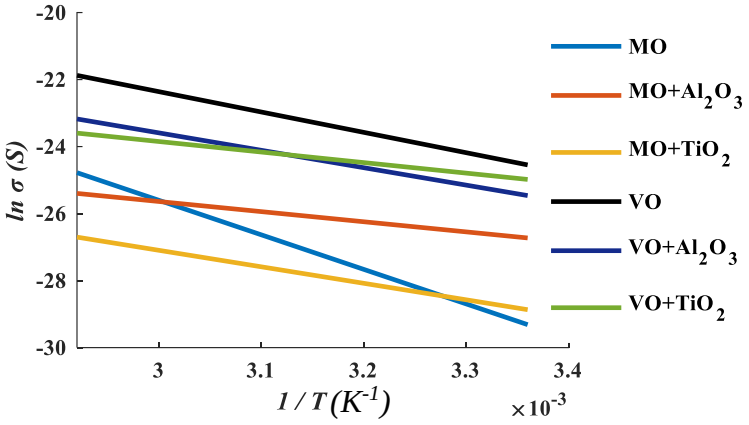


**Fig. 3.5.** Graph for calculating the activation energy for different samples.

Table 3.2. Activation energy of nanofluids based on Mineral oil and Vegetable oil

| Samples | Activation Energy in eV | Samples | Activation Energy in eV |
|---|---|---|---|
| MO | 0.36 | VO | 0.39 |
| MO+$TiO_2$ | 0.22 | VO+$TiO_2$ | 0.26 |
| MO+$Al_2O_3$ | 0.28 | VO+$Al_2O_3$ | 0.25 |

It can be observed from Table 3.2 that, vegetable oil has highest activation energy among all prepared samples. However, presence of nanoparticles in the base oil degrades the activation energy. This may be due to the fact that, bond between nanoparticles with the base molecule increase the rate of molecular interaction [232]. The nanoparticles become negatively charged when it traps the electrons from base oil and have electrical double layer repulsion force. This repulsion forces are responsible for the increment in reaction rate further reduce the activation energy. It should be mentioned here that, by evaluating the activation energy of the insulating samples, the remaining life of the insulation can be predicted.

### *3.5.4. Nonlinearity Study in Dielectric Response Current*

From the PDC experiment, the conduction current is calculated by the difference between polarization and depolarization current. However, it should be stated here that, the effect of conduction current is negligible during polarization when the magnitude of applied voltage is less than 100V, since the charge inoculation from the HV electrode is insignificant at a stress less than 1 kV and insulation considered as linear system. When the voltage applied crosses 100V, significant deviancy between polarization current and depolarization current can be noticed, which is due to the presence of non-linearity inside the dielectric. The main reason for this non-linearity of the insulating medium is the injection of the space charge close to the electrodes at the time of polarization [105]. The amassing of space charges near the electrodes leads to the space charge polarization and moves through the bulk of insulating material. This phenomenon of charge amassing and amputation of space charges (through holes and electrons) are considered as non-linear matter which is related to the change in voltage magnitude [105]. Since the amassing and exclusion of space charges are mainly influenced by the condition of dielectric, these non-linear phenomena can be utilized as decisive factors for the assessment of insulation condition. Therefore, the non-linearity of the dielectric medium can be studied with the expression presented in (3.7).

$$I_{cond} = aV^{b} \tag{3.7}$$

Here, $I_{cond}$ and $V$ indicate the conduction current and the applied voltage, respectively. Further, it can also be stated that (3.7) behaves like a linear equation for b is equal to 1, which dictates that the insulation can be stipulated as a linear system for the unity value of b.

A major issue in the transformer insulation is that, in their composite insulation, both hydrophobic (oil) and hydrophilic (paper) materials are presents. When the temperature elevation is higher, the moisture migration in between those two materials will occurs which further hamper the moisture equilibrium state of transformer. Moreover, there are many studies [82] which states that relaxation current is very sensitive to the temperature elevation. This is due to the fact that with temperature elevation charge

mobility is increased which in turn leads to impose the non-linearity on PDC measurement.

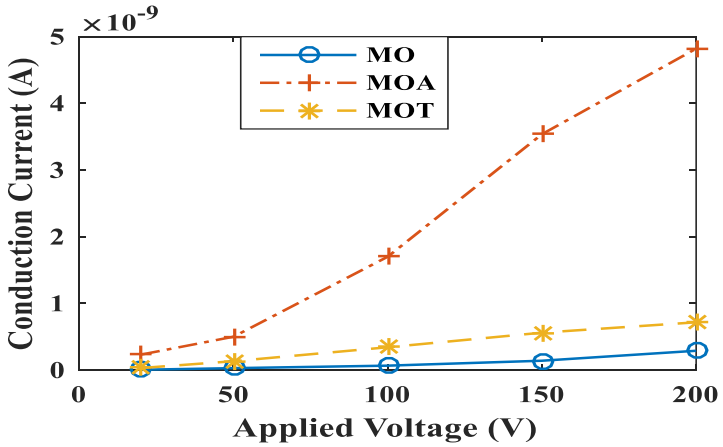


Fig. 3.6. Variation of conduction current with applied voltage of MO its nanofluids.

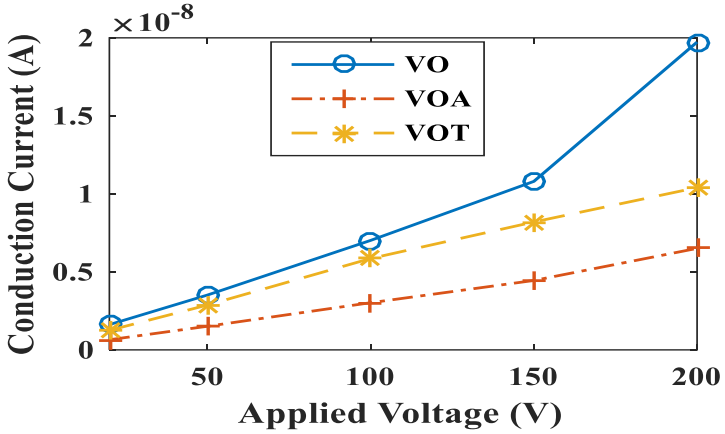


Fig. 3.7. Variation of conduction current with applied voltage of VO and its nanofluids.

The conduction current at 25°C for all the nanofluid samples along with their base oils were recorded at five different voltage levels i.e. 20V, 50V, 100V, 150V and 200V, from the polarisation and depolarisation current measurements. Fig. 3.6 shows the conduction current for for mineral oil and

its nanofluids with the aforemention voltage levels and Fig. 3.7 is same for natural ester based oil and its nanofluids respectively. From Table 3.3, it can be observed that, nonlinearity in conduction current is maximum for mineral oil. However, by dispersing nanoparticles nonlinearity in conduction current can be reduced. Alumina nanofluid for both oil has shown more linear behaviour.

Table 3.3. Non-linearity parameters for different samples.

| | **MO** | **MO+ $TiO_2$** | **MO+ $Al_2O_3$** | **VO** | **VO+ $TiO_2$** | **VO+ $Al_2O_3$** |
|---|---|---|---|---|---|---|
| **a** | 2.63E-14 | 3.21E-13 | 8.76E-12 | 1.12E-10 | 7.69E-11 | 3.87E-11 |
| **b** | **1.744** | **1.471** | **1.186** | **0.9462** | **0.9298** | **0.9577** |

## *3.5.5. Dielectric Dissipation Factor*

Using IDAX 300 , dielectric dissipation factor (*tanδ*) were obtained through FDS measurement for both the pure oil as well as the nanofluids. The variations of *tanδ* of mineral oil along with the mineral oil based nanofluids (MO+$Al_2O_3$ and MO+$TiO_2$) at 25˚C, have been shown in Fig. 3.8. In the case of vegetable oil (VO), the *tanδ* profiles of VO and both the nanofluids (VO+$Al_2O_3$ and VO+$TiO_2$) at 25˚C have been shown in Fig. 3.9.

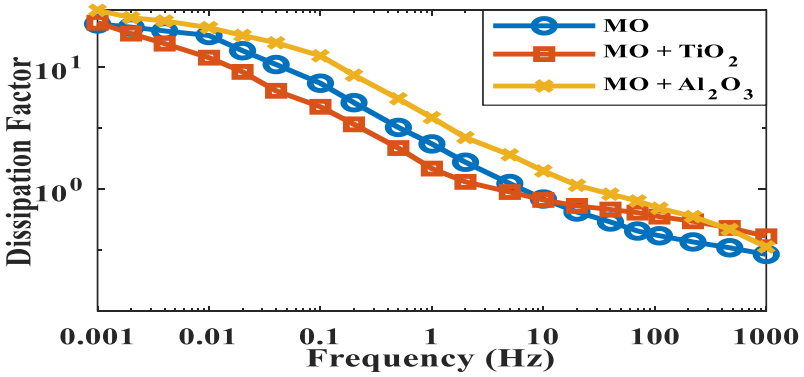


**Fig. 3.8.** Variation of *tanδ* for pure MO and nanoparticle-based MO at 25˚C.

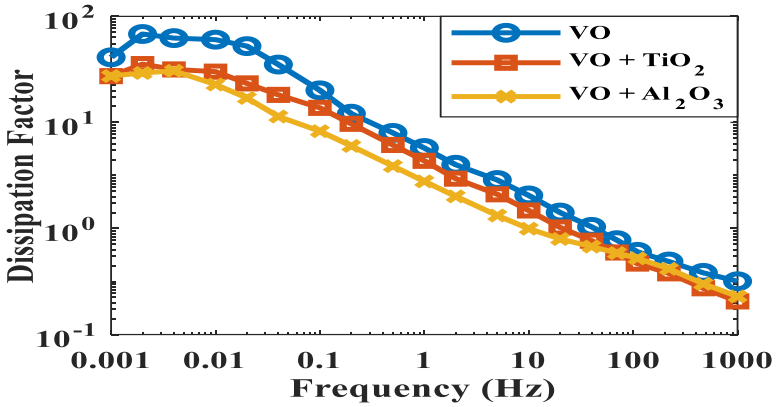


**Fig. 3.9**. Variation of *tanδ* for pure VO and nanoparticle-based VO at 25°C.

### 3.5.5.1. Effect of Nanoparticles on *tanδ*

It may be observed from Fig. 3.8 that the *tanδ* profile of both pure mineral oil as well as nanofluids (MO+$Al_2O_3$ and MO+$TiO_2$) decreases as the frequency increases. The decrement of *tanδ* value with increasing frequency may be due to the fact that as the frequency of the excitation voltage decreases, the time period increses. Therefore, the dipoles as well as the free electrons in the dielectric are under the influence of a particular polarity in the applied field for a longer time. This fact drives the dipoles to align more toward the applied field. Like the dipoles, electrons also get sufficient time to move towards the anode. The above two processes enhance the interactions due to the alignment of dipoles and the movement of the electrons towards anode. The interactions result in increment of frictional loss and hence dielectric dissipation factor (*tanδ*) [224]. It may also be observed that the *tanδ* value of nanofluid (MO+$TiO_2$) is higher than the corresponding value of pure MO at higher frequency range. This may be due to the unbalaced crystal structure of $TiO_2$ nanoparticles. The molecular structure of $TiO_2$ nanoparticles has been shown by Fig.3.10. It may be observed from Fig.3.10 that the interactomic distance between one Ti-O atom is nearly 1.988Å, whereas the distance between another Ti-O bond is around 1.944Å [26]. This unbalance structure of the $TiO_2$ nanoparticles develop the strong polarization

characteristics in the crystal [233]. It is reported in [233] that the relaxation times of polar crystal, $TiO_2$ typically ranges from $10^{-13}$ to $10^{-3}$ s. Therefore, the unbalanced structure of $TiO_2$ molecules in crystal takes part in dipolar/ionic polarization during FDS near to kHz range. This explain the polarization process at higher frequency range, which causes large intractions due to the polar crystal $TiO_2$ in nanofluids that results in higher value of *tanδ* at higher frequency range.

On the other hand, It may be observed from Fig. 3.8 that the *tanδ* value of nanofluid ($MO+TiO_2$) at lower frequency range is lower than the corresponding value of pure MO. Sun *et al* reported that the relative permittivity of nanofluid decreases if the nanoparticle concentration ($TiO_2$) in mineral oil is higher than 0.06g/l [233]. This may be due to the presence of hydroxyl group at the surface of the nanoparticles. It is to be mentioned that Ti atom has affinity to the hydroxyl ($OH^-$) group (present within the water molecules in nanofluids) [234]. Therefore, application of strong electric field, which persists for longer time (i.e at lower frequency) causes development of a bond with the hydroxyl ($OH^-$) group (as shown in Fig.3.11). Sun *et al* reported that the hydroxyl group (on $TiO_2$ crystal) makes loose bonding with the cellulosic chains (in mineral oil) which weakens the polarization capability of the nanoparticles at lower frequency range [233]. Another theory (the three core model) proposed by Tanaka [235] says that the third core may slowly develop bindings with the existing oil molecules, which in turn reduces the polarization capability of the nanofluid. This in turn reduces the corresponding *tanδ* value as the reduction of polarization process decreases the interactions among the dipoles during FDS measurement.

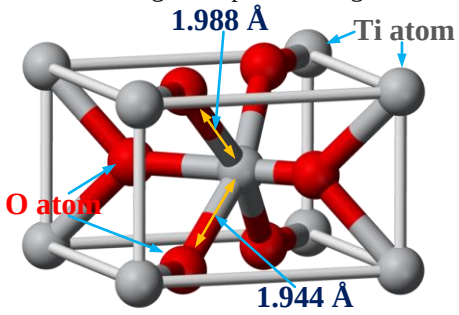


**Fig. 3.10.** Typical crystal structure of $TiO_2$ nanoparticles [236].

It may also be observed from Fig. 3.8 that the *tanδ* value of nanofluid MO+$Al_2O_3$ is higher than the correponding value of pure mineral oil throughout the entire frequency range of 1 mHz to 1 kHz. Mansour *et al* reported that unlike $TiO_2$, $Al_2O_3$ absorbs $H^+$ ions from the water molecules, which creates a bond with its O atom [234] (as shown in Fig. 3.11). This phenomenon results in development of dipoles through the bonding created by O-H. The development of the dipole at the surface of $Al_2O_3$ results in strong polarization characteristics, which is active during FDS measurement. The development of strong polarization chracteristics of nanofluid (MO+$Al_2O_3$) results in higher frictional loss during FDS measurement, which in turn enhances value of *tanδ.*

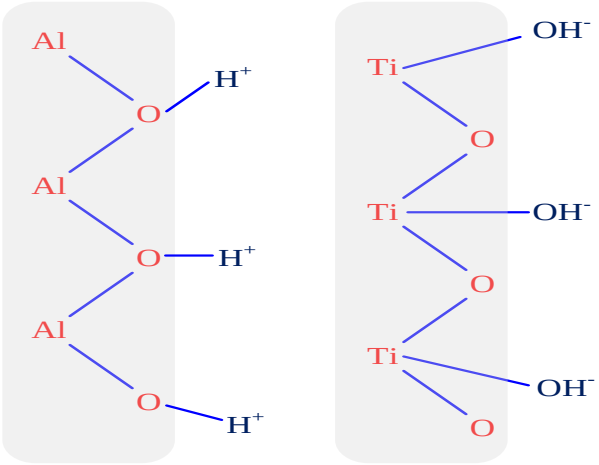


**Fig. 3.11**. Formation of bonding with water molecules in nanofluids [224].

It may be observed from Fig. 3.9 that unlike MO, the *tanδ* values of both the nanofluids are lower than the corresponding value of vegetable oil throughout the entire frequency range from 1 mHz to 1 kHz. Li *et al* reported that VO is a weak dielectric material [237]. Therefore, under applied electric field, the polarization current becomes lower than the corresponding value of conduction current. It is well known fact that the free electron in the dielectric material is responsible for the conduction current. This conduction current generally determines the *tanδ* value in the biodegradable vegetable

oil. However, for nanofluids, the nanoparticles ($Al_2O_3$ and $TiO_2$) dispersed within VO gets polarized under the applied field [237]. This polarized nanoparticles trap the free electron under applied field during FDS measurement [237]. This trapping of highly mobile free electrons results in reduction of free electron cocentration within the vegetable oil and develops negetively charged nanoparticles. The mobility of these negetively charged nanoparticles are lower in comparison with the free electrons. This in turn reduces the magnitude of the conduction current through the nanofluids during FDS measurement. The reduction of the conduction current decreases the corresponding *tanδ* value of the nanofluids in comparison with the pure VO as observed from Fig. 3.9.

3.5.5.2. Effect of temperature on dielectric parameter

In order to investigate the effect of temperature on the dielectric properties of VO, MO and the nanofluids, corresponding *tanδ* profiles have been evaluated from FDS measurement performed at 25˚C, 50˚C, 60˚C, 70˚C and 80˚C respectively.

*3.5.5.2.1. Effect of Temperature on tanδ for Pure Oil*

The variation of *tanδ* profiles of pure mineral and vegetable oil at 25˚C, 50˚C, 60˚C, 70˚C and 80˚C have been shown in Fig. 3.12 and 3.13, respectively. It may be observed from Fig. 3.12 and 3.13 that the *tanδ* values (for entire frequency range of 1 mHz to 1 kHz) for both the pure mineral and vegetable oil increase with temperature. Setayeshmehr *et al.* reported that increment of temperature enhances the activation energy within the oil molecules [238]. Therefore, the conduction current of the dielectric material increases with temperature. This leads to increment of the conduction loss which in turn results in subsequent increment of *tanδ* value.

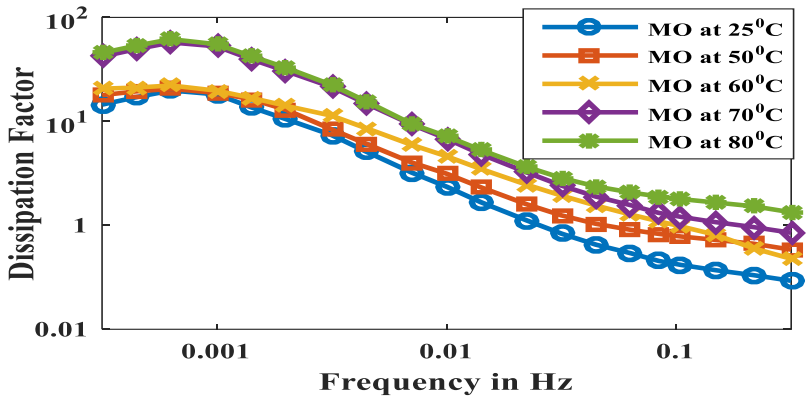


**Fig. 3.12.** Variation of *tanδ* for pure MO at different temperatures.

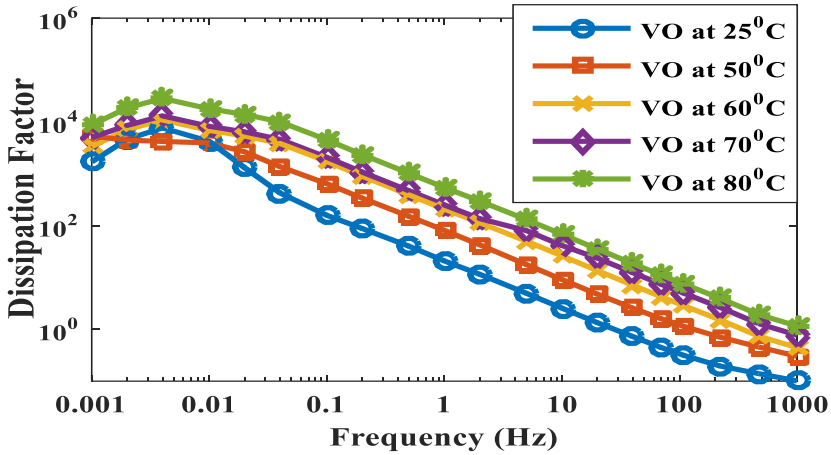


**Fig. 3.13.** Variation of *tanδ* for pure VO at different temperatures.

### *3.5.5.2.2. Temperature Effect on tanδ for Nano Particles Based Mineral Oil*

The variation of *tanδ* profiles of both the mineral oil based nanofluids (MO+$TiO_2$ and MO+$Al_2O_3$) at 25˚C, 50˚C, 60˚C, 70˚C and 80˚C have been shown in Fig. 3.14 and 3.15, respectively. An interesting fact can be observed

from Fig. 3.14 the variation of *tanδ* profiles at the above-mentioned temperatures. The *tanδ* values at 50˚C for MO+$TiO_2$ are closer to the corresponding values at 25˚C at higher frequency range, whereas the *tanδ* values at 50˚C are lower than the corresponding values at 25˚C at lower frequency ranges. On the other hand, reverse pattern can be observed at 70˚C. The *tanδ* values at 70˚C are higher than the corresponding values at 25˚C throughout the entire frequency range. The same pattern is followed for the *tanδ* values at 80˚C, since with temperature increment activation energy has been increased which leads to the increment of dielectric loss.

In the case of MO+$Al_2O_3$, same pattern of *tanδ* profiles at 25˚C, 50˚C and 70˚C is followed like MO+$TiO_2$. The *tanδ* values at 50˚C are lower than the corresponding values at 25˚C throughout the entire frequency range. On the other hand, the *tanδ* values at 70˚C are higher than the corresponding values at 25˚C though the differences are relatively lower unlike MO+$TiO_2$.This may occur due to de-trapping and bonding phenomena of charges in nanofluids. It is reported in [239] that, the magnitude of detrapped charge in the case of the nanofluids become maximum if the temperature is nearly 25˚C. On the other hand, the rate of change of detrapped charge decreases as the temperatures increases further [239]. Therefore, the number of detrapped charges does not change significantly as the temperature increases beyond 25˚C. These detrapped charges make bonds with nanoparticles as reported in [239]. As the temperature increases beyond 25˚C, the number of free charges within nanofluids decreases due to the higher rate of bonding with nanoparticles than the rate of generated detrapped charges. This phenomena result in reduction of interactions during FDS. This reduction of interaction leads to decrease in overall dielectric loss and consequently, the *tanδ* value when temperature rises from 25˚C to 50˚C. As temperature increases further, the thermal conductivity of the charges become significant which then plays the major role to determine the values of *tanδ*. As reported in [240], the enhancement of thermal conductivity of nanoparticles may be due to primarily four reasons (Brownian motion of nanoparticle, liquid layering, nanoparticle aggregation, radiative heat transfer). Increase in thermal conductivity in turn, enhances the overall dielectric loss, which results in increase of corresponding *tanδ* values. Therefore, *tanδ* value for both the nanofluids (MO+$Al_2O_3$ and MO+$TiO_2$) increases due to increase in temperature from 50˚C to 80˚C, as observed in Fig. 3.14 and 3.15.

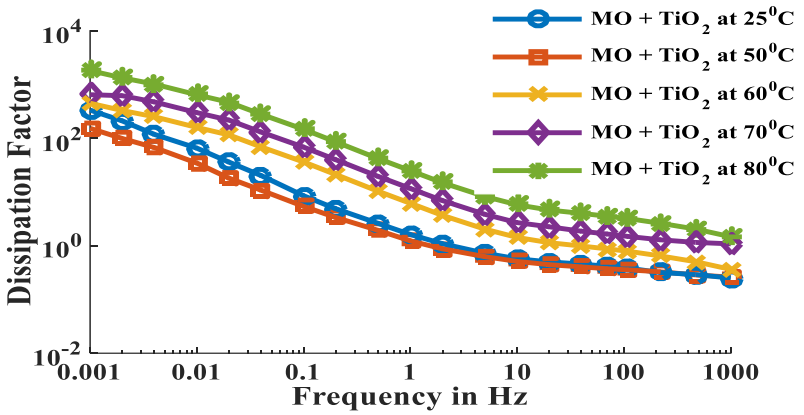


**Fig. 3.14.** Variation of *tanδ* for pure MO with $TiO_2$ at different temperatures.

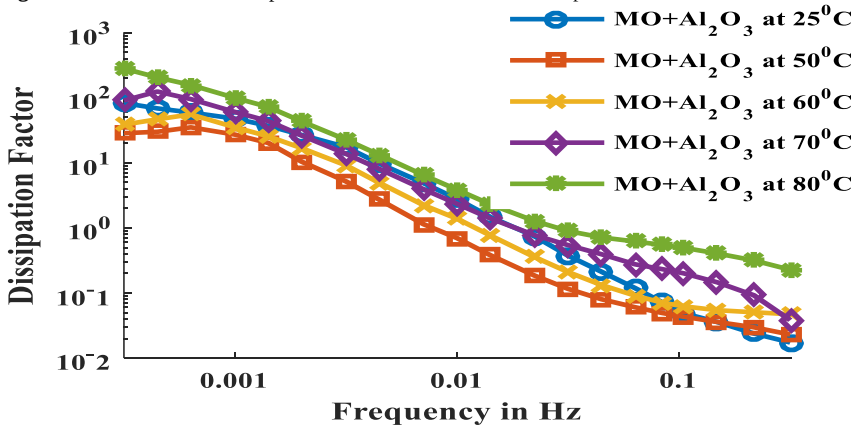


**Fig. 3.15.** Variation of *tanδ* for pure MO with $Al_2O_3$ at different temperatures.

### *3.5.5.2.3. Temperature Effect on tanδ for Nano Particles Based Vegetable Oil*

In the case of VO based nanofluids, the variation of *tanδ* profile at different temperatures has been shown in Fig. 3.16 and 3.17, respectively. It may be observed from Fig. 3.16 and 3.17 that the *tanδ* value increases as the temperature increases for both the nanofluids (VO+$TiO_2$ and VO+$Al_2O_3$).

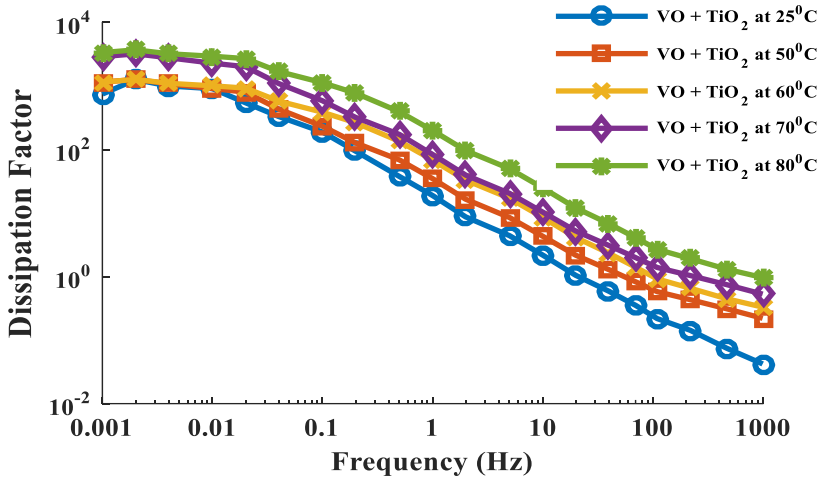


**Fig. 3.16.** Variation of *tanδ* for pure VO with $TiO_2$ at different temperatures.

In the case of VO, free electrons are primarily responsible for the dielectric current under applied electric field, which contribute to *tanδ* value. Besides, dispersion of nanoparticles ($TiO_2$ and $Al_2O_3$) in VO traps the free electrons which results in reduction of *tanδ* value in comparisons with the corresponding values for pure VO. However, as the temperature increases, the trapped electrons acquire thermal energy. If the acquired thermal energy becomes higher than the energy required to de-trap, then the trapped electrons are released. For both the nanofluids (VO+$TiO_2$ and VO+$Al_2O_3$), the concentration of free electron becomes higher as the measurement temperature increases. Therefore, the conduction currents of the nanofluids increase with tempeature, which in turn enhances the value of corresponding *tanδ*. This fact has been reflected in Fig. 3.16 and 3.17, respectively. The *tanδ* profiles of both the nanofluids (VO+$TiO_2$ and VO+$Al_2O_3$) are higher with temperature.

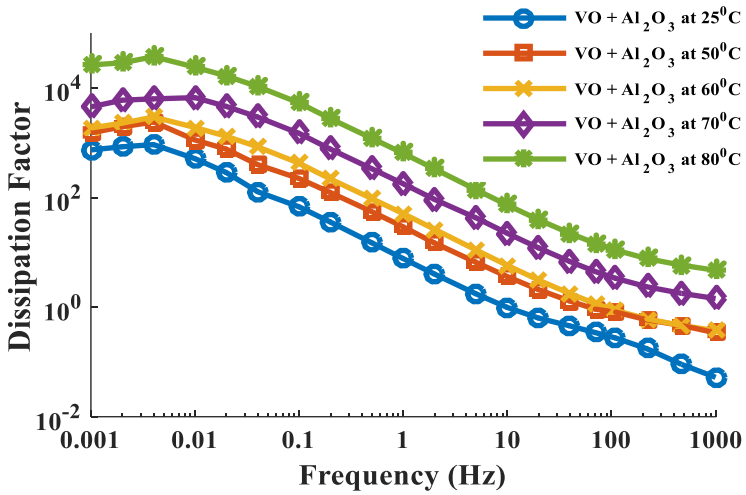


**Fig. 3.17.** Variation of *tanδ* for pure VO with $Al_2O_3$ at different temperatures.

Table 3.4. Percentage changes of tan Delta value at power frequency (50Hz) for different temperatures.

| Dielectrics | *tanδ* value *at* 25˚C | % changes of *tanδ* value | | | |
|---|---|---|---|---|---|
| | | 50˚C | 60˚C | 70˚C | 80˚C |
| MO | 0.039 | 181 | 454 | 495 | 637 |
| MO+ $TiO_2$ | 0.066 | 011 | 116 | 372 | 466 |
| MO+ $Al_2O_3$ | 0.087 | 021 | 018 | 165 | 173 |
| VO | 0.072 | 252 | 877 | 950 | 967 |
| VO+$TiO_2$ | 0.042 | 127 | 293 | 463 | 542 |
| VO+$Al_2O_3$ | 0.046 | 183 | 288 | 386 | 412 |

Moreover, the changes of the *tanδ* values with temperature of the pure oils and nanofluids at power frequency range have been evaluated at power frequency (50 Hz) for comparison purpose and are tabulated in Table 3.4. It may be observed from Table 3.4 that the percentage changes of *tanδ* values at different temperatures due to dispersion of nanoparticles in both mineral and vegetable oils are lower in comparison with the pure oils. This facts illustrate that that presence of nanoparticles in oils reduces the dielectric loss and improves the dielectric properties.

### *3.5.6. Correlation between Dielectric Dissipation loss and LFD of Real Capacitance*

From the FDS measurement the real capacitance of each sample has been obtained. The variation of real capacitance of MO and VO with their nanofluids at 25˚C has been depicted in Fig. 3.18 and 3.19 respectively.

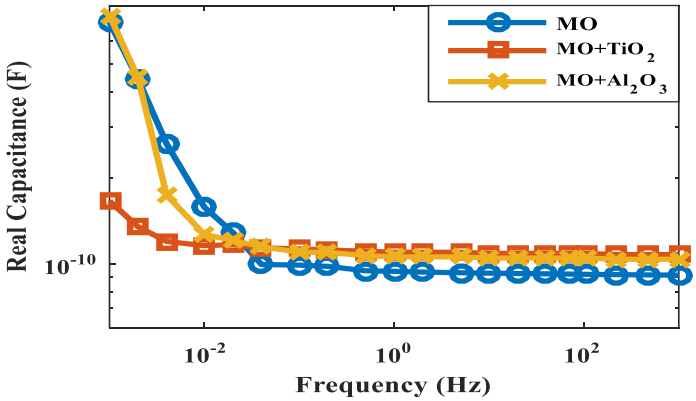


**Fig. 3.18.** Variation of real capacitance for pure MO and nanofluids.

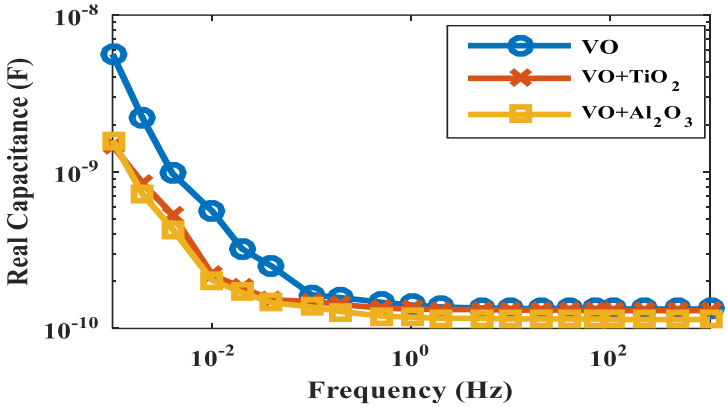


**Fig. 3.19.** Variation of real capacitance for pure VO and nanofluids.

This study proposes an empirical equation (3.8) to describe the relation between *tanδ* and low frequency dispersion i.e. change in real capacitance.

$$\tan\delta = a \times \Delta C^{b} \tag{3.8}$$

Where parameter a and b are depends on the electrode materials, temparature and types of liquid dielectric. These parameters are obtained through nonlinear regression method with $R^2$>0.95 and are presented in table 3.5. Change of real capacitance vs *tanδ* curve for measured value and values obtained from the proposed model have been plotted for different prepared samples in Fig. 3.20. As ac conductivity is lower at low frequency and rise in temparature, electrode polarisation has been reduced owing to reduction in ionic hopping time.

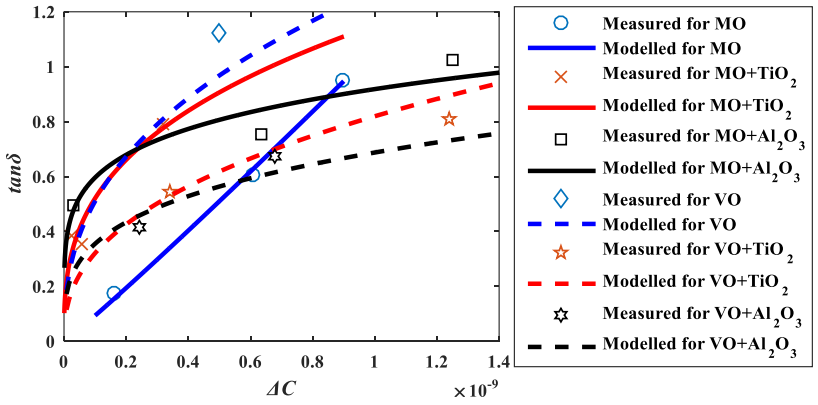


**Fig. 3.20.** Change of *tanδ* against change in real capacitance in MO, VO and their nanofluids.

**Table 3.5.** Parameters of proposed model for correlating *tanδ* and LFD of real capacitance.

| Dielectrics | a | b | Dielectrics | a | b |
|---|---|---|---|---|---|
| **MO** | 3.156E+6 | 1.0532 | **VO** | 4863 | 0.3979 |
| **MO+ $TiO_2$** | 1452 | 0.3445 | **VO+$TiO_2$** | 3767 | 0.4069 |
| **MO+ $Al_2O_3$** | 44.79 | 0.1876 | **VO+$Al_2O_3$** | 260.8 | 0.2866 |

Again different dielectrics show diverse adsorption behaviour i.e. liquid electrode interface which may hinder the electron transfer, as a consequence the test samples may have different electrode polarisation effect hence LFD of real capacitance is lower. The pattern of changing *tanδ* losses with LFD of real capacitance for different dielectric can be observed by the parameter values at Table 3.5 and in the Fig. 3.20. For same ΔC and same temparature, *tanδ* losses are higher in case of nanofluids based on mineral oil due to strong polarisation effects. But in the case of vegetable oil based nanofluids, the reverse phenomenon has been observed. The reason behind the fact is trapping of highly mobile free electrons which results in reduction of free electron cocentration within the vegetable oil and develops negetively charged nanoparticles.

## 3.6. Inference

In the chapter, semi-conducting nanoparticle, $TiO_2$ (titania), and a non-conducting nanoparticle, $Al_2O_3$ (alumina), based nanofluids have been prepared in laboratory for investigation of their dielectric properties. From experimental measurements and analysis, it was observed that the conductivity of Alumina nanofluids based on mineral oil nominally increased with increase in applied voltage is higher than the conductivity of Titania nanofluids based on mineral oil which increased slightly with applied voltage. In the case of natural ester-based oil (FR3) as base oil, Alumina nanofluids showed the same nature. It was also observed that the mineral oil shows much non-linear behaviour and with addition of nanoparticles, the degree of non-linearity can be improved with reduceing the value of the parameter 'b' comes close to the value of unity. Alumina based nanofluid based on mineral oil provide better linear property than Titania based mineral oil. But there is no such improvement in nonlinearity in case of addition of nano particle with natural based ester oil. It may be observed from the reported results that the presence of $Al_2O_3$ (alumina) in mineral oil increases corresponding *tanδ* values, whereas dispersion of $TiO_2$ (titania) decreases the corresponding *tanδ* values compared to pure mineral oil. On the other hand, a reverse phenomenon has been observed for vegetable oil. It has been observed that the presence of alumina in vegetable oil reduces the *tanδ* values while comparing with the titania-based vegetable oil. Moreover, the FDS have been conducted at 25°C, 50°C, 60°C, 70°C and 80°C respectively, on

pure mineral and vegetable oils and nanofluids to investigate the effect of temperature on their dielectric properties. It has been observed that the *tanδ* values at each frequency increases for both the pure mineral and vegetable oils with tempearture. In the case of mineral oil based nanofluids, a peculiar behaviour has been observed with increasing temperature from the corresponding *tanδ* profiles. As the temperature increases from 25˚C to 50˚C, *tanδ* values decreases and again increases as the temperature is raised to 70˚C and higher. In the case of VO based nanofluids, the *tanδ* values increase with the tempearture monotonically. Besides the investigations on LFD to calculate ΔC can provide an idea about aging of the insulation. For same ΔC and same temparature, *tanδ* losses are higher in case of nanofluids based on mineral oil but in the case of vegetable oil based nanofluids, the reverse phenomenon has been observed.

From the detailed discussion about the comparative study on the dielectric properties of nanofluids with mineral and vegetable oil, it can be inferred that, by dispersing nanoparticles dielectric properties like dc conductivity, nonlinearity in conduction current, *tanδ* profile can be improved. However, activation energy of the nanofluids are found to be decreased. Further, there is a increase in viscosity after dispersing nanoparticles which is not desirable. Considering these facts, further investigation is needed for searching the new class of insulation. Therefore, in the next chapter, hybrid nanoparticles have been dispersed and their corresponding nanofluids are subjected to the dielectric experiments.

# Chapter 4

# Hybrid Nanofluids: Dielectric Characteristics Investigations by Dielectric Spectroscopy

## 4.1. Introduction

From the previous chapter, it has been found that, dispersion of nanoparticles in mineral and vegetable oil can enhance some dielectric properties like dc conductivity, *tanδ* etc. but fails to improve viscosity, activation energy etc. In addition, according to the fact stated in [241, 242], $Al_2O_3$ (Alumina) shows enhanced stability in oil but lacks to provide good thermal properties and having lower breakdown strength. Moreover, $TiO_2$ (Titania) based nanofluids shows the better result in terms of improving breakdown strength [243, 244]. Further, with the higher temperature, $TiO_2$ based nanofluids also show better dielectric properties [244]. Furthermore, hybrid nanofluid based on alumina, titania and silicon dioxide dispersing in water improve viscosity [245]. From the literature [246], it can be noticed that employing fly ash-Cu hybrid nanoparticle improves the thermophysical properties like thermal conductivity, specific heat of the water. In case of oil filled transformers, CTs, PTs, circuit breakers, bushings cables and condensers, mineral oil has been used for insulation and cooling purposes. However, it has some detrimental drawbacks like very prone to fire hazards, higher electrical conductivity, non-biodegradability etc. So, hybrid nanofluids can be a good replacement of the mineral oil as next generation insulation which can be used in the aforementioned application. It should be mentioned here that, there are many researches investigating electrical, thermal, chemical properties of nanofluids with a single nanoparticle can be found. However, there are very few researches on the dielectric behavior of the hybrid nanofluids as an insulating medium of the transformer.

Considering this fact, in this chapter, $Al_2O_3$ (Alumina) and $TiO_2$ (Titania) have been chosen to prepare hybrid nanofluid dispersing on either mineral oil or vegetable oil. In this study, an effort has been made to prepare a stable biodegradable hybrid nanofluids and investigate their dielectric properties besides comparing with virgin mineral and vegetable oil.

## 4.2. Preparation of Nanofluids & Experimental Procedures

In this study, hybrid nanofluids (i.e. mixing of two different types of nanoparticles in either mineral oil or in vegetable oil) were prepared using the following procedure as shown in Fig. 4.1. For the preparation of hybrid nanofluids, 80 mg of surface modified $TiO_2$ and $Al_2O_3$ nanoparticles were mixed in three proportions (i.e. 30 mg $TiO_2$ with 50 mg $Al_2O_3$, 40 mg $TiO_2$ with 40 mg $Al_2O_3$ and 50 mg $TiO_2$ with 30 mg $Al_2O_3$ as referred in Table 4.1).

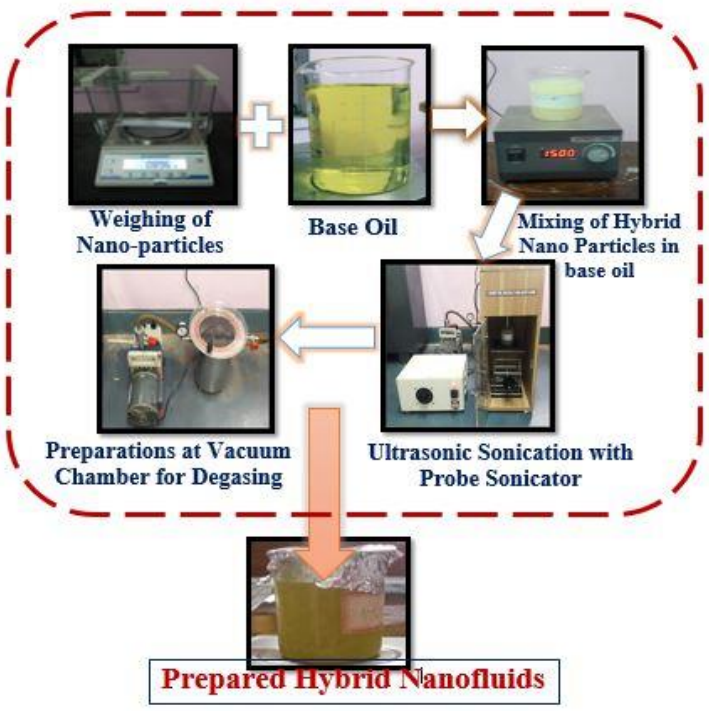


**Fig. 4.1.** Preparation of hybrid nanofluids.

Thereafter, those mixed nanoparticles were dispersed within either 800ml of mineral oil or 800 ml of vegetable oil. This mixture was stirred by a magnetic stirrer at a speed of 1200 rpm for 45 minutes to prepare a hybrid nanofluid concentration of 0.1 g/l. Next, ultrasonic probe sonicator was used for 6 hours for sonication process of the mixture. In the preparation of the

nanofluids, 2ml of oleic acid was used as surfactant for surface modification. As reported in [231], a combination of magnetic stirring and ultra-sonication with surface modified nanoparticles can provide stable nanofluids. During the stirring and sonication process, some microbubbles were formed which need to be eliminated for the sake of clear investigation of their dielectric characteristics. For this purpose, the mixture was subjected to a vacuum chamber at less than 1 kPa for about 2 hours followed by heating at 50°C for 1 hour. After the preparation, the mixture was allowed to relax for 2 hours before conducting experiment.

Table 4.1 Nomenclature of the hybrid samples according to the proportion of the nanoparticles

| Nanoparticle Proportions | | Base Oil | Nomenclature |
|---|---|---|---|
| $TiO_2$ | $Al_2O_3$ | | |
| 30 mg | 50 mg | Mineral Oil | MOA5T3 |
| 40 mg | 40 mg | | MOA4T4 |
| 50 mg | 30 mg | | MOA3T5 |
| 30 mg | 50 mg | Vegetable Oil | VOA5T3 |
| 40 mg | 40 mg | | VOA4T4 |
| 50 mg | 30 mg | | VOA3T5 |

In order to study the uniformity of the nanoparticles throughout the base matrix, the diameter distribution of the prepared hybrid nanoparticles was evaluated by DLS instrument [247]. The diameter distribution of the nanoparticles in the base oil was typically from 40 nm to 80 nm as shown in Fig. 4.2. This fact from the particle size distribution measurement indicates that nano particles are uniformly dispersed within the base liquid dielectric and can be subjected to PDC and FDS measurement to get proper condition assessment.

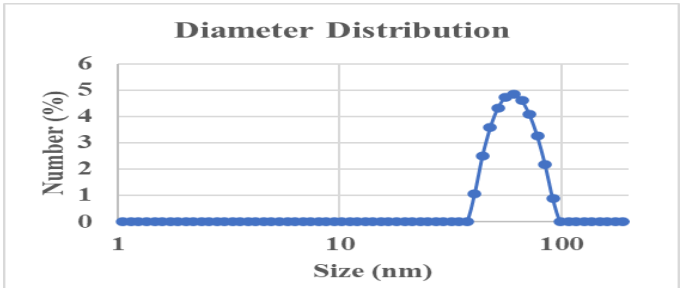


**Fig. 4.2**. Diameter distribution of nanoparticles in nanofluid through DLS instrument.

After the preparation of stable hybrid nanofluids, the electrode setup was dipped into the samples for the experiments. Dielectric properties of the hybrid nanofluids were investigated through conducting PDC and FDS

measurements employing DIRANA$^{TM}$ and IDAX 300, respectively (as shown in Chapter 2: Fig. 2.14 and Fig. 2.15, respectively). The PDC measurement was conducted on various voltage stages (50V, 100V, 150V, 180V and 200V) whereas the voltage magnitude for FDS measurement was fixed at $140V_{rms}$. Both the measurements were conducted at 25˚C, 40˚C, 50˚C, 60˚C, 70˚C and 80˚C to have a clear idea about the temperature effect on their dielectric properties.

## 4.3. Results & Discussion

### *4.3.1. Estimation of Viscosity*

Table 4.2 represents the corresponding values of viscosity of the prepared hybrid nanofluids comparing with pure oils and their nanofluids with single nanoparticles.

Table 4.2 Results from Viscosity measurement of prepared dielectric samples at 25°C

| Samples | Viscosity (cP) | Samples | Viscosity (cP) |
|---|---|---|---|
| MO | 13 | VO | 50 |
| MO+$TiO_2$ | 14.58 | VO+$TiO_2$ | 51.42 |
| MO+$Al_2O_3$ | 15.06 | VO+$Al_2O_3$ | 53.58 |
| MOA5T3 | 15.52 | VOA5T3 | 53.28 |
| MOA4T4 | 15.01 | VOA4T4 | 52.61 |
| MOA3T5 | 13.25 | VOA3T5 | 50.84 |

It may be observed from Table 4.2 that, viscosity of the nanofluids can be reduced by introducing hybrid nanoparticles in the base liquid dielectric instead of single nanoparticle. Moreover, higher amount of titania in the hybrid nanoparticles ensure lower viscosity among the nanofluids. The observed reduction in viscosity with higher Titania content may be attributed to multiple factors:

a) Particle morphology and interaction: Titania nanoparticles used in hybrid oil may have exhibited lower surface interaction or better dispersion in the base oil, resulting in less hindrance to fluid flow compared to the hybrid oil having higher Alumina.

b) Stability and sedimentation: Although Titania has a higher density, the hybrid formulation may have enhanced stability due to synergistic interactions between $Al_2O_3$ and $TiO_2$, reducing agglomeration and improving dispersion.

## *4.3.2. Estimation of DC Conductivity*

From the PDC measurement, the dc conductivity of each sample can be estimated by (Chapter 1: Equation (1.17)). Calculated conductivity for different hybrid and single nanofluids (for mineral oil and vegetable oil base) at 25°C, 40°C, 50°C, 60°C, 70°C and 80°C have been shown in Fig. 4.3 and Fig. 4.4, respectively. From the Fig. 4.3 and Fig. 4.4, it can be observed that conductivity increases with temperature. It is due to the fact that conduction current mainly is caused due to free charge present in the dielectric. Further, with increasing temperature, more number of free charge gain high thermal energy to enter into the conduction band which in turn increases the conductivity. From the Fig. 4.3, it can also be observed that the rate of the increment of conductivity for hybrid nanofluid reduces with temperature increment (upto 80°C) when amount of $TiO_2$ is higher than the amount of $Al_2O_3$ (for MOA3T5). Presence of $Al_2O_3$ attracts moisture and O atom (in $Al_2O_3$) in the alumina has an affinity towards the $H^+$ ions present in the moisture and produces hydroxyl group ($OH^-$) [233]. It has also been reported in [25] that, Ti atom has higher affinity to the hydroxyl group ($OH^-$) which is produced by $Al_2O_3$ present in hybrid nanofluids as shown in Fig. 4.5. This bonding makes an obstacle which may trap the free electrons moving towards anode. As the amount of $TiO_2$ increases, bonding with hydroxyl group increases which in turn enhances the obstacles. As a consequence, reductions of the mobility of those free electrons which results in reduction of the conductivity [234]. Again, it should be mentioned here that, when nanoparticles trap the free electrons, become negatively charged particles whose mobility is lower than the free electrons which reduces the conductivity. Further, MOA4T4 composition may offer an enhanced

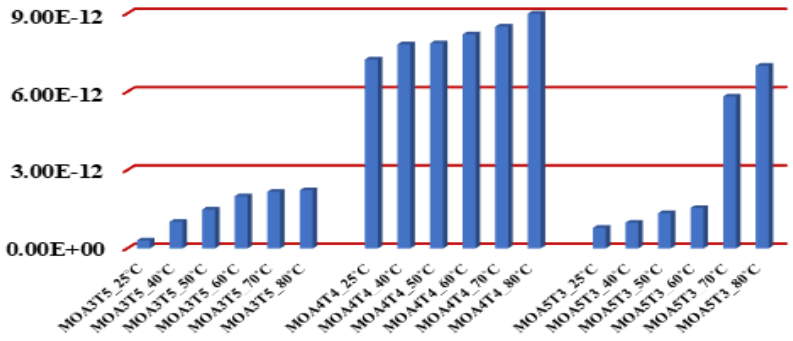


**Fig. 4.3.** Conductivity at different temperatures of mineral oil-based hybrid nanofluids.

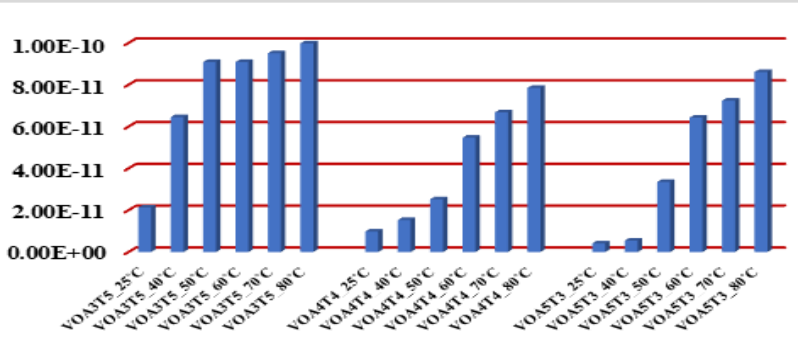


Fig. 4.4. Conductivity at different temperatures of vegetable oil-based hybrid nanofluids.

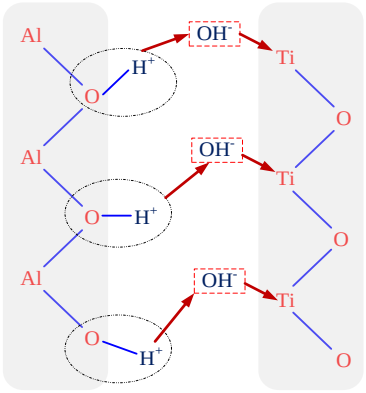


Fig. 4.5. Formation of bonding between nanoparticles through hydroxyl ions.

interfacial charge transport mechanism, where the mixed oxide interface promotes higher electron hopping or ionic conduction pathways compared to other samples. For the vegetable oil based nanofluids, presence of alumina shows better result in the case of conductivity not only in hybrid nanofluids but also in single nanofluid. As reported in [237], VO is a weak dielectric and moisture ingression is higher than mineral oil resulting a greater number of free electrons present in the vegetable oil. This fact leads to higher conductivity than mineral oil-based dielectric. It is reported in [233] that, the presence of alumina can attract $H^+$ ions from moisture and make hydroxyl ions. So, higher amount of alumina can produce more hydroxyl ions. These ions further attached with Ti atom and restrict the movement of free charges. Further, it can be observed that high amount of alumina with titania i.e.

VOA4T4 and VOA5T3 shows better result than single nanofluid with alumina. This is due to the bonding of Ti atom to $OH^-$ ions as shown in Fig. 4.5.

### *4.3.3. Estimation of Activation Energy*

Moreover, to calculate activation energy, *ln(σ)* has been plotted against inverse of temperature in Kelvin for different prepared samples as shown in Fig. 4.6. From the slope of the curve, activation energy has been calculated employing (3.4) (discussed in Chapter 3: Section 3.4.3) and measured values have been shown in Table 4.3.

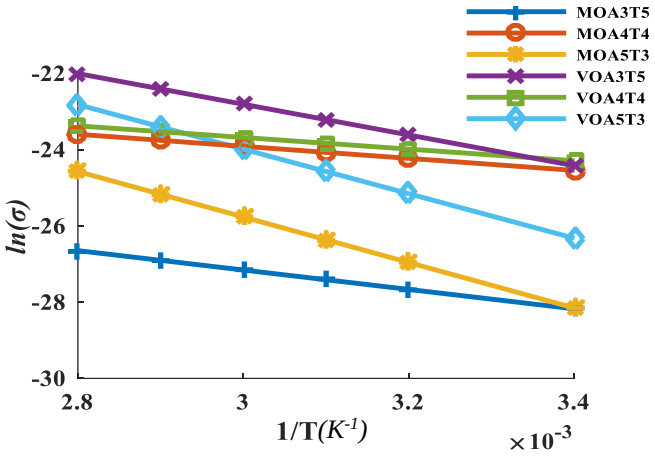


Fig. 4.6. Graph for calculating the activation energy for different samples.

Table 4.3 Activation energy of nanofluids based on Mineral and Vegetable oil

| Samples | Activation Energy in eV | Samples | Activation Energy in eV |
|---|---|---|---|
| MO | 0.36 | VO | 0.39 |
| MO+$TiO_2$ | 0.22 | VO+$TiO_2$ | 0.26 |
| MO+$Al_2O_3$ | 0.28 | VO+$Al_2O_3$ | 0.25 |
| MOA3T5 | 0.35 | VOA3T5 | 0.35 |
| MOA4T4 | 0.44 | VOA4T4 | 0.43 |
| MOA5T3 | 0.52 | VOA5T3 | 0.50 |

It can be observed from Table 4.3 that, presence of high amount of alumina in hybrid nanofluids offers more activation energy than other dielectric samples. This is due to the fact that more alumina may offer strong bonding with titania through $OH^-$ ions for both base fluids. So, to overcome

this potential barrier, more energy is needed hence offers more activation energy. It is to be mentioned here that, the activation energy is an important parameter for estimating the remaining life of the insulation.

## *4.3.4. Study on Non-linearity in Conduction Current*

### 4.3.4.1. Effect of Voltage on Non-linearity

For investigating the linearity of the prepared dielectrics, $I_{cond}$ at 25°C have been depicted for MO and VO based hybrid nanofluids as shown in Fig. 4.7a, and 4.7b, respectively and have been fitted with (Chapter 3, Equation (3.7)) for different levels of applied voltage (50V, 100V, 150V, 180V and 200V). Thereby, the value of the power (*b)* at the aforementioned voltage have been calculated for all prepared samples and presented in Table 4.4.

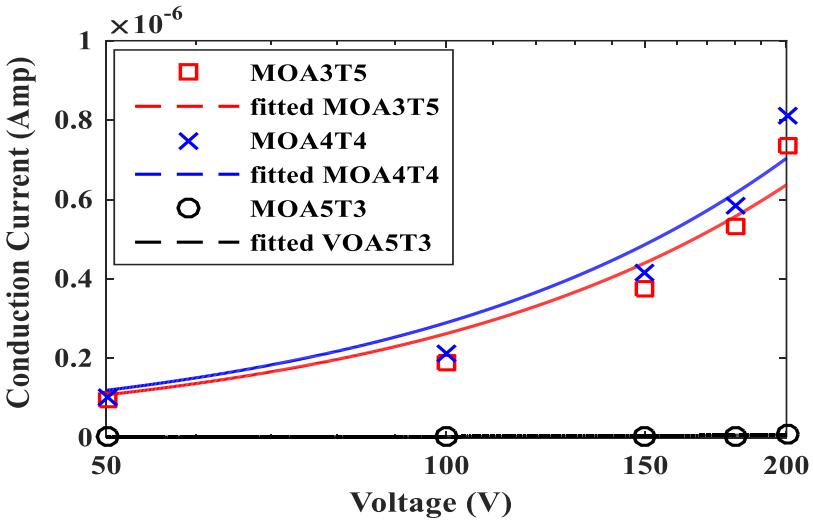


(a)

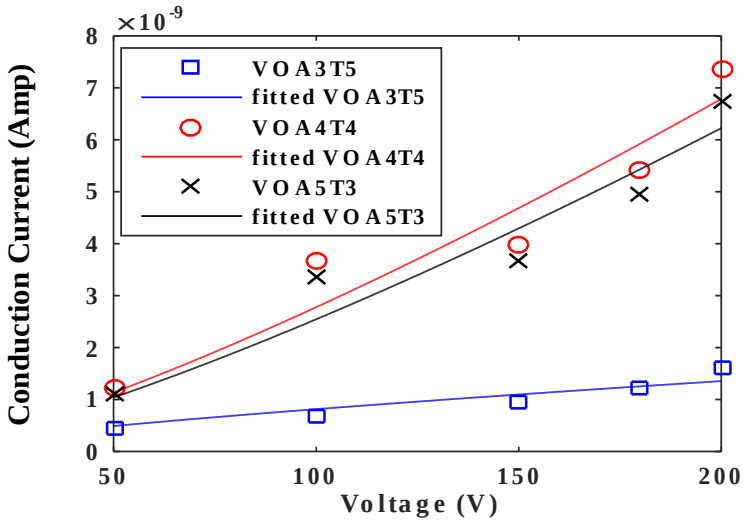


(b)

Fig. 4.7. $I_{cond}$ at various voltage level for (a) MO based and (b) VO based hybrid nanofluids.

Table 4.4 Parameters for Investigating the Non-Linearity for Various Samples Due to Voltage

| Samples | *a* | *b* | Samples | *a* | *b* |
|---|---|---|---|---|---|
| **MO** | 2.63E-14 | **1.744** | **VO** | 1.12e-10 | **1.346** |
| **MOT** | 3.21E-13 | **1.471** | **VOT** | 7.95E-10 | **1.281** |
| **MOA** | 8.76E-12 | **1.186** | **VOA** | 3.46E-11 | **1.233** |
| **MOA3T5** | 7.63E-12 | **1.369** | **VOA3T5** | 7.36E-12 | **1.089** |
| **MOA4T4** | 6.36E-13 | **1.285** | **VOA4T4** | 2.56E-10 | **1.082** |
| **MOA5T3** | 7.27E-11 | **1.085** | **VOA5T3** | 6.70E-12 | **0.792** |

From Table 4.4, it can be noticed that, mineral oil and vegetable oil exhibit maximum nonlinearity. By introducing nanoparticles in the base matrix, the degree of nonlinearity can be reduced. Moreover, more linear nature of conduction current has been noticed by introducing hybrid nanoparticles.

4.3.4.2. Effect of Temperature on Non-linearity

For the study of non-linearity of the dielectric system owing to temperature elevation, $I_{cond}$ at 200V have been plotted for MO and VO based

hybrid nanofluids as shown in Fig. 4.8a, and 4.8b, respectively for different levels of temperatures (25˚C, 40˚C, 50˚C, 60˚C, 70˚C and 80˚C).

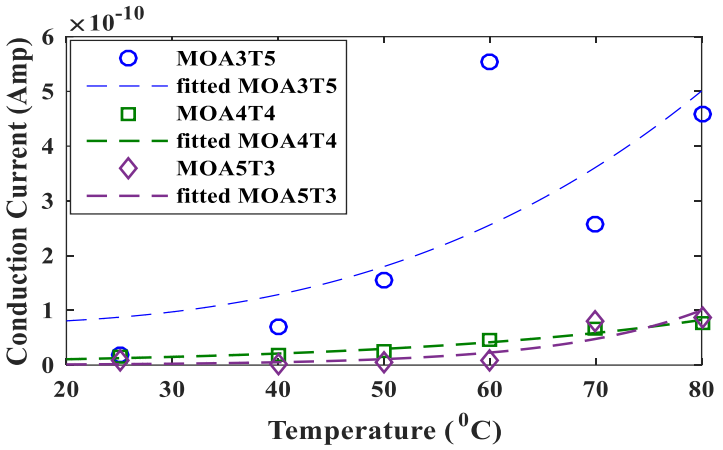


(a)

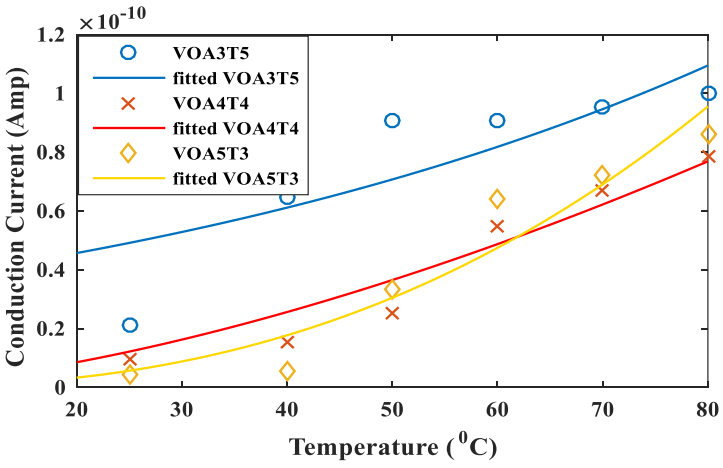


(b)

Fig. 4.8. $I_{cond}$ at various temperatures for (a) VO based nanofluids and (b) hybrid nanofluids.

Using regression method, the relationship between temperature and conduction current has been established as presented in (4.1). Thereby, the value of the power (*d)* is decided the degree of nonlinearity due to temperature elevations which have been evaluated for all prepared samples and presented in Table 4.5.

$$I_{cond} = c \times e^{d \times t} \tag{4.1}$$

Table 4.5 Parameters for Investigating the Non-Linearity for Various Samples Due to Temperature

| Samples | *c* | *d* | Samples | *c* | *d* |
|---|---|---|---|---|---|
| **MO** | 5.242e-14 | **0.083** | **VO** | 9.894e-12 | **0.050** |
| **MOT** | 4.638e-13 | **0.072** | **VOT** | 5.385e-12 | **0.044** |
| **MOA** | 4.563e-13 | **0.081** | **VOA** | 2.707e-13 | **0.073** |
| **MOA3T5** | 4.962e-12 | **0.035** | **VOA3T5** | 3.412e-11 | **0.015** |
| **MOA4T4** | 4.908e-12 | **0.059** | **VOA4T4** | 3.168e-12 | **0.041** |
| **MOA5T3** | 3.865e-12 | **0.062** | **VOA5T3** | 1.915e-12 | **0.049** |

From Table 4.5 it can be observed that, the nonlinearity effect due to temperature elevation can be reduced using hybrid nanofluids. This improvement is due to the fact that, in hybrid nanofluids, a stronger bond has been created in the surface of Titania and Alumina via hydroxyl ions as shown in Fig. 4.5 [248]. Moreover, conduction current can be modelled with simultaneous variation of voltage and temperature as presented in (4.2). The corresponding conduction current is shown in Fig. 4.9. Here, A and B are constants which depends on the insulating materials. From Fig. 4.9 it can be observed that, with higher voltage and higher temperature more nonlinearity of the conduction current has been noticed.

$$I_{cond} = AV^{b} \times e^{B \times t} \tag{4.2}$$

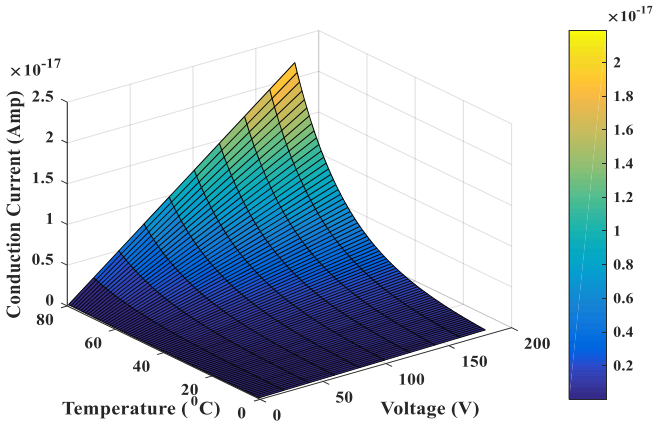


**Fig. 4.9.** Conduction current with simultaneous change of voltage and temperature.

## *4.3.6. Dielectric Dissipation Factor*

### 4.3.6.1. Effect of Nanoparticles on *tanδ*

The FDS measurement employing IDAX 300 of Hybrid nanofluids based on mineral oil and vegetable oil at 25˚C have been compared with the single nanoparticle based nanofluid as shown in the Fig. 4.10 and Fig. 4.11, respectively. From the both Figures, it can be observed that, the dielectric dissipation factor (*tanδ)* decreases with increasing frequency. It is obvious due to the fact that, initially lesser number of dipoles are intending to allign towards the applied field which gradually increases with time. So, at low frequency, most of the dipoles are trying to take part in dipolar polarisation and may interact with free electrons which increase the frictional losses hence the dielectric loss.

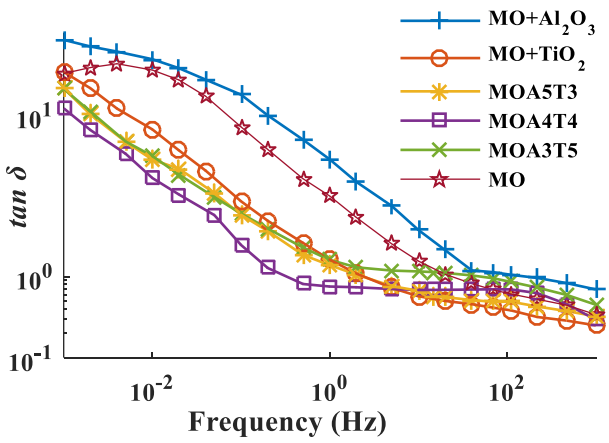


Fig. 4.10. Variation of *tanδ* for mineral oil based nanofluid at $25^0$C.

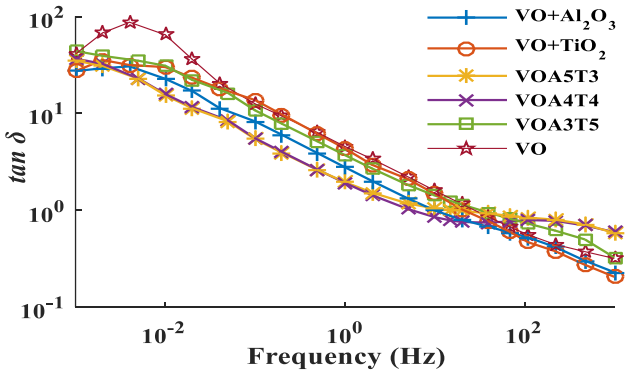


Fig. 4.11. Variation of *tanδ* for vegetable oil based nanofluid at $25^0$C.

From the Fig. 4.10, it can also be observed that the *tanδ* profiles of mineral oil based hybrid nanofluids show better result than the nanofluid consisting single nanoparticle (from low frequency to power frequency range). Among the mineral oil based hybrid nanofluids, 50% alumina with 50% titania (MOA4T4) shows least dielectric loss factor below power frequency range. In the lower frequency range, nanoparticles are exposed to electric field for longer time. So Ti and Al atoms gradually create a bond with water molecules as shown in Fig. 4.5 as Ti and Al atom have their affinity to absorb hydroxyl ($OH^-$) ion and $H^+$ ion, respectively in their surface[233]. Again, electronegetivity of oxygen (O atom) is 3.5 which is higher than the electronegativity of Ti atom (which is 1.54). So, oxygen (O atom) atom present in the alumina attracks $H^+$ ions more quickly and makes $OH^-$ hydroxyl group which in turn has a tendency to attached with the Ti atom. This fact leads to the reduction in relative permittivity in the presence of multiple nanoparticles. According to the three core model reported in [237], third core may develop some attachments with oil molecules. This fact weakens the polarisation phenomena in the lower frequency range which in turn plays a vital role for lower the dielectric loss. However, in the higher frequency ranges (in Fig. 4.10), a peculier trend can be observed where hybrid oil consisting more $TiO_2$ nanoparticle exhibits higher dielectric losses than the other two types of hybrid nanofluids. This is due to the unbalanced crystal structure of $TiO_2$ atom which has been shown in Chapter 3, Fig. 3.10. This imbalance crystal atom causes strong polarisation in the higher frequency range i.e. near kHz range.

Fig. 4.11 shows some improvement in the *tanδ* profile in the case of hybrid nanofluids than the single nanofluids. Again for bio-degradable oil,

conduction current dominant over polarisation current [237]. As free electrons are more responsible for the conduction current, the friction during the movement of the free electrons is the main reason for dielectric loss. However, presence of the nanoparticle in base oil, traps those free electrons which result in reduction of the dielectric losses. Besides, as discussed in section 4.3.2, the conductivity in nano-dielectric reduces when the amount of $Al_2O_3$ is higher. This phenomenon in turn reduces the dielectric loss resulting the reduction of *tanδ.*

4.3.6.2. Effect of Temperature on *tanδ*

FDS measurement of the prepared hybrid nanofluids have been conducted at 25˚C, 40˚C, 50˚C, 60˚C, 70˚C and 80˚C, respectively to examine the effect of temperature on the dielectric properties of hybrid nanofluids.

*4.3.6.2.1. Temperature Effect on tanδ for MO Based Hybrid Nanofluids*

The temparature effect on the dielectric losses in the hybrid nanofluids has been discussed in this section. Fig. 4.12, 4.13 and 4.14 shows the teparature effects of the hybrid nanofluids referred as MOA3T5, MOA4T4 and MOA5T3, respectively.

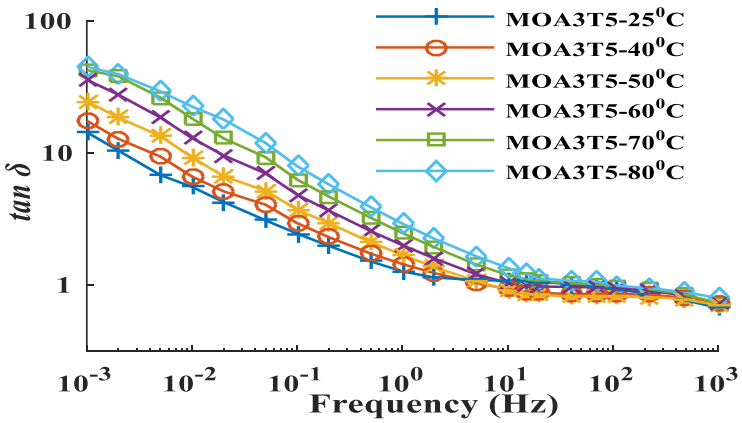


Fig. 4.12. Variation of *tanδ* for Mineral oil with higher Titania nanoparticles at different temperatures.

All the three cases revealed that, with the increase of temparature from 25°C to 80°C, the values of *tanδ* increase throughout the frequency range

from 1mHz to 1kHz. But the rate of increment of dielectric loss with incresing temperature, is higher in the low frequency range and negligible in the case of high frequency range. Again, with higher amount of titania present in the base fluid shows relatively less change in dielectric loss at higher frequency ragnes in comparison with lower frequency ranges as shown in Fig. 4.12. This is due to the fact that at lower frequencies, electrons gain relatively higher amount of thermal energy which consequently enhances the conduction current. As a consequence, conduction losses are higher which leads to the high dielectric losses.

Moreover, at higher temparature, thermal conductivity is more responsible for dielectric loss. Thermal conductivity further depends on the radiative heat transfer, brownian motion of nanoparticle, nanoparticle aggregation [240]. These factors are also aggravated with temparature increment. As a result, enhancement of the thermal conductivity can be experienced which in turn leads to high dielectric losses at high temparature. From the pattern in the above graphs, it can be concluded that more amount of $TiO_2$ can minimize this increment of thermal conductivity as shown in the Fig. 4.13 and 4.14. This is due to the fact that presence of Ti atom leads to bonding with the $OH^-$ group which may not be broken totally with temparature rise upto 80°C. Hence, the number of free electrons are not as much as in case of other nanofluids. This fact in turn resists the rate of increment of the dielectric loss.

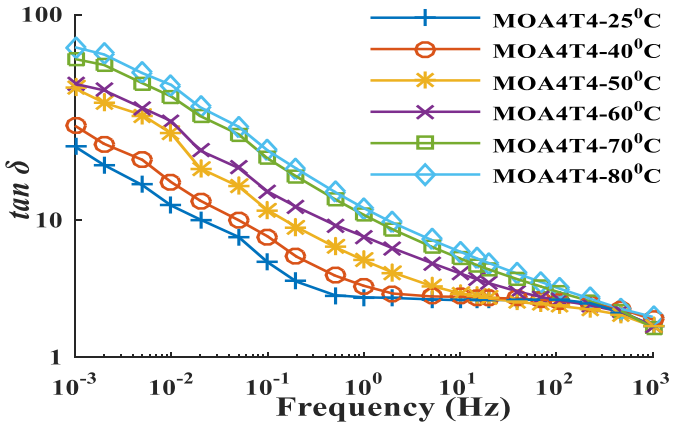


Fig. 4.13. Variation of *tanδ* for Mineral oil with equal amount of Titania and Alumina nanoparticles at different temperatures.

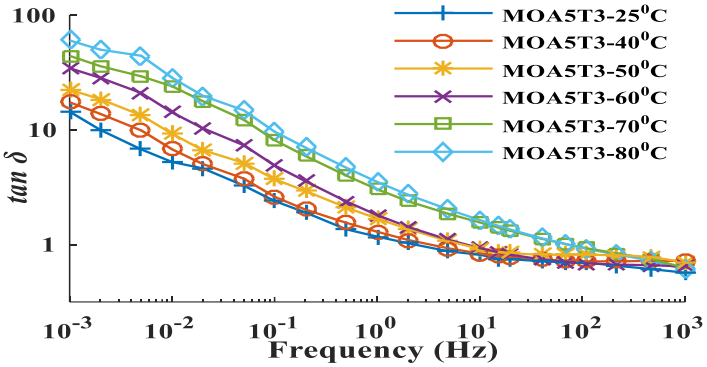


Fig. 4.14. Variation of *tanδ* for Mineral oil with higher Alumina nanoparticles at different temperatures.

### *4.3.6.2.2. Temperature Effect on tanδ for Vegetable Oil Based Hybrid Nanofluids*

Fig.s 4.15, 4.16 and 4.17 shows the teparature effects of the hybrid nanofluids referred as VOA3T5, VOA4T4 and VOA5T3, respectively. From these Fig.s, it can be observed that the dielectric losses are relatively higher with increasing temparature for the lower frequency range (i.e. from 1mHz to 50Hz). It may also be observed from the Fig.s 4.16 and 4.17 that, the *tanδ* value at higher frequency range (above power frequency ranges) at 25°C dielectric loss is maximum and decreased at 40°C. Then with increasing temparature dielectric losses also increase after 40°C.

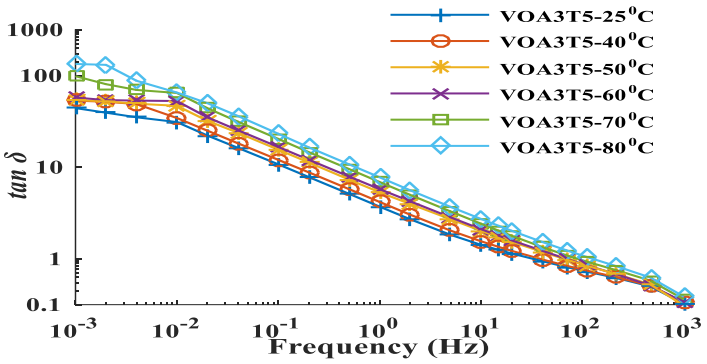


Fig. 4.15. Variation of *tanδ* for Vegetable oil with higher Titania nanoparticles at different temperatures.

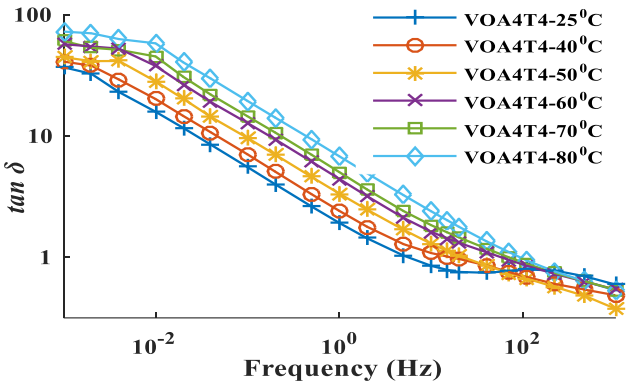


Fig. 4.16. Variation of *tanδ* for vegetable oil with equal amount of Titania and Alumina nanoparticles at different temperatures.

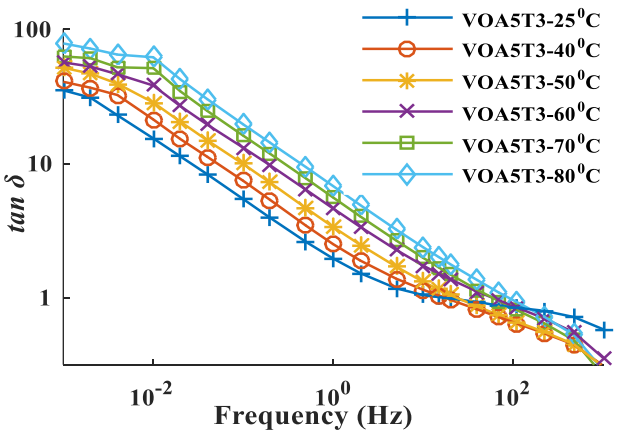


Fig. 4.17. Variation of tanδ for vegetable oil with higher Alumina nanoparticles at different temperatures.

As discussed in the section 4.3.2, dielectric losses are determined by the movement of free electrons. However, presence of nanoparticles in the vegetable oil ensures the trapping of the free electrons which furthur reduces the dielectric losses. As the temperature increases, the moisture ingression within VO increases which results in increment of formation of hydroxyl group. Presence Al and Ti atom generate a bond with hydroxyl group which resist the movement of electron and hence the *tanδ* value reduces.

## 4.4. Inference

In the present investigations, hybrid nanofluids have been prepared by mixing with a semiconducting type nanoparticle ($TiO_2$) and a non-conducting type nanoparticle ($Al_2O_3$) in a certain ratio. Therefore, the dielectric properties like dc conductivity, activation energy and *tanδ* profiles of the prepared dielectric liquid samples have been compared with the nanofluids consisting single nanoparticle. For this purpose, PDC and FDS measurement have been conducted employing DIRANA and IDAX 300, respectively at 25°C, 40°C, 50°C, 60°C, 70°C and 80°C. From the results, the key findings have been summarized as

a) The conductivity of Hybrid nanofluid is reduced when amount of $TiO_2$ is higher than the amount of $Al_2O_3$. Even with the temperature rise, higher amount of $TiO_2$ can resist the conductivity increment to a lower limit in the case of mineral oil base. For the vegetable oil based nanofluids, presence of higher amount of alumina shows better result in the case of conductivity than the presence of titania.
b) Presence of higher amount of alumina in both the base oils offers more activation energy.
c) From this study it can be stated that, high value of voltage greater than 100V and temperature are two factors responsible for nonlinearity presence in dielectric response. Hybrid nanofluids can also decrease the effect of nonlinearity due to both voltage and temperature.
d) The hybrid nanofluids based on mineral oil, 50% alumina with 50% titania shows least dielectric loss factor at lower frequency range.
e) For the mineral oil based nanofluids, the values of *tanδ* will increase throughout the frequency range from 1mHz to 1kHz. But the rate of increment of dielectric loss with temperature increase, is higher in the low frequency range and in the case of high frequency this change is negligible. Presence of higher amount of Titania in the base fluid showed minimum change in dielectric loss at high frequencies.
f) For the vegetable oil based nanofluids, the dielectric losses increases with increasing temparature upto 80°C from the lower frequency range i.e. from 1mHz to 50Hz (power frequency). But at the higher frequency range dielectric losses are highest at 25°C and then dielectric losses are lower with increasing frequency.
g) Higher amount of $TiO_2$ nanoparticle presence in the base oil ensure the higher breakdown strength than other prepared dielectric samples for the both base oil.

From this discussion, it can be observed from the experimental results that hybrid nanofluids can be a better choice than single nanofluids and the base oils (mineral oil or vegetable oil) for a power engineer with improved dielectric properties. Further, it can be concluded that the VOA4T4 (Vegetable oil with 50% Titania and 50% Alumina) is the most suitable insulating fluid among the test samples used for the investigation.

In this chapter, nanoparticles were mixed for the preparation of nanofluids. It is to be stated here that, for the environmental issue, vegetable oil has been chosen over mineral oil. However, vegetable oil has major problems like high cost, higher viscosity and higher moisture ingression. In view of this issue, mixed oil i.e. certain amount of mineral oil is replaced with vegetable oil, has been considered for base oil. Therefore, in the next chapter, mixed oil based nanofluids have been prepared and their dielectric properties have been compared with existing oils to investigate their applicability as an alternative to transformer oil.

# Chapter 5

# Mixed Oil based Nanofluids: Dielectric Characteristics Investigations by Dielectric Spectroscopy

## 5.1. Introduction

From the previous chapter, it has been observed that, by mixing of nanoparticles, insulating properties can be enhanced. Further, to find a new class insulating liquid, several studies have been conducted on mixed insulating oil where two or more types of oils are mixed in a certain ratio. It should be stated here that, by blending a certain proportion of mineral oil with esters, viscosity can be reduced, Oxidation stability may be enhanced, especially in sealed systems, Hence, it enables gradual transition from mineral oil systems in aging transformers, aiding utilities in extending equipment life without complete fluid replacement. Fofana *et al.* [249] prepared mixed oils by mixing with mineral oil and synthetic ester (MIDEL 7131) at different ratio for investigation. Again in 2006, Perrier *et al* recommended the mixed oils in which ratio of mineral oil and synthetic ester was 4:1 [250]. According to Takahashi *et al*, blending of oil containing 80% vegetable oil and 20% mineral oil, shows better dielectric properties [251]. Though the uses of mixed oils show better performance in transformer, however, its dielectric characteristics degrades with time. Therefore, regular condition assessment of the mixed oils within transformer is necessary for its reliable operation. In order to assess the condition of mixed oils-based insulation, Polarization and Depolarization Current (PDC) and Frequency Domain Spectroscopy (FDS) are popularly used [222]. In this chapter, vegetable and mineral oils have been blended in a certain ratio to prepare mixed-oil samples. Moreover, effect of titania and alumina on the mixed oil samples have been investigated by preparing mixed-oil based nanofluids. Therefore, PDC and FDS on the mixed-oil and nano-particles based oils have been conducted at 25℃, 40℃, 50℃, 60℃, 70℃ and 80℃ to understand the dielectric properties like non-linearity in conduction current, dc Conductivity, activation energy etc. Moreover, a

statistical modeling approach has been proposed to understand the variation in the dielectric parameters of the oil. A correlation among the three parameters i.e. frequency, temperature, and two dielectric parameters has been established.

## 5.2. Preparation of Nanofluids & Experimental Procedures

In this section, the procedures for the preparation of mixed-oil and mixed oil based nanofluids have been explained. Mixture of mineral oil (MO) and vegetable oil (VO) (basic properties of these base oils has been presented in Chapter 1, Table 1.1) were chosen as base oil. Besides, $TiO_2$ and $Al_2O_3$ nanoparticles were dispersed within mixed oils to prepare nanoparticles based mixed-oil. The preparation of the mixed oil and mixed oil based nanofluids have been depicted in Fig. 5.1.

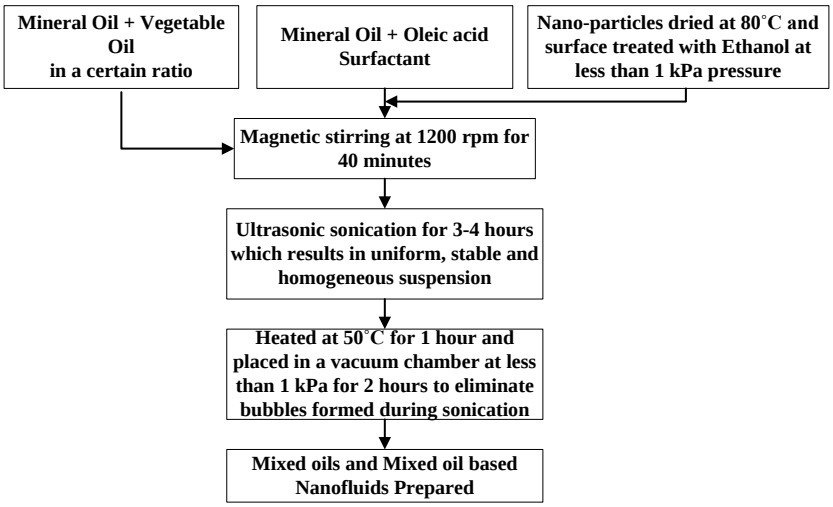


Fig. 5.1. Flowchart for mixed oil-based sample preparation.

Before taking the samples for the experimental purpose, the samples were kept rest for 3 hours for settling from its agitated state. The mixture proportion of the mixed dielectrics has been given in Table 5.1. The particle size distribution of the nanoparticles in the mixed oil were evaluated by DLS measurement and the average diameter distribution has been found within 40

nm to 80 nm as given in Fig. 5.2 which ensures the uniformity of the prepared nanofluids [230].

Table 5.1 Nomenclature of The Prepared Samples

| Mixed Dielectrics | Mixture Proportion | Mixed Oils with Nano-particles | Prepared Nanofluids |
|---|---|---|---|
| **S1** | MO 70% + VO 30% | **S1T** | S1+ $TiO_2$ |
| | | **S1A** | S1+ $Al_2O_3$ |
| **S2** | MO 75% + VO 25% | **S2T** | S2+ $TiO_2$ |
| | | **S2A** | S2+ $Al_2O_3$ |
| **S3** | MO 80% + VO 20% | **S3T** | S3+ $TiO_2$ |
| | | **S3A** | S3+ $Al_2O_3$ |
| **S4** | MO 90% + VO 10% | **S4T** | S4+ $TiO_2$ |
| | | **S4A** | S4+ $Al_2O_3$ |

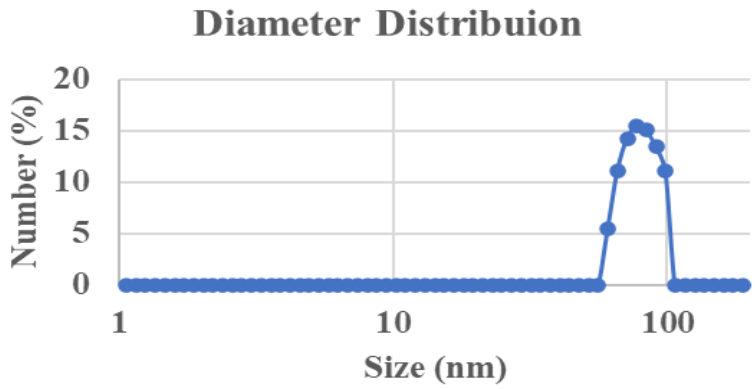


Fig. 5.2. Nanoparticle distribution in nanofluids by DLS.

After the preparation of mixed oil-based samples, the electrode setup was dipped into the samples for the dielectric experiments. Dielectric properties of the mixed oil-based samples were investigated through conducting PDC and FDS measurements employing DIRANA™ and IDAX 300, respectively (as shown in Fig. 2.14 and Fig. 2.15, respectively). The PDC measurement was conducted on various voltage stages (50V, 100V, 150V, 180V and 200V) whereas the voltage magnitude for FDS measurement was fixed at $140V_{rms}$. Both the measurements were conducted at 25˚C, 40˚C, 50˚C, 60˚C, 70˚C and 80˚C to have a clear idea about the temperature effect on their dielectric properties.

## 5.3. Results & Discussion

### *5.3.1. Estimation of Viscosity*

The viscocity of the prepared test samples were measured by viscometer and the corresponding values have been presented in Table 5.2. From the Table 5.2, it can be observed that, among the mixed oils, viscosity of samples S1 to S4 are reducing and becomes lowest in case of S4. In order to investigate further, the viscosity of another sample (with MO 95% + VO 5%) was measured. It was found that, the viscosity of the new sample was 35.7 cP. This result implies that further enhancement of MO beyond 90% in the mixed oil, does not significantly improve the viscosity. Therefore, the viscosity of S4 (with MO 90% + VO 10%) mixed with nano-particles are providing the best results.

Table 5.2 Viscosity of test Samples at 25°C

| Samples | Viscosity (cP) | Samples | Viscosity (cP) |
|---|---|---|---|
| **MO** | 13 | **S2T** | 37.8 |
| **VO** | 50 | **S3T** | 35.9 |
| **S1** | 41.6 | **S4T** | 34.1 |
| **S2** | 36.4 | **S1A** | 40.8 |
| **S3** | 35.6 | **S2A** | 36.1 |
| **S4** | 35.8 | **S3A** | 35.2 |
| **S1T** | 42.6 | **S4A** | 33.9 |

In case of nano-particles based oil, it can further be observed from Table 5.2 that, the viscosity is minimum for S4A (MO 90% + VO 10% with alumina). Moreover, in case of nanofluids, it can be observed that alumina based mixed oil exhibit lower viscosity than titania based mixed oil.

### *5.3.2. Estimation of DC Conductivity*

From the PDC measurement, the dc conductivity of the prepared samples have been calculated by (Chapter 1, Equation 1.17). Calculated conductivity for mixed oils, mixed oil based titania and alumina nanofluids at 25°C, 40°C, 50°C, 60°C, 70°C and 80°C have been presented in Fig.s 5.3, 5.4 and 5.5, respectively. From the Fig.s 5.3 and 5.4, it can be observed that conductivity increases with temperature. It is due to the fact that conduction current mainly is caused due to free charge present in the dielectric. Further, with increasing temperature, more number of free charge gain high thermal energy to enter into the conduction band which in turn increases the conductivity.

From Fig. 5.3 it can be observed that, dc conductivity can be reduced by introducing mixed oils than the pure oils. Among mixed oils, S4 shows most reduced conductive property. Again, from the Fig. 5.4 and 5.5, it can also be observed that the rate of the increment of conductivity for mixed oil based nanofluid reduces with temperature increment (upto 80˚C). It is to be stated here that, Ti atom has higher affinity to the hydroxyl group ($OH^-$).

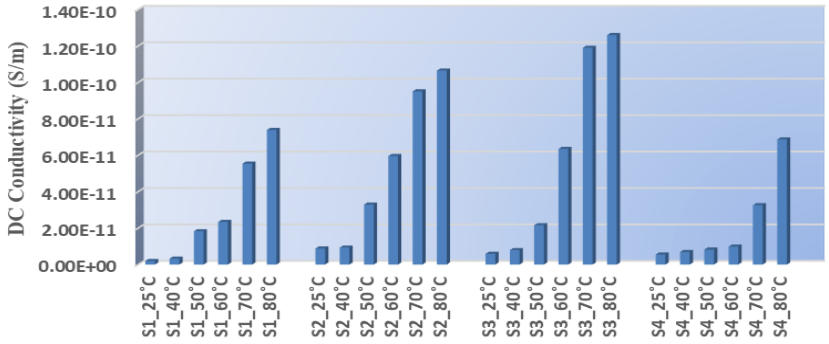


Fig. 5.3. Conductivity at different temperatures of various mixed oils.

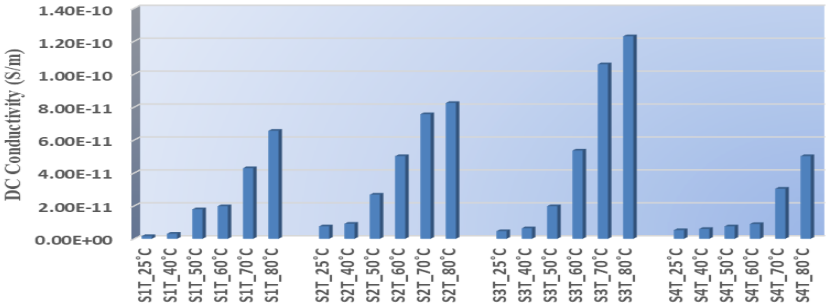


Fig. 5.4. Conductivity at different temperatures of mixed oil-based titania nanofluids.

Again, presence of $Al_2O_3$ attracts moisture and O atom in the alumina has an affinity towards the H+ ions present in the moisture and produces hydroxyl group ($OH^-$) [252]. This bonding makes an obstacle which may trap the free electrons moving towards anode. As a consequence, reductions of the mobility of those free electrons which results in reduction of the conductivity. Again, it should be mentioned here that, when nanoparticles trap the free electrons, become negatively charged particles whose mobility is lower than the free electrons which reduces the conductivity. From Figs. 5.3, 5.4 and

5.5 it can be revealed that S4A and S4T shows the better results in terms of dc conductivity.

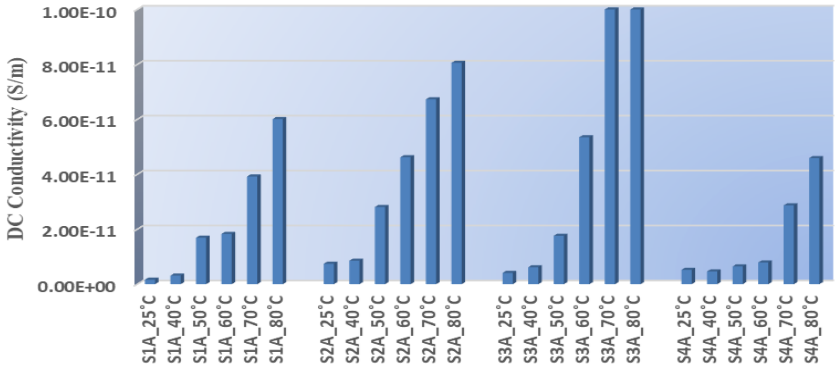


Fig. 5.5. Conductivity at different temperatures of mixed oil-based alumina nanofluids.

## *5.3.3. Estimation of Activation Energy*

Next, to determine the activation energy of the test samples, $ln(\sigma)$ is plotted against inverse of temperature ($K^{-1}$) as presented in Fig. 5.6. Thereafter, activation energy of the test samples has been evaluated from the slope of the curves using (3.4) (discussed in Chapter 3, Section 3.4.3) and has been given in Table 5.6.

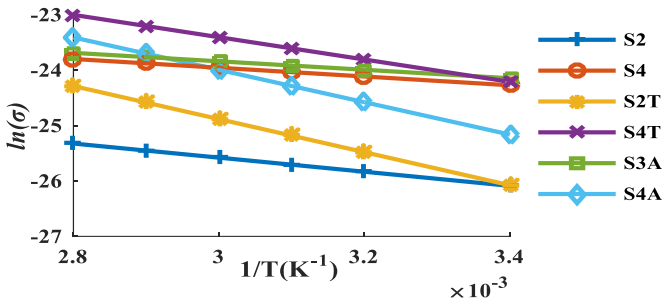


Fig. 5.6. Graph for determining the activation energy for prepared test samples.

Table 5.3 Activation Energy of Mixed Oil and Nanofluids

| Samples | $E_g$ in eV | Samples | $E_g$ in eV |
|---|---|---|---|
| **MO** | 0.58 | **S2T** | 0.66 |
| **VO** | 0.52 | **S3T** | 0.69 |
| **S1** | 0.58 | **S4T** | 0.68 |
| **S2** | 0.41 | **S1A** | 0.64 |
| **S3** | 0.65 | **S2A** | 0.63 |
| **S4** | 0.62 | **S3A** | 0.72 |
| **S1T** | 0.61 | **S4A** | 0.75 |

It may be observed from Table 5.3 that, presence of $Al_2O_3$ in mixed oil based nanofluids offers more activation energy than other prepared samples. As discussed above, the mixed oil based nanofluids containing $Al_2O_3$ absorbs the electrons resulting requirement of higher energy to break the barrier and hence hinder the movement of electrons towards the anode.

## *5.3.4. Results from Non-linearity Study in Conduction Current*

For investigating the linearity of the prepared mixed oil-based samples, $I_{cond}$ at 25°C have been depicted for mixed oils and mixed oil based nanofluids as shown in Fig. 5.7a, 5.7b and 5.7c, respectively and have been fitted with (Chapter 3, Equation 3.7) for different levels of applied voltage (50V, 100V, 150V, 180V and 200V). Thereby, the value of the power (*b)* at the aforementioned voltage have been calculated for all prepared samples and presented in Table 5.4.

It may be observed from Table 5.4 that, the value of *b* for mineral oil is highest in comparison with the pure vegetable oil and other prepared samples. Higher value of *b* indicates the existence of higher non-linearity which illustrates the higher possibility of space charge polarization [253]. This fact in turn indicates that, the field distribution becomes more distorted near the windings of the mineral oil-filled transformer during its operation. This distorted field distribution is responsible for accelerating its degradation process. Moreover, it may also be observed from Table 5.4 that, the value of *b* for the mixed oils dispersed with $Al_2O_3$ is lower in comparisons with the other prepared samples. This is due to the fact that, the Al atoms (within $Al_2O_3$) have an affinity towards $H^+$ ions which in turns develop a covalent bond [222].

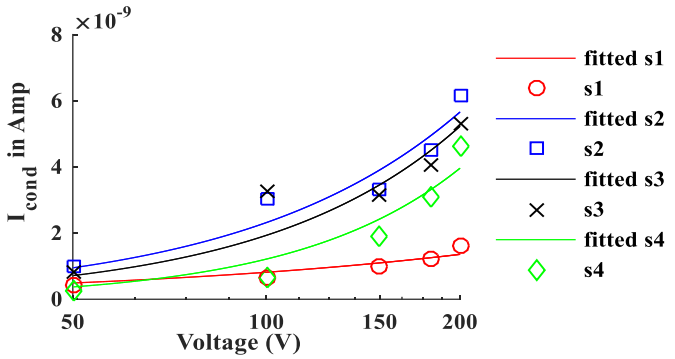


(a)

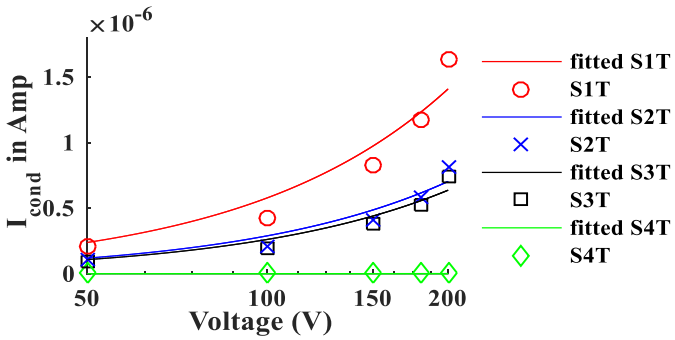


(b)

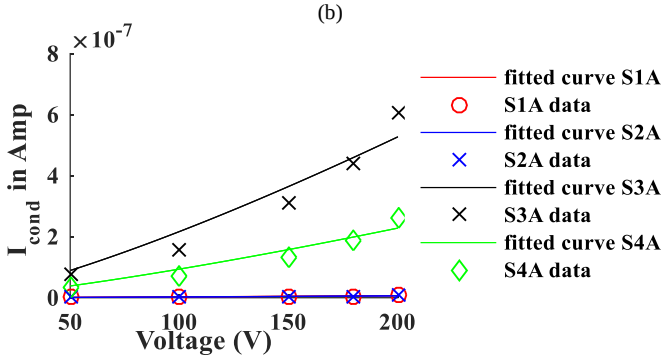


(c)

Fig. 5.7. Conduction current at different voltage level for (a) mixed oil and (b) mixed oil with titania and (c) mixed oil with alumina.

This covalent bond absorbs the space charges which are developed near electrodes. This phenomenon reduces the possibility of the space charge polarization and hence shows less non-linearity which in turn indicates the relatively less degradation of the insulation. It is to be mentioned here that, the value of the conductivity and the dielectric constant mainly is dependent on two mechanisms i.e. alignment of dipoles in the direction of applied field and movement of charge carriers. The dependency of conductivity and dielectric constant on the frequency mainly observed from the lower frequency to power frequency (50 Hz) ranges. At this frequency ranges, the charge carriers respond when the dielectric is applied to electric field. As the frequency reduces, more number of dipoles as well as charge carriers participate in polarization process (mainly due to space-charge polarization or interfacial polarization) resulting variation of conductivity and the dielectric constant [234]. However, in the higher frequency ranges (above 50Hz) significant numbers of charge carriers do not get ample time to respond when alternating field is applied [224]. Hence, it may be stated that the conductivity and the dielectric constant mainly change below power frequency ranges and remain almost unchanged in higher frequency ranges.

Table 5.4 Parameters for Non-linearity Study of Different Samples

| **Samples** | ***a*** | ***b*** | **Samples** | ***a*** | ***b*** |
|---|---|---|---|---|---|
| **MO** | 2.63e-14 | **1.744** | **S2T** | 7.95E-10 | **1.281** |
| **VO** | 1.12e-10 | **1.346** | **S3T** | 7.20E-10 | **1.281** |
| **S1** | 2.79E-11 | **1.533** | **S4T** | 3.46E-11 | **1.233** |
| **S2** | 6.17E-12 | **1.287** | **S1A** | 7.36E-12 | **1.089** |
| **S3** | 2.60E-12 | **1.436** | **S2A** | 6.70E-12 | **0.792** |
| **S4** | 4.72E-13 | **1.305** | **S3A** | 5.94E-10 | **1.081** |
| **S1T** | 1.58E-09 | **1.782** | **S4A** | 2.56E-10 | **1.082** |

## *5.3.5. Dielectric Dissipation Factor*

The FDS measurement employing IDAX 300 of mixed oils and mixed oil based nanofluids at 25˚C have been shown in the Fig. 5.8 and Fig. 5.9, respectively. From the both Fig.s, it can be observed that, the dielectric dissipation factor (*tanδ)* decreases with increasing frequency. It is obvious due to the fact that, initially lesser number of dipoles are intending to allign towards the applied field which gradually increases with time. So, at low frequency, most of the dipoles are trying to take part in dipolar polarisation and may interact with free electrons which increase the frictional losses hence the dielectric loss.

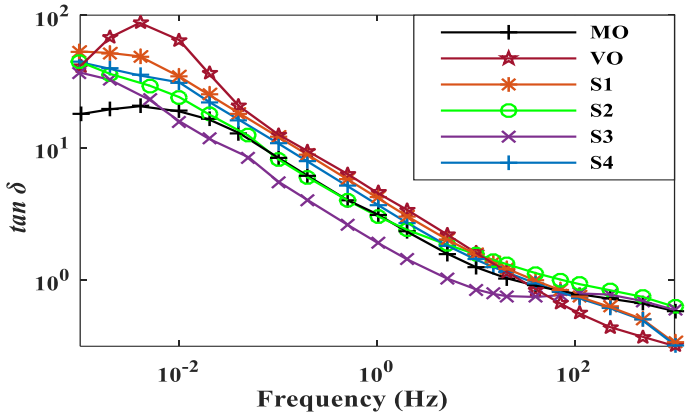


Fig. 5.8. Variation of *tanδ* for different prepared mixed oil at $25^0$C.

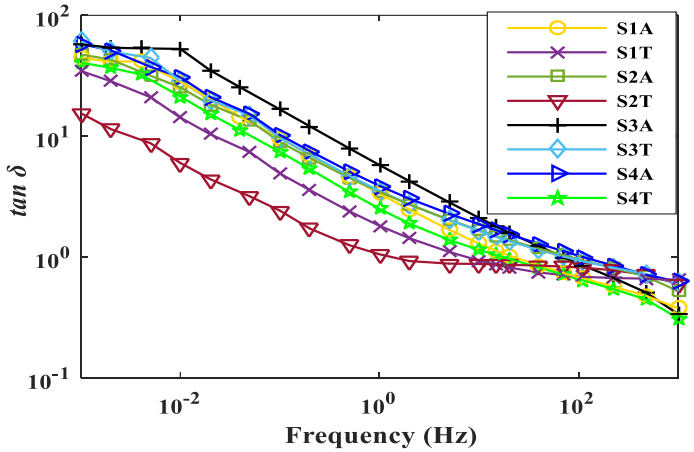


Fig. 5.9. Variation of *tanδ* for mixed oil based nanofluid at $25^0$C.

The comparative study from the Fig. 5.8 and 5.9 of the prepared samples indicates that, *tanδ* profile of S2 dispersed with $TiO_2$ becomes lower whereas the *tanδ* shows higher value for pure vegetable oil. Owing to the more tendency of moisture ingression, the *tanδ* becomes higher for the vegetable oil. However, presence of nano-particles within oils improves its ac conductivity.

## 5.3.6. Quantitative Effect of Temperature on the Dielectric Parameters

To investigate the quantitative effect of temperature on the $\varepsilon'$ and *tanδ*, statistical modeling is executed at different frequencies. This statistical model investigates how these dielectric parameters ($\varepsilon'$ and *tanδ*) are varied with temperature. For this purpose, the $\varepsilon'$ and *tanδ* values at different temperature are fitted with fourth order polynomial regression equation as shown in (5.3) [254].

$$y = P_1 t^4 + P_2 t^3 + P_3 t^2 + P_4 t + P_5 \tag{5.3}$$

Where *P5* is the intercept, $P_1$, $P_2$, $P_3$, and $P_4$ are the coefficients. In (5.3), *t* indicates temperature in °C and y-axis is either $\varepsilon'$ or *tanδ.* This fitting procedure has been repeated at each frequency. The regression models for $\varepsilon'$ and *tanδ* values have been shown in Fig. 5.10 and 5.11, respectively. From Fig. 5.10 it may be observed that, the increment of $\varepsilon'$ with temperature is more prominent at higher frequency range. Further, it may be observed from Fig. 5.11 that, the *tanδ* values of the prepared samples increase with temperature. This increment of *tanδ* with temperature becomes more prominent at lower frequency.

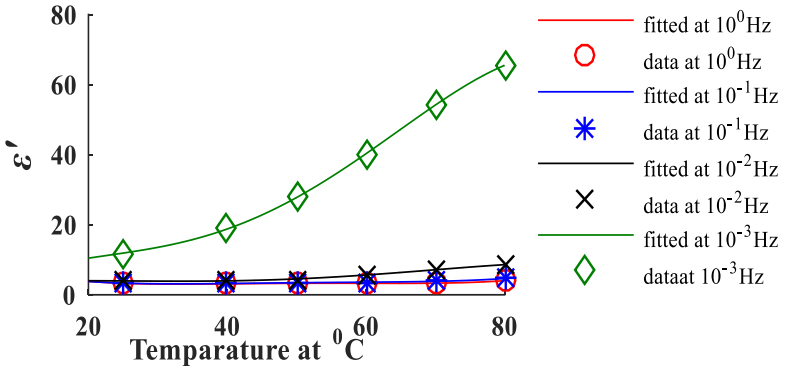


(a)

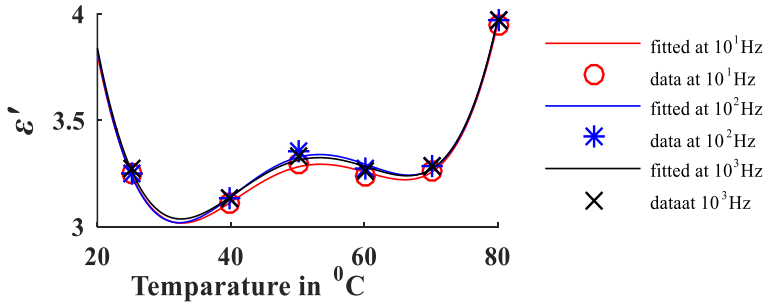


(b)

Fig. 5.10. Variation of $\varepsilon'$ with temperature at (a) lower frequency (1 mHz to 1Hz) and (b) higher frequency (10Hz to 1kHz).

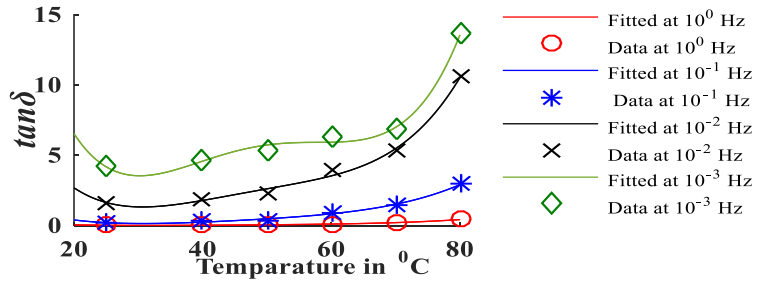


(a)

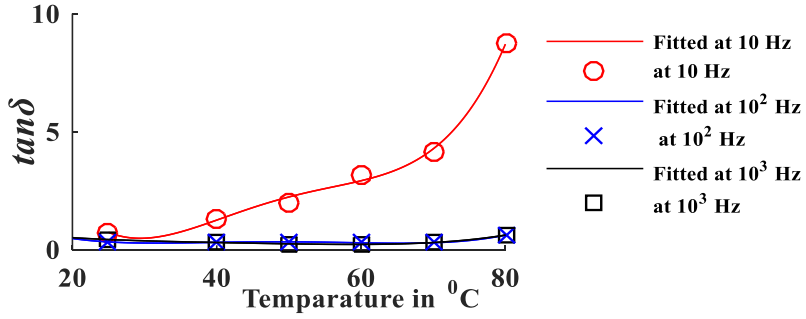


(b)

Fig. 5.11. Variation of *tanδ* with temperature at (a) lower frequency (1 mHz to 1Hz) and (b) higher frequency (10Hz to 1kHz).

It is also to be noted here that, the coefficient values ($P_1$, $P_2$, $P_3$, $P_4$ and $P5$) can be evaluated by (5.4 and 5.5). Using (5.4), the coefficients values at different frequencies (1000Hz, 100Hz, 10Hz, 1Hz, 0.1Hz, 0.01Hz and 0.001Hz) have been evaluated as given in Table 5.5 and 5.6 for $\varepsilon'$ and $tan\delta$, respectively.

$$P_i = \sum_{i=1}^{5} A_i f^{B_i} + C_i \tag{5.4}$$

$$T = \begin{bmatrix} 1 & t_1 & t_1^2 & t_1^3 t_1^4 \\ 1 & t_2 & t_2^2 & t_2^3 t_2^4 \\ . & . & . & . \; . \\ 1 & t_n & t_n^2 & t_n^3 t_n^4 \end{bmatrix}; P = \begin{bmatrix} P_5 \\ P_4 \\ P_3 \\ P_2 \\ P_1 \end{bmatrix}; y = \begin{bmatrix} y_1 \\ y_2 \\ . \\ . \\ y_n \end{bmatrix};$$

$$y=TP$$
$$T^T y = T^T TP$$
$$(T^T T)^{-1} T^T y = P \tag{5.5}$$

Table 5.5 Model Parameters for Dielectric Constant With Respect To Temperature

| Parameters | Dielectric Constant ($\varepsilon'$) magnitude | | | | | | |
|---|---|---|---|---|---|---|---|
| | 1000 Hz | 100 Hz | 10 Hz | 1 Hz | 0.1 Hz | 0.01 Hz | 0.001 Hz |
| $P_1$ | 2.065E-06 | 2.146E-06 | 2.004E-06 | 1.88E-06 | 1.474E-06 | -1.01E-06 | -7.698E-06 |
| $P_2$ | -0.0004 | -0.0004 | -0.0004 | -0.0004 | -0.0003 | 0.0002 | 0.0013 |
| $P_3$ | 0.0307 | 0.0319 | 0.0298 | 0.0281 | 0.0225 | -0.0109 | -0.0679 |
| $P_4$ | -0.9510 | -0.9857 | -0.9247 | -0.8786 | -0.7182 | 0.2352 | 1.6530 |
| $P_5$ (Intercept) | 13.6000 | 13.9200 | 13.3100 | 12.9100 | 11.3100 | 2.2990 | -4.9420 |
| $R^2$ | 0.9969 | 0.9961 | 0.9973 | 0.9988 | 0.9999 | 0.9995 | 0.9991 |

Table 5.6 Model Parameters for tan-delta with respect to Temperature

| Parameters | *tanδ* magnitude | | | | | | |
|---|---|---|---|---|---|---|---|
| | 1000 Hz | 100 Hz | 10 Hz | 1 Hz | 0.1 Hz | 0.01 Hz | 0.001 Hz |
| $P_1$ | 2.474E-07 | 7.024E-07 | 6.097E-06 | 2.616E-05 | 0.0002 | 0.0009 | 0.0024 |
| $P_2$ | -4.22E-05 | -0.0001 | -0.0011 | -0.0047 | -0.0313 | -0.1871 | -0.4650 |
| $P_3$ | 0.0027 | 0.0095 | 0.0837 | 0.3326 | 2.2290 | 13.2200 | 32.7500 |
| $P_4$ | -0.0865 | -0.2814 | -2.4780 | -10.1600 | -68.1200 | -396.8000 | -969.3000 |
| $P_5$ (Intercept) | 1.4640 | 3.2990 | 26.4800 | 115 | 775 | 4527 | 1.093E+04 |
| $R^2$ | 0.9756 | 0.9907 | 0.9968 | 0.9948 | 0.9952 | 0.9949 | 0.9954 |

The $R^2$ (which is more than 95%) values given in Table 5.5 and 5.6 shows the very good fitting of the $\varepsilon'$ or *tanδ* by the regression model. The variation of coefficients ($P_1$, $P_2$, $P_3$, $P_4$ and $P5$) with frequency (as shown in Table 5.5 and 5.6) have been fitted and the corresponding correlation have been shown in (5.5).

Table 5.7 Model Parameters with respect to Different Frequencies

| | Dielectric Constant ($\varepsilon'$) magnitude | | | | | *tanδ* magnitude | | | | |
|---|---|---|---|---|---|---|---|---|---|---|
| | $P_1$ | $P_2$ | $P_3$ | $P_4$ | $P_5$ | $P_1$ | $P_2$ | $P_3$ | $P_4$ | $P_5$ |
| *A* | 6.842 E-06 | 0.001 | -0.003 | 0.092 | 8.545 E-11 | 2.599 E-05 | -0.004 | 0.328 | -10.03 | 113.30 |
| *B* | 0.065 | -0.153 | -0.451 | -0.439 | 0.2195 | -0.6050 | -0.825 | -0.830 | -0.830 | -0.833 |
| *C* | -6.93 E-06 | -0.007 | 0.031 | -0.971 | 1.584 E-10 | 1.217 E-05 | -0.001 | 0.0108 | -0.307 | 3.347 |

The values of the parameters ($A_i$, $B_i$ and $C_i$) of (5.4) have been given in Table 5.7. By combining the (5.3) and (5.4), a general equation for estimating $\varepsilon'$ or *tanδ* at any temperature and frequency, have been derived and have been given by (5.6).

$$y(f,t) = \sum_{i=1}^{5} P_i t^{5-i} = \sum_{i=1}^{5} (A_i f^{B_i} + C_i) t^{5-i} \tag{5.6}$$

In (5.6), *y(f,t)* indicates $\varepsilon'$ or *tanδ* at any frequency and temperature. The significance of (5.6) is that, for a given value of frequency and temperature, the values of $\varepsilon'$ or *tanδ* can be evaluated for all the prepared test samples. For the validation of (5.6), *tanδ* (at 40 Hz, 25°C and 40°C) and $\varepsilon'$ (at 5 Hz, 25°C and 40°C) of the prepared sample has been evaluated using IDAX300 and

calculated through (5.6). The error between two results have been presented in Table 5.8. From Table 5.8, it can be observed that errors are within 12.11% which validate (5.6).

Table 5.8 Validation of (5.6) with IDAX300

| | Using IDAX300 | Using (15) | Error |
|---|---|---|---|
| *tanδ at* 25°C and 40 Hz | 6.359 | 5.589 | 12.11% |
| *tanδ at* 40°C and 40 Hz | 31.568 | 33.988 | 7.66% |
| *ε' at* 25°C and 5 Hz | 13.04 | 13.89 | 6.52% |
| *ε' at* 40°C and 5 Hz | 28.04 | 29.49 | 5.17% |

## 5.4. Inference

In this chapter, mixed oils have been prepared by mixing vegetable oil with mineral oil in a certain ratio. Further, $TiO_2$ and $Al_2O_3$ have been chosen for preparing mixed oil based nanofluids. Therefore, the dielectric properties like viscosity, dc conductivity, activation energy, *tanδ* of the prepared test samples have been compared with the conventional pure oils. Moreover, to study the effect of temperature on dielectric parameters, PDC and FDS measurement have been conducted at 25°C, 40°C, 50°C, 60°C, 70°C and 80°C. From the consequences, the key outcomes can be summarized as

a) Viscosity of samples S1 to S4 are reducing and becomes lowest in case of S4. Again, viscosity of S4 (with MO 90% + VO 10%) mixed with nano-particles are providing the best results among mixed oil based nanofluids.

b) 75% MO with 25% VO results more linear than the other mixed dielectrics. Again, Alumina nanoparticles dispersed in mixed dielectrics shows the least degree of nonlinearity.

c) Again, by dispersing $Al_2O_3$ in mixed oil, viscosity and nonlinearity in the conduction current can be reduced by 34% and 54%, respectively.

d) Alumina based nanofluids can enhance activation energy by 22.7% than base oil samples.

e) From the dc conductivity and *tanδ* analysis, it can be found that, S2 (75%MO + 25% VO) with $TiO_2$ showed the least at lower frequency.

f) A statistical modeling is executed at different frequency to understand the variation in the dielectric properties of the oil, and an expression involving all three parameters of frequency, temperature, and dielectric parameters (dielectric constant and *tanδ*) have been derived.

From the chapters 3, 4 and 5, it can be observed that, in search of new class of insulation, nanofluids, hybrid nanofluids and mixed oil based nanofluids shows enhanced dielectric properties in terms of viscosity, dc conductivity, nonlinearity study, $tan\delta$ and temperature dependency. Therefore, for evaluating an insulating oil for application in transformer, two important parameters i.e. breakdown voltage and ac conductivity should be studied. In view of this context, in the next chapter, all the prepared samples have been compared in terms of breakdown voltage and ac conductivity to investigate the quality of these prepared samples.

# Chapter 6

# Comparative Study on AC Breakdown Characteristics and AC Conductivity of Different Prepared Nanofluids

## 6.1. Introduction

Previous chapters of this thesis revealed that, $TiO_2$ or $Al_2O_3$ nanoparticles dispersed in mineral or vegetable oil can enhance dielectric parameters. Moreover, few literatures reported that dispersion of $SiO_2$ and $Al_2O_3$ nanoparticles in the transformer oil, the breakdown voltages can be improved by 9% and 12%, [255], respectively and for $TiO_2$ nanofluid it is about 19% with respect to transformer oil [256]. It should be mentioned here that, the quality of the oil can be determined by breakdown voltage measurement of the dielectric. However, it has been found that most of researches on nanofluids for transformer applications were conducted choosing mineral oil as base oil in which single nanoparticle was dispersed.

In this chapter, three types of nanofluids (as discussed in chapter 3, 4 and 5) were taken for experiment. To investigate the quality of the prepared nanofluids, AC breakdown voltages (ACBDV) of these prepared nanofluids were measured in the laboratory. A statistical method i.e. Weibull distribution function was adopted for estimating the average ac breakdown voltages with 1%, 10%, and 50% risk probabilities which are considered as very important parameters for the design of the power system equipment. Therefore, the conformity test of the experimental data was conducted to ensure whether those data-set follow the Weibull distribution or not. The breakdown of the oil mainly due to the amount of free charges presence in the oil. These charges are important factor for occurring the electron avalanches phenomenon. Hence, from the conductivity value, the number of charges i.e. the main reason of the breakdown voltage can be understood. Therefore, the prepared nanofluids were subjected to Frequency Domain Spectroscopic (FDS) measurement to determine the ac conductivity, an important parameter for any dielectric. Moreover, the effect of nanoparticles on ac conductivity at different stages of frequencies have been studied by ladder phenomenon occurred in ac conductivity.

## 6.2. Brief Theory on Statistical Analysis of AC Breakdown Voltage: by Weibull Distribution

Weibull distribution is regarded as the most used statistical law for evaluating the breakdown voltage of the insulating materials. (6.1) indicates the cumulative Weibull distribution function where $V_b$, $\alpha$ and $\beta$ indicates as the measured data of breakdown voltages, scale parameter (which is associated with the scattering of the measured data and specifies the degree of failure) and shape parameter (which is considered as the slope of the Weibull plot), respectively [257, 258].

$$F(\mathrm{V}_b \mid \alpha, \beta) = (1 - e^{-(\frac{V_b}{\alpha})\beta}) \tag{6.1}$$

To ensure whether the measured data would follow the Weibull distribution, the Anderson - Darling [259] hypothesis test has been conducted to determine the *p-value* which is considered as the probability that determines the confirmation against the null hypothesis. It is a well-known fact that, lesser *p*-values is basically stronger indication against the null hypothesis. Typically, a significance level (α) of 0.05 has been indicated to check whether the measured data follow Weibull distribution or not [259]. Then, it can be concluded that, for each sample's dataset, if the calculated *p*-values is more than the significance level of 0.05, it directs that dataset follow Weibull distribution.

## 6.3. Brief Theory on Ladder Phenomenon Observed in Complex Conductivity obtained from FDS

From the FDS scan, the ac conductivity ($\sigma'$) of different prepared samples have been calculated using (6.2) [260].

$$\sigma' = \frac{C'' \times \varepsilon_0 \omega}{C_0} \tag{6.2}$$

Where $C''$, $C_0$ and $\varepsilon_0$ have been considered as imaginary part of complex capacitance, geometric capacitance and permittivity in free space, respectively. $\sigma'$ curve strongly depends on the frequency at higher frequency ranges whereas, $\sigma'$ curves remains constant at the lower frequency ranges which reflect the frequency independence. The $\sigma'$ curve (from frequency ranges 1 mHz to 1 kHz) comprises of three stages having different slopes. In this context, the threshold frequency is regarded as a point where $\sigma'$ curves changes its slopes. This phenomenon of slope changes of the $\sigma'$ curves are

considered as the ladder phenomenon [261]. To illustrate this ladder phenomenon as per Jonscher's law, (6.3) is considered [262].

$$\sigma'(\omega) = \sigma_{dc} + K_1 f^m + K_2 f^n \tag{6.3}$$

Where, $\sigma'(\omega)$ and $\sigma_{dC}$ are defined as the ac conductivity which is frequency dependent and dc conductivity, respectively. Here, $K_1$ and $K_2$ are the constants depends on the factors like temperature and insulating material characteristics. Additionally, *m* and *n* are considered as the power-law indexes (typically value becomes within 0 to 1) of the testing frequency *f*.

## 6.4. Preparation of Test Oil Samples & Experimental Procedures

A beaker containing 400ml of mineral or vegetable oil has been heated at 50˚C for 48 hours followed by vacuum treatment keeping pressure less than 1 kPa for another 48 hours to ensure fully removal of moisture from the oils. Even-after the pouring of prepared samples into the breakdown-test cell, the aforementioned heat and vacuum treatment was conducted for ensuring the fully removal of microbubbles. Next, three types of nanofluids were prepared followed by the procedure discussed in chapter 3, 4 and 5. Then, 400ml of the nanofluids samples were subjected to the aforementioned treatment and were poured into the breakdown-test cell.

TABLE 6.1. Nomenclature of the prepared samples

| Name | Prepared samples | Name | Prepared samples |
|---|---|---|---|
| MO | Mineral oil | VO | Vegetable oil |
| MOA | MO+ $Al_2O_3$ | VOA | VO+ $Al_2O_3$ |
| MOT | MO+ $TiO_2$ | VOT | VO+ $TiO_2$ |
| MOA3T5 | MO+30mg $Al_2O_3$+50 mg $TiO_2$ | VOA3T5 | VO+ 30mg $Al_2O_3$+50 mg $TiO_2$ |
| MOA4T4 | MO+40mg $Al_2O_3$+40 mg $TiO_2$ | VOA4T4 | VO+40mg $Al_2O_3$+40 mg $TiO_2$ |
| MOA5T3 | MO+50mg $Al_2O_3$+30 mg $TiO_2$ | VOA5T3 | VO+50mg $Al_2O_3$+30 mg $TiO_2$ |
| S1 | MO 90% + VO 10% | S1T<br>S1A | S1+ $TiO_2$<br>S1+ $Al_2O_3$ |
| S2 | MO 80% + VO 20% | S2T<br>S2A | S2+ $TiO_2$<br>S2+ $Al_2O_3$ |
| S3 | MO 75% + VO 25% | S3T<br>S3A | S3+ $TiO_2$<br>S3+ $Al_2O_3$ |
| S4 | MO 70% + VO 30% | S4T<br>S4A | S4+ $TiO_2$<br>S4+ $Al_2O_3$ |

The nomenclatures of the prepared samples have been presented in Table 6.1. After the preparation of stable nanofluids, the samples were subjected to AC breakdown voltage test using the oil breakdown test kit (as described in section 2.2.2.6). Moreover, the electrode setup was dipped into the samples for the FDS measurements employing IDAX 300 as shown in Fig. 2.15 (in Chapter 2) for the estimation of ac conductivity.

## 6.5. Results & Discussion

### *6.5.1. Average AC Breakdown Voltages (ACBDV) Analysis Viscosity*

The variation of the average power frequency breakdown voltage of the pure mineral oil, vegetable oil and their nanofluids (first and second types) are presented using box-plot in the Fig. 6.1. A boxplot is basically defined by five points of Data i.e. minimum, maximum, sample median, and the two quartiles (first and third). It is to be stated here that, solid square in the box plot indicates that most of the distribution of group data are nearer to the upper quartile (black in Figs. 6.1 and 6.2). Again, hollow Square in the box plot indicates that, most of the distribution of group data are nearer to the lower quartile.

From Fig. 6.1, it can be observed that, average ACBDV is higher for pure vegetable oil than pure mineral oil. However, dispersion of the nanoparticles in the base oil shows improvement in ACBDV. Among the nanofluids, Titania based nanofluids exhibit higher breakdown voltages. It is well-known fact about the dispersion of $TiO_2$ in nanofluids that, hydroxyl ($OH^-$) ions are attached on the surface of Ti atoms and becoming a negatively charged particles [256]. In case of dispersion of $Al_2O_3$ in nanofluids, O atoms in Alumina absorbs $H^+$ ions which further creates hydroxyl ions and becomes a negatively charged particles. The mobility of these negatively charged particles is slower than electrons which further results in reducing the propagation velocity of electrons in the base oil by scavenging the electrons [256]. As a consequence, resistance against streamer development is increased.

Furthermore, it can be observed from Fig. 6.1 that, hybrid nanoparticles exhibit improved ACBDV for both base oils. For the samples MOA3T5 and VOA3T5, the ac breakdown voltage is enhanced by 71% and 67%, respectively in comparisons with the base oils. It is to be mentioned here that, in the presence of electric field, bond has been developed with Ti atom and hydroxyl ($OH^-$) atom. Another fact has been observed for $Al_2O_3$ that, unlike

$TiO_2$, $Al_2O_3$ absorbs $H^+$ ions which further creates hydroxyl ions. Moreover, in the case of hybrid nanofluids, $Al_2O_3$ is responsible for generating hydroxyl ($OH^-$) ions which is attached with $TiO_2$ by creating a bond as shown in Fig. 4.5 (in Chapter 4). This bond has more capability to capture free electrons. Hence, reduce the possibility of streamers development.

Fig. 6.2 represents the average value of ACBDV for mixed oil and third type of nanofluids using box-plot. It can be noticed that, average ACBDV for mixed oil is improved than mineral oil. However, this improvement of ACBDV cannot surpass the same for vegetable oil.

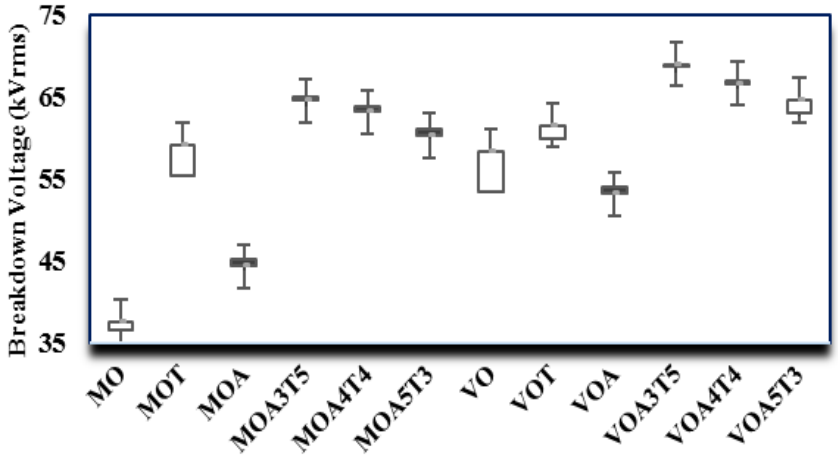


**Fig. 6.1.** ACBDV for mineral and vegetable oil based nanofluids and their hybrid nanofluids.

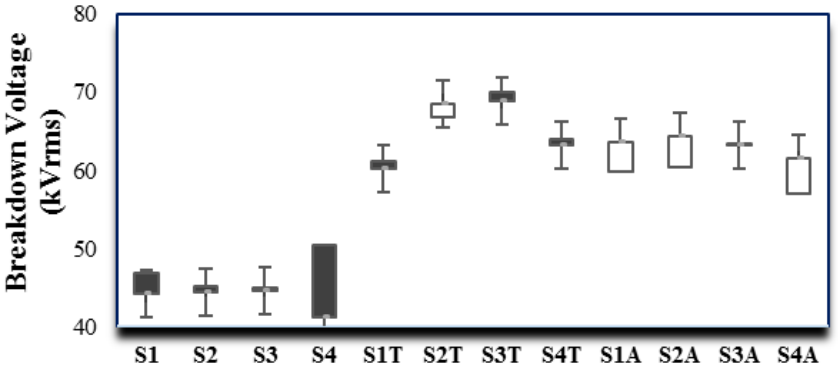


**Fig. 6.2.** ACBDV for mixed oil and their nanofluids.

Further it has been revealed that, presence of nanoparticles (both $TiO_2$ and $Al_2O_3$) can provide enhancement of the average ACBDV of mixed oil even comparing with vegetable oil. Among the mixed oil based nanofluids, dispersion of Titania in the mixed oil shows better results. This improvement may be owing to the fact that, Titania nanoparticles scavenge more electrons and traps the electrons resulting slower movement of these negatively charged particles which further provide more resistance against streamer development. So, it can be concluded that, sample S3T shows most improvement of ACBDV from pure oils. Moreover, it is to be mentioned here that the BDV under DC voltage is lower than the AC voltage. This discrepancy may be explained by analyzing with the injected space charge which depends on the type of voltage i.e. AC or DC. Under the application of DC voltages, homo-charges are injected which makes the base oil more conducting [263]. This fact in turn decreases the BDV under DC voltage. However, during the application of AC voltages, hetero-charges are injected which neutralize themselves [263]. The neutralization phenomena among the hetero-charges reduces the effective free charges which in turn enhances the BDV of the liquid samples under AC voltage.

### *6.5.2. Statistical analysis of Experimental Data of ACBDV by Weibull Distribution*

Figs. 6.3 to 6.7 show the Weibull plot of the average value of the pure oils and prepared nanofluids.

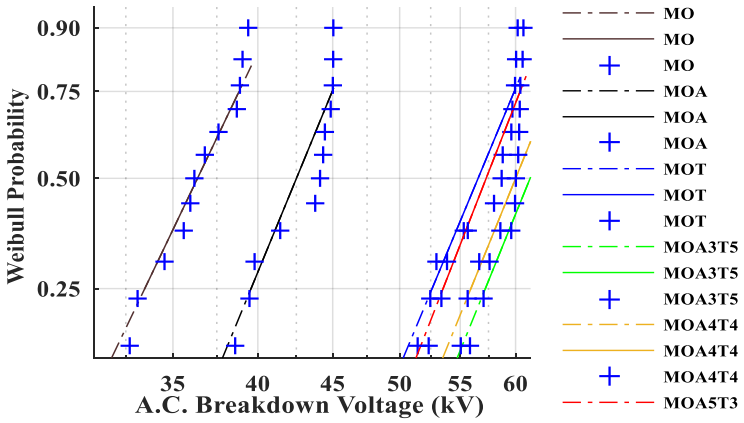


**Fig. 6.3.** Weibull distribution for ACBDV of mineral oil and its nanofluids.

From Figs. 6.3 to 6.7, *p* value has been calculated and has been presented in Table 6.2. From Table 6.2, it can be observed that, the p-values of all the measurement points (except S1T and S4A) are above 0.05 which further indicates that, the measurement points would follow the Weibull distribution.

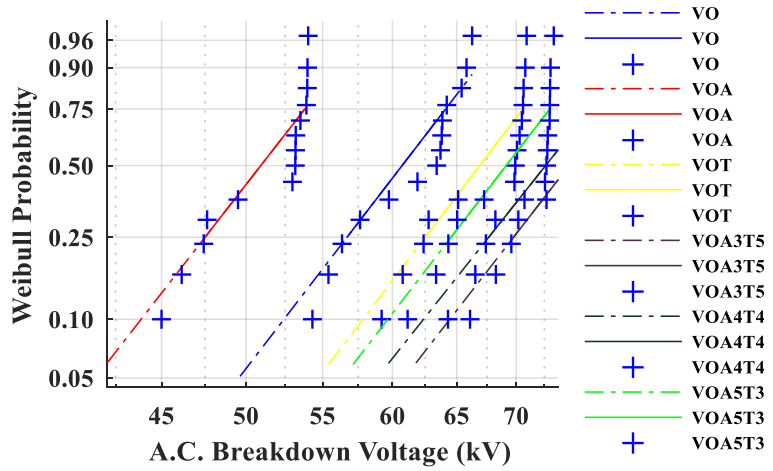


**Fig. 6.4.** Weibull distribution for ACBDV of vegetable oil and its nanofluids.

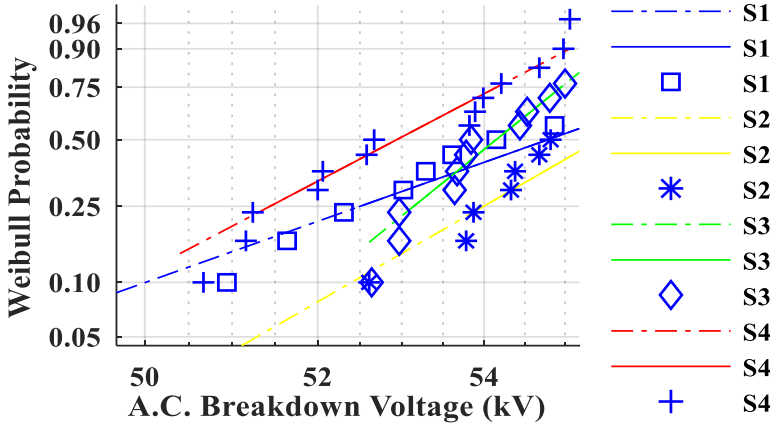


**Fig. 6.5.** Weibull distribution for ACBDV of mixed oil.

From these plots, the ACBDV breakdown voltage of prepared samples at 1%, 10% and 50% breakdown risk probabilities have been estimated which

has been presented in Table 6.3. It is very important to estimate the ACBDV at 1% cumulative probability which can provide an estimation of the lowest possible ACBDV. Hence, this 1% cumulative probability value provides an indication about the reliability of liquid dielectric. It should be mentioned here that, for determination of safety coefficient for electrical equipment design, breakdown at 50% cumulative probability risk has been considered.

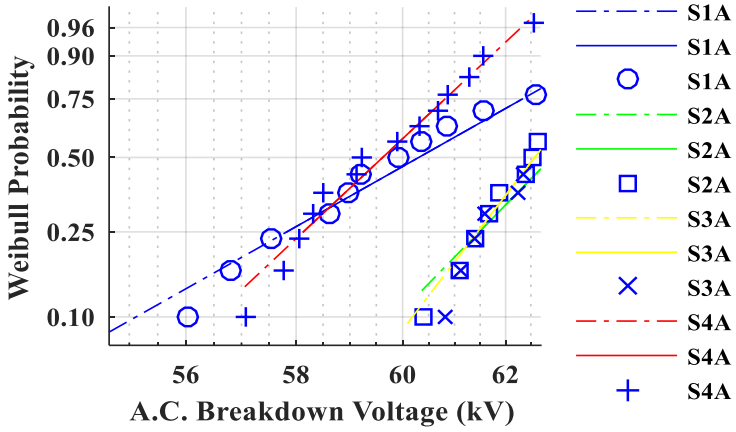


**Fig. 6.6.** Weibull distribution for ACBDV of Alumina dispersed in mixed oil.

From Table 6.3, it can be seen that at the lowest possible breakdown, hybrid nanofluids exhibit improved breakdown strength than the pure oil as well as nanofluids consisting only Titania or Alumina. This may also be due to the presence of the bond as discussed in Chapter 4, Section 4.3.2, which can more actively participated in electron scavenging mechanism to restrict the streamer propagation [218]. Another theory of a potential well model which is proposed by Takada *et al.* [264] suggests that, it will suppress the formation of space charge in the base matrix when the dispersion of the nanoparticles having higher permittivity in the base matrix results in a deeper trap well. It has been revealed by Lv *et al.* [265] that, dispersion of nanoparticles in the base oil aggravates the process of trapping and de-trapping in shallower traps which helps in the faster transfer of charge carriers and enhance the dielectric strength of the base oil. According to the Xu *et al.* [266] energy band theory, by introducing trapping and de-trapping process, the effective energy of the charge carriers can be decreased.

According to Electronic band theory, accumulation of charge layer is developed in the interface of electrode and liquid in equilibrium state for

equalizing the Fermi level of the dielectric and the metal electrodes. The corresponding energy levels of negative and positive ionized state are increased due to the formation of a series of trap sites for the nanoparticles. Now, for the case of hybrid nanofluids, their strong bond formation (as shown in Fig. 4.5) results in higher energy level to trap more number of charges.

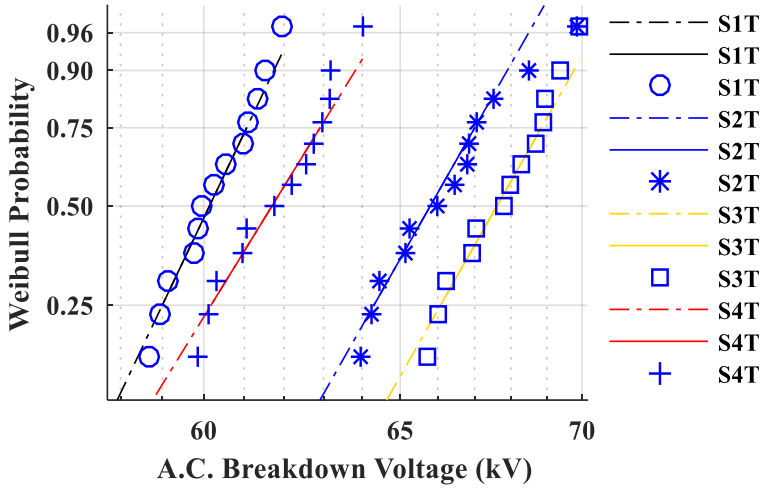


**Fig. 6.7.** Weibull distribution for ACBDV of Titania dispersed in mixed oil.

It is reported in [257] that, the electric potential well due to an induced dipole moment of nanoparticles under the application of electric field are responsible for developing a trapping site for charge carriers. Due to strong bond formation (as shown in Fig. 4.5 in Chapter 4) of hybrid nanofluids, the induced dipole moment is higher than other nanofluids consisting single nanoparticle which further results in more trapping sites. Moreover, due to the high dielectric constant of the nanoparticles, the trapped depth and the effective range of potential well is higher in the case of hybrid nanofluids. Due to these facts, hybrid nanofluids are capable to suppress more space charge formation hence, resist the formation of streamers. This fact in turn helps in the improvement of the insulating performance of the nanofluids. So, from Table 6.3, it can be further concluded that, samples S2T, S3T and S4T can be considered as better liquid dielectric for 1, 10 and 50% breakdown probabilities among all the prepared samples.

As discussed in Chapter 3, section 3.4.4.1, Titania nanoparticles have affinity towards hydroxyl ions. So, Titania nanoparticles in the mixed oil

adsorb the hydroxyl ions which results in induced dipole moment and results in higher effective range of potential well and trapped depth. That is why, S2T, S3T, and S4T samples may trap more charge carriers hence, resist the formation of streamers. However, it can be observed from Table 6.2 that, breakdown data of S1T sample does not follow Weibull distribution.

Table 6.2. Conformity based on *p*-value, $\alpha$ and $\beta$ for Weibull distribution plots of the ACBDV of various nanofluids

| **Samples** | ***p* value** | **Conformity** | $\alpha$ | $\beta$ |
|---|---|---|---|---|
| MO | 0.18 | Accepted | 37.3335 | 16.1763 |
| MOT | 0.41 | Accepted | 58.1588 | 18.7259 |
| MOA | 0.42 | Accepted | 43.6383 | 18.8950 |
| MOA3T5 | 0.48 | Accepted | 63.1322 | 18.6577 |
| MOA4T4 | 0.49 | Accepted | 61.9477 | 18.7276 |
| MOA5T3 | 0.49 | Accepted | 59.0082 | 18.7167 |
| VO | 0.47 | Accepted | 62.832 | 17.2444 |
| VOT | 0.46 | Accepted | 68.7675 | 19.0664 |
| VOA | 0.45 | Accepted | 52.2923 | 18.7744 |
| VOA3T5 | 0.49 | Accepted | 76.9679 | 18.8648 |
| VOA4T4 | 0.47 | Accepted | 74.7862 | 18.7072 |
| VOA5T3 | 0.50 | Accepted | 71.2050 | 19.0093 |
| S1 | 0.12 | Accepted | 55.6814 | 22.2361 |
| S2 | 0.06 | Accepted | 56.1918 | 29.7389 |
| S3 | 0.29 | Accepted | 54.6595 | 54.4578 |
| S4 | 0.67 | Accepted | 53.6311 | 40.1761 |
| S1T | 0.03 | Not Accepted | 60.5841 | 57.0562 |
| S2T | 0.36 | Accepted | 66.8359 | 35.3551 |
| S3T | 0.28 | Accepted | 68.1987 | 50.6330 |
| S4T | 0.38 | Accepted | 62.2799 | 46.9629 |
| S1A | 0.16 | Accepted | 61.2346 | 23.5856 |
| S2A | 0.32 | Accepted | 63.3051 | 49.8505 |
| S3A | 0.06 | Accepted | 63.1424 | 58.7059 |
| S4A | 0.03 | Not Accepted | 60.2947 | 38.6244 |

So, any conclusion cannot be drawn for S1T. However, from Average AC Breakdown Voltages analysis it may be observed that breakdown voltage of

S1T is lower than S2T, S3T, and S4T samples. Again, unlike Titania, Alumina nanoparticles have a tendency to introduce more moisture content in the base matrix due to its hygroscopic nature.

Table 6.3 ACBDV at various breakdown probabilities for different prepared nanofluids

| Samples | E (kV) at 1% | E (kV) at 10% | E (kV) at 50% |
|---|---|---|---|
| MO | 4.955 | 12.272 | 25.392 |
| MOT | 23.661 | 35.144 | 48.262 |
| MOA | 18.051 | 26.602 | 36.303 |
| MOA3T5 | 28.422 | 40.277 | 53.265 |
| MOA4T4 | 28.209 | 39.780 | 52.403 |
| MOA5T3 | 26.922 | 37.936 | 49.943 |
| VO | 26.963 | 39.031 | 52.503 |
| VOT | 30.608 | 43.622 | 57.953 |
| VOA | 22.613 | 32.656 | 43.844 |
| VOA3T5 | 35.151 | 49.502 | 65.139 |
| VOA4T4 | 33.220 | 47.391 | 63.007 |
| VOA5T3 | 33.183 | 46.302 | 60.478 |
| S1 | 12.869 | 29.593 | 47.691 |
| S2 | 6.582 | 22.508 | 49.321 |
| S3 | 22.432 | 38.842 | 44.674 |
| S4 | 25.162 | 38.482 | 46.242 |
| S1T | 2.158 | 9.878 | 33.438 |
| S2T | 46.119 | 54.294 | 61.882 |
| S3T | 46.255 | 55.000 | 63.191 |
| S4T | 45.489 | 52.261 | 58.413 |
| S1A | 15.331 | 28.579 | 47.085 |
| S2A | 42.197 | 56.054 | 63.269 |
| S3A | 12.645 | 26.281 | 47.246 |
| S4A | 2.658 | 16.025 | 67.656 |

Due to this fact, number of charge carriers are more in the base oil than the Titania based nanofluids. This in turn results in lower breakdown voltage for S1A, S3A, and S4A than S2T, S3T, and S4T. These facts in turns resist to

form the breakdown channel (resisting to bridges between anode and cathode). Therefore, it can be stated that, oil with nanoparticles have better insulating properties and can be considered as better insulation for transformers or capacitors.

From the above discussion, it can be stated that, the probable reasons of the breakdown voltage are the streamer development in the insulating oils. This streamer development is mainly due to the electron avalanches phenomenon. So, the number of free charges is an important factor for occurring the electron avalanches phenomenon. Hence, from the conductivity value, the number of charges i.e. the main reason of the breakdown voltage can be understood.

### *6.5.3. AC Conductivity*

From the FDS scan, the ac conductivity ($\sigma'$) of different prepared samples have been calculated using (6.2) [260] and has been shown in Figs. 6.8-6.11 for different prepared samples.

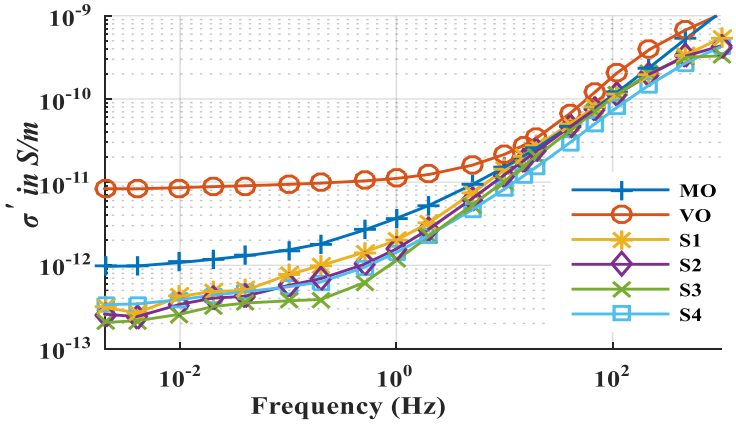


**Fig. 6.8.** AC conductivity for pure and mixed oils.

The values of $\sigma_{dc}$, $K_1$, $K_2$, $m$ and $n$ for different samples have been presented in Table 6.4. From Figs. 6.8-6.11, the ladder phenomenon of ac conductivity has been described. It can be seen from Fig. 6.8-6.11 that, the first threshold frequency is 1 Hz i.e. in the first stage (below 1 Hz), ac conductivity does not depend on frequency so, $\sigma'$ can be considered as dc conductivity.

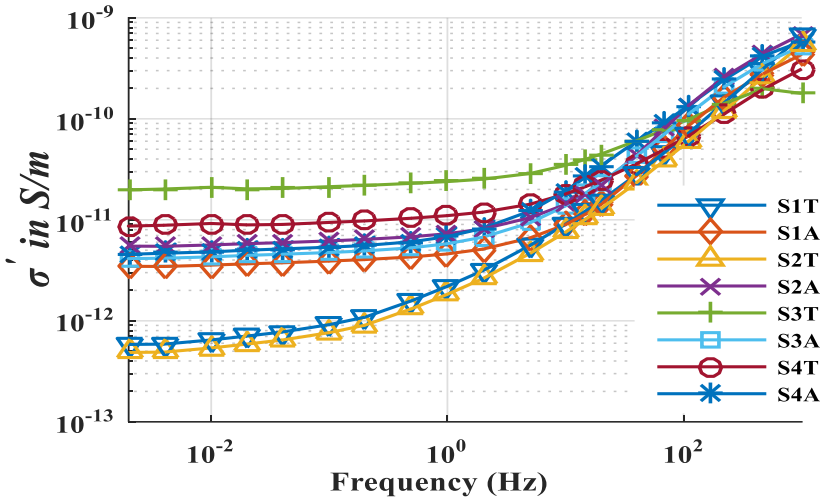


**Fig. 6.9.** AC conductivity for mixed oils based nanofluids.

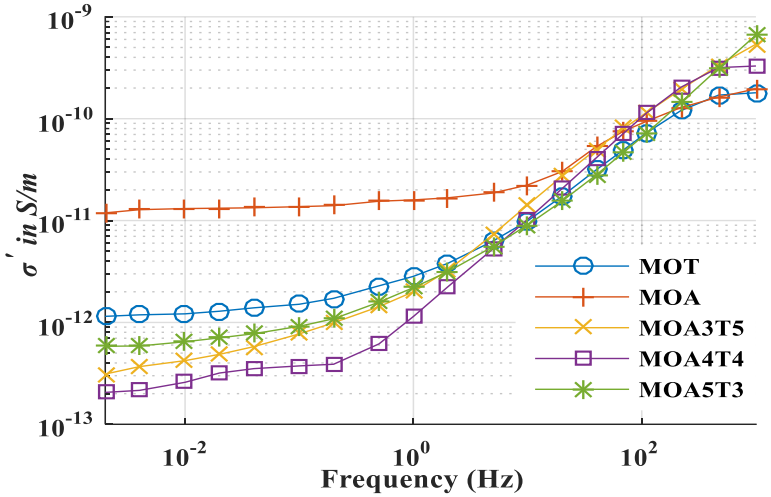


**Fig. 6.10.** AC conductivity for mineral oil based nanofluids.

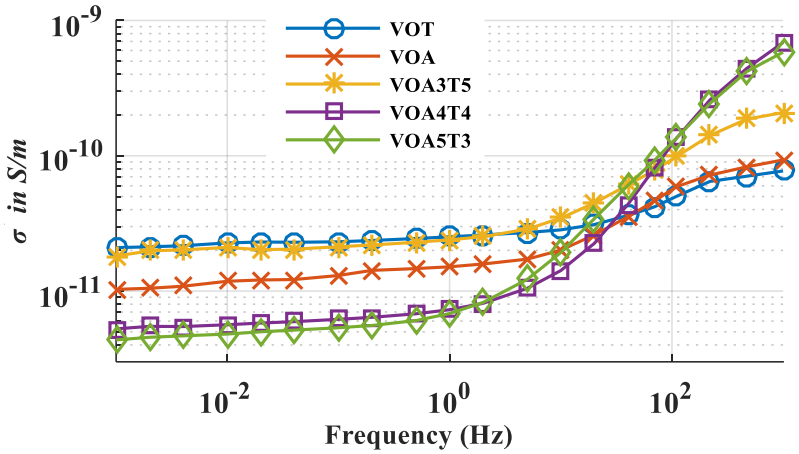


**Fig. 6.11.** AC conductivity for vegetable oil based nanofluids.

In this stage, by dispersing hybrid nanofluids in mineral oil can reduce the conductivity to the lowest limit among the prepared samples. Then, from Figs. 6.8-6.11, next threshold frequency has been pointed at 100 Hz. So, from 1 Hz to 100 Hz i.e. in the second stage, the variation of $\sigma'$ becomes nonlinear with the change in frequency. Therefore, beyond 100 Hz i.e. in the third stage, AC conductivity becomes more nonlinear with the increment of frequency. However, in the second and third stage, mixed oil and their Titania based nanofluids shows least value of slope i.e. reduce the conductivity in higher frequency. *m* and *n* of all the stages are different for different samples. Thus, it can be understood that, the frequency dependency of ac conductivity for different samples is different. This is due to the fact that, value of *m* and *n* is dependent on the dipolar polarization and interfacial polarization which is not similar for different samples [261, 253]. It can be observed from Fig. 6.11 that, the ac conductivity of VOA3T5 is higher than that of VOA. This discrepancy may be due to the unbalanced molecular structure of $TiO_2$ nanoparticles. In $TiO_2$ nanoparticles, different interatomic distances between one Ti-O atom can be observed. Again, VO has an affinity towards moisture. Therefore, this unbalanced molecular structure mainly responsible for strong polarization characteristics in the crystal due to more possibility of Ti-O interaction in the presence of more moisture in base oil which in turn results in higher conduction current.

Table 6.4 Parameters of (6.3) for different samples

| Samples | $\sigma_{DC}$ (S/m) | $K_1$ | m | $K_2$ | n |
|---|---|---|---|---|---|
| MO | 4.54E-12 | 5.94E-12 | 0.473 | -2.15E-12 | 0.830 |
| MOT | 1.74E-12 | -1.15E-12 | 0.934 | 4.89E-12 | 0.757 |
| MOA | 1.45E-11 | -1.02E-10 | 0.792 | 1.00E-10 | 0.655 |
| MOA3T5 | 2.93E-13 | 2.78E-12 | 0.684 | 9.39E-11 | 0.097 |
| MOA4T4 | 6.20E-13 | 6.25E-12 | 0.957 | 5.62E-11 | 0.157 |
| MOA5T3 | 4.63E-13 | 4.50E-10 | 0.485 | -5.44E-09 | 0.141 |
| VO | 9E-11 | -5.70E-13 | 0.917 | 7.43E-12 | 0.757 |
| VOT | 1.23E-11 | 6.27E-11 | 0.110 | 8.44E-11 | 0.389 |
| VOA | 1.22E-11 | 3.51E-10 | 0.490 | -3.39E-10 | 0.337 |
| VOA3T5 | 2.25E-12 | -8.87E-11 | 0.655 | 6.31E-11 | 0.706 |
| VOA4T4 | 1.18E-12 | 1.16E-09 | 0.045 | 9.91E-12 | 0.822 |
| VOA5T3 | 1.31E-12 | 9.94E-12 | 0.950 | -1.47E-12 | 0.439 |
| S1 | 6.51E-13 | 1.21E-11 | 0.567 | -9.45E-11 | 0.053 |
| S2 | 7.53E-13 | 1.33E-11 | 0.934 | -1.04E-11 | 0.568 |
| S3 | 4.66E-13 | 1.34E-09 | 0.337 | -1.00E-10 | 0.794 |
| S4 | 1.23E-13 | 4.61E-09 | 0.165 | -4.72E-09 | 0.262 |
| S1T | 4.24E-13 | -2.78E-11 | 0.153 | -9.11E-11 | 0.538 |
| S2T | 5.13E-11 | -9.37E-13 | 0.817 | -2.82E-11 | 0.084 |
| S3T | 3.04E-11 | 4.82E-11 | 0.145 | 5.95E-12 | 0.869 |
| S4T | 9.27E-12 | 2.59E-11 | 0.144 | 7.25E-12 | 0.622 |
| S1A | 2.35E-12 | 9.66E-12 | 0.748 | 2.26E-10 | 0.083 |
| S2A | 3.52E-12 | 1.38E-09 | 0.442 | -4.15E-11 | 0.961 |
| S3A | 2.19E-12 | 5.09E-12 | 0.800 | -1.38E-12 | 0.911 |
| S4A | 1.92E-12 | 7.91E-10 | 0.401 | -2.47E-09 | 0.239 |

## 6.6. Inference

This investigation mainly focused on the investigation on the effect of $TiO_2$, $Al_2O_3$ and their mixture on the ac dielectric properties (average power frequency breakdown voltages and ac conductivity) when dispersed in the mineral oil, vegetable oil or their mixture. After the preparation of the nanofluids, ac breakdown voltage measurement and FDS measurement have been conducted. From the ACBDV experiment, the breakdown voltages for each sample with 1%, 10%, and 50% risk probabilities has been estimated using Weibull distribution. Besides, ac conductivity has been calculated from FDS scan. From the experimental results, the following inferences can be drawn.

i. Average ACBDV is higher for pure vegetable oil than pure mineral oil. Among the nanofluids, Titania based nanofluids exhibit higher breakdown voltages than the pure oils.

ii. Hybrid nanoparticles exhibit improved ACBDV for both base oils. For the samples MOA3T5 and VOA3T5, the ac breakdown voltage can be enhanced by 71% and 67%, respectively than the base oils.

iii. The average ACBDV for mixed oil is improved than mineral oil. However, this improvement of ACBDV cannot surpass the same for vegetable oil. Further it has been revealed that, presence of nanoparticles (both $TiO_2$ and $Al_2O_3$) can provide enhancement of the average ACBDV of mixed oil even comparing with vegetable oil. Therefore, sample S3T shows most improvement of ACBDV from pure oils.

iv. From the Weibull distribution analysis, it can be observed that, samples S2T, S3T and S4T can be considered as better liquid dielectric for 1%, 10% and 50% breakdown probabilities among all the prepared samples.

v. In the first stage of ladder phenomenon of ac conductivity, by dispersing hybrid nanofluids in mineral oil can reduce the conductivity to the lowest limit among the prepared samples. However, in the second and third stage of ladder phenomenon of ac conductivity, mixed oil and their Titania based nanofluids reveal least value of slope i.e. reduce the conductivity in higher frequency.

From this chapter, the quality of the different prepared oil has been investigated considering ac breakdown voltage and ac conductivity to search the next generation dielectric for transformer. However, for the transformer insulation, moisture has been considered as the biggest enemy for insulation condition which in turn reduce the transformer life. In this context, in the next chapter, moisture content in transformer insulation has been assessed using dielectric spectroscopy.

# Chapter 7

# Moisture Assessment of Nano-particles based Composite Insulation by Dielectric Spectroscopy

## 7.1. Introduction

From the previous chapters, different types of nanofluids have been prepared and their dielectric properties have been investigated for searching a new class of insulation. In this chapter, a significant threat for a transformer insulation i.e. moisture is considered for assessment to predict the transformer insulation condition. Therefore, condition-based monitoring of these insulating oils is essential for the prolonged life of the transformer [1]. Among various developed methods, measurement of polarization and depolarization current (PDC) and frequency domain spectroscopy (FDS) are probably extensively used technique to assess the insulation condition [16, 17]. In PDC, insulation is generally applied by a steady excitation voltage which results in the dielectric response current. This current mainly consists of two main components which are regarded as conduction and polarization current. Insulation resistance is primarily responsible for the conduction current whereas the polarization current magnitude is decided by the dipolar polarization phenomenon inside it. It is to be mentioned here that, the dipolar characteristics of oil and paper in power transformer insulation are not similar and needs to be investigated for proper diagnosis of their condition. Considering this, various researchers have modelled the dipolar characteristics of oil and paper using different mathematical expression among which extended Debye model is popular [18]. However, in extended Debye model, the insulation is modelled by number of dipoles having distinct relaxation frequencies [18]. In practice, it has been observed that, depending on the aging status and condition, the insulation can have dipoles with minor differences of relaxation frequencies which are not considered when modelled through extended Debye model. Therefore, insulation characteristics modelled by extended Debye model can introduce error. In order to minimize this error, relaxation frequency distribution (RFD) based

state-of-art technique has been proposed in this work for investigating the insulation characteristics of transformer. The proposed RFD scheme takes the close relaxation times into account to model the dielectric response current. In frequency domain, the method is known as frequency domain spectroscopy (FDS) [9]. From the FDS measurement, parameters like complex capacitance, dielectric loss factors can be determined to predict the condition of the insulating medium [9]. It is reported in [10] that, the peak of the complex capacitance and dielectric dissipation factor from FDS appears at low frequency. So, factors like moisture, temperature affects more in low frequency ranges which results in Low Frequency Dispersion (LFD) of the parameters like complex capacitance. Further, Low Frequency Dispersion (LFD) has been chosen as a parameter to estimate ac conductivity [11] and dielectric dissipation factor [12]. Moreover, with aging of the insulating oil, moisture is produced within the oil as a byproduct of aging. Further this moisture migrates from oil to paper and vice versa. This ingression of moisture in oil and paper degrades their dielectric properties. This degradation of insulation can be predicted using the LFD of complex capacitance.

In this chapter, few insulations model have been developed for investigation purpose. The insulation models are either oil (mineral or vegetable) or nano-fluids ($TiO_2$ and $Al_2O_3$ dispersed in mineral or vegetable oil) impregnated. The percentage moisture content of the insulation models is kept different for investigating the efficacy of the suggested method in wide variation of moisture. Based on the depolarization (relaxation) current, the RFD spectra of each insulation model have been evaluated. The RFD spectrum of each insulation model have been studied and few parameters are identified which are sensitive to the insulation condition. Another parameter i.e. LFD of complex capacitance has also been used for estimate the insulation condition. Besides, another important parameter i.e. activation energy, has also been correlated with RFD spectrum. Based on the value of activation energy, remaining life of the dielectric can be predicted which further helps in constructing the maintenance plan of the power transformer on condition basis.

## 7.2. Theoretical background

### *7.2.1. Modelling of Relaxation Phenomenon of Liquid Dielectric*

As per conventional Maxwell or Debye model (DBM), dielectric response function *r(t)* for an insulation may be represented in (7.1) [19-20].

$$r(t) = \frac{k}{\tau_{DBM}} e^{(-\tau/\tau_{DBM})} \tag{7.1}$$

When steady voltage ( $E(t) = E_0 U(t)$ ) is applied to an insulating material, the polarization process starts and this polarization may be represented by (7.2) [21]. $\tau_{DBM}$ represents relaxation time constant in Debye model.

$$Pol(t) = \varepsilon_0 E_0 \int_0^t r(t) dt \tag{7.2}$$

$$or, \quad \frac{d}{dt} Pol(t) = \varepsilon_0 E_0 r(t) \tag{7.3}$$

In (7.3), dielectric response function *r(t)* can be replaced by (7.1) and can be altered as (7.4).

$$\frac{d}{dt} Pol(t) = \varepsilon_0 E_0 \frac{k}{\tau_{DBM}} e^{(-\tau/\tau_{DBM})} \tag{7.4}$$

The above equation can further be modified as

$$Pol(t) = \int \frac{d}{dt} Pol(t) dt = \varepsilon_0 E_0 \frac{k}{\tau_{DBM}} \int e^{(-\tau/\tau_{DBM})} dt$$

$$= \frac{\varepsilon_0 E_0 k}{\tau_{DBM}} (-\tau_{DBM}) e^{(-\tau/\tau_{DBM})} + \lambda$$

$$= -\tau_{DBM} \varepsilon_0 E_0 \frac{k}{\tau_{DBM}} e^{(-\tau/\tau_{DBM})} + \lambda$$

$$= -\tau_{DBM} \varepsilon_0 E_0 r(t) + \lambda \tag{7.5}$$

Here, $\varepsilon_0$, $\lambda$ and *r(t)* are the permittivity of free space, integrating constant and insulation response function, respectively. It is well-known fact that, the nature of *r(t)* is monotonically decreasing [21]. As a consequence, *r(t)* becomes 0 after sufficiently long time. $\lim_{t\to\infty} r(t) = 0$ .

Thereafter, the electric field applied for sufficiently long time, (7.5) may be represented as

$$\lim_{t\to\infty} Pol(t) = 0 + \lambda$$

$$or, \ \lambda = \lim_{t\to\infty} Pol(t) \tag{7.6}$$

The dielectric polarization *Pol(t)* in (7.5) can further be modified using (7.4) and (7.6) as

$$\frac{d}{dt}Pol(t) = \varepsilon_0 E_0 \frac{k}{\tau_{DBM}} e^{(-\tau/\tau_{DBM})}$$

$$Pol(t) = -\tau_{DBM}\frac{d}{dt}Pol(t) + \lim_{t\to\infty} Pol(t) \tag{7.7}$$

At final and stable state i.e. $t\to\infty$,

$$\lim_{t\to\infty} Pol(t) = Pol_0 = \varepsilon_0 E_0 \int_0^\infty r(t)dt = \varepsilon_0 E_0 \chi_0 \tag{7.8}$$

Where, the susceptibility at final and stable state is indicated as $\chi_0$ and it can be estimated by $\chi_0 = \int_0^\infty r(t)dt$

By putting (7.8) to (7.7), $\tau_{DBM}$ can be denoted as (7.9) which can be regarded as the insulation response consisting single relaxation time,

$$\tau_{DBM}\frac{d}{dt}Pol(t) + Pol(t) = \lim_{t\to\infty} Pol(t) = \varepsilon_0 E_0 \chi_0 \tag{7.9}$$

Equation (7.9) has been modified in respect of relaxation frequency ($\nu = (1/\tau_{DBM})$) and can be represented in (7.10) [16],

$$\frac{1}{\nu}\frac{d}{dt}Pol(t) + Pol(t) = \varepsilon_0 E_0 \chi_0 \tag{7.10}$$

As reported in [19-22], DBM relaxation mechanism only consider single relaxation of the dipoles which is regarded as spherical in shape. However, in the practical dielectric material, multiple relaxation processes take place at the same time and considering their condition, these relaxation processes may have different frequencies. Therefore, it is very challenging task to isolate the close relaxation times inside the insulating material. So, relaxation current modelling using some existing approaches like Debye model may differs from the actual relaxation current (measured) [17, 19, 21]. The suggested RFD scheme deliberates the close relaxation times to model the relaxation current of liquid dielectric. Therefore, it can be said that the modelling of insulation using RFD method provides better about inherent characteristics of the insulation. In the case of liquid nano-dielectrics, molecules interact with their axis of rotation which in turn possess different relaxation processes. This phenomenon ensures that the frequency distribution of the relaxation model for the liquid nano-dielectrics occurs over an extensive range of

frequency. Moreover, for understanding the relaxation model of the liquid nano-dielectrics, the corresponding time domain depolarization (relaxation) current data is recorded and is transformed into frequency domain to obtain the distribution of relaxation frequencies. The *r(v)* is the distribution density function which indicates the distinct relaxation of individual dipole group having different frequency (*v*). So, the rate of change of relaxation of the total polarization ($Pol_{total}$) with respect to relaxation frequency (*v*) is considered as the distribution density function (*r(v)*) [21].

$$r(\nu) = \frac{1}{Pol_{total}} \frac{dPol_{total}}{d\nu} \tag{7.11}$$

$$\nu r(\nu) \equiv R(\nu) \tag{7.12}$$

*R(v)* can also be represented in terms of the depolarization current as (7.13).

$$i(t) = Pol_{0total} \int_0^\infty R(\nu) e^{-t\nu} d\nu \tag{7.13}$$

Here, $Pol_{0total}$ denotes the entire polarization occurs inside the insulating medium considering stable state. In discrete domain, (7.13) can alternately be represented by a series of discrete equation with combination of ($\nu_m$, $R_m$) which is represented in (14).

$$i_{di}(t_{di}) = Pol_{0total} \sum_{\substack{m=1 \\ i=1,2,\ldots N}}^{N} \Delta\nu_m R_m(\nu_m) e^{-t_{di}\nu_m} \tag{7.14}$$

The matrix corresponding to the (7.14) may be ill-conditioned. So, it is very difficult task to determine the solution of this equation. Few techniques for obtaining the solution of this sort of equations are demonstrated in [20-22]. In this work, the estimation of the frequency distribution spectrum of the relaxation procedure has been conducted by incorporating a numerical iterative process to the measured relaxation current.

## *7.2.2. Activation Energy using Debye Model Parameters*

In extended Debye model, the insulation is modelled by combination of *R-C* parameters which are evaluated from the corresponding dielectric relaxation current [23]. The *R* parameters are sensitive to the temperature. It is reported in [24] that, the variation of *R* with temperature as shown in (7.15).

$$R_{T_2} = R_{T_1} \times \exp\left(-\frac{E_a}{K} \times \left(\frac{1}{T_1} - \frac{1}{T_2}\right)\right) \tag{7.15}$$

Where $R_{T_1}$ and $R_{T_2}$ indicate the geometric dc resistance at temperature $T_1$ and $T_2$, respectively. In case of insulation under test, the activation energy can be evaluated if the branch resistance of extended Debye model is known at two different temperatures [24]. It should be mentioned here that, the dielectric relaxation current of insulation under test can be utilized for deriving its extended Debye model [23]. Therefore, it is well-understood that, if the relaxation current of insulation under test are measured at two different temperatures, the corresponding extended Debye model can be derived at those two temperatures. Based on the corresponding branch resistance values at the two temperatures, the activation energy of the dielectric can be evaluated. Therefore, from the activation energy value, the remaining life of the insulation can be determined under a fixed thermal stress based on isothermal accelerated ageing of the oil as given in IEC60216 standard [25]. A correlation has been derived between activation energy and RFD parameter

## 7.3. Experimental Procedures

### *7.3.1. Determination of Paper Moisture Content*

After preparing the insulation prototypes (as shown in Fig. 2.12 in Chapter 2), the overall moisture level of the samples was determined by Dry-weight method [26]. During preparation, insulation prototypes contained residual moisture which needed to be eliminated. For this purpose, the insulation prototypes were heated at 80°C for 72 hours. Thereafter, the insulation prototypes were kept in the vacuum chamber at a pressure of 1kPa for 72 hours. Then the weight of the moisture free insulation prototypes ($W_o$) was measured using precision balance. Again, those insulation prototypes were exposed to air for ingression of the desired moisture. Next, the weight of the prototype samples ($W_m$) was recorded. Based on $W_m$ and $W_o$, the percentage moisture content (%*pm*) was calculated by (7.16) which were verified through FDS (using IDAX300).

It is to be mentioned here that total 30 different types of test samples were developed with different moisture contents. Out of 30 types test samples, 24 types test samples [MO (with paper moisture-0.52%, 1.14%, 2.08% and 3.16%), MOT (with paper moisture-0.55%, 1.09%, 2.07% and 3.12%), MOA (with paper moisture-0.58%, 1.11%, 2.15% and 3.06%), VO (with paper moisture-0.53%, 1.05%, 2.17% and 3.08%), VOT (with paper moisture-0.65%, 0.61%, 0.54% and 0.41%) and VOA (with paper moisture-0.47%, 0.42%, 0.37% and 0.32%)] were used for deriving the empirical relationship

for estimation of sample moisture content. On the other hand, remaining 6 types test samples [(MO with pm 1.58%, MOT with pm 1.63%, MOA with pm 1.72%, VO with pm 2.59%, VOT with pm 2.54% and VOA with pm 2.39%)] have been used to validate the proposed relationships.

$$\%pm = \frac{W_m - W_o}{W_o} \times 100\% \tag{7.16}$$

### *7.3.2. Oil-paper Impregnation Procedure*

After estimation of paper moisture, the insulation samples were impregnated in the base fluids (MO and VO) and prepared nanofluids. For this purpose, the insulation prototypes were immersed in the base fluids (MO and VO) and each nanofluids were kept at a constant pressure (vaccum) at 30°C for 72 hours to ensure proper impregnation process. The impregnated samples were placed in a sealed vessel. The placement of the test samples within the sealed vessel reduces the possibility of induction of significant error due to the environmental issue.

## 7.4. Results & Discussion

### *7.4.1. Result from PDC measurement of oil impregnated samples*

The measurement of PDC has been conducted for each prepared sample. The results from polarization and depolarization current measurement for both the mineral and vegetable oil impregnated insulation samples have been presented in Fig. 7.1.

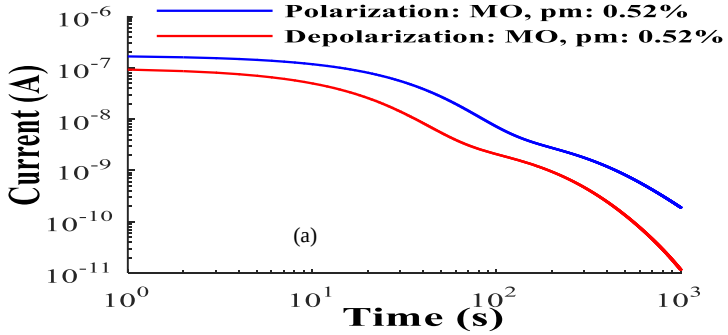

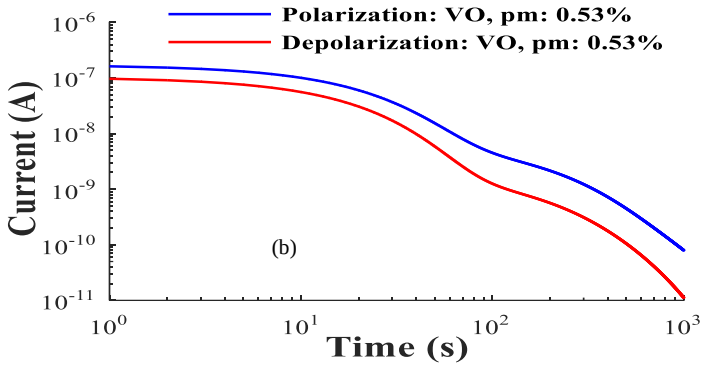


Fig. 7.1. PDC results for (a) mineral and (b) vegetable oil impregnated paper transformer insulation.

## *7.4.2. Analysis of PDC considering Frequency Distribution Function*

The frequency domain distribution function of each oil-paper samples has been assessed using the corresponding depolarization current data considering appropriate procedure as discussed in section 7.2.1. The relaxation frequency domain distribution function for mineral oil-paper samples (having different moisture) have been shown in Fig. 7.2. Since, the recorded data is discrete in nature, the determination of the overall *R(v)* function, iterative method has been incorporated as reported in [20-22]. It can be noticed from Fig. 7.2 that the relaxation frequency domain distribution (RFD) contains multiple peaks at different frequency ranges. The peak at higher frequencies (0.1 Hz range) can be considered due to the relaxation of the dipoles in oil as their relaxation time becomes lower (in the range of 10s and lower) [32]. On the other hand, the peak at 0.01Hz frequency range represents the dipolar relaxation in paper insulation as their relaxation times become in the range of 100s and above [32]. Therefore, the peak near to 0.1 Hz has been considered as the dipolar relaxation of oil whereas the peak near 0.01Hz has been considered due to the dipolar relaxation in paper. It should be mentioned here that, there are third relaxation peak (having relatively lower value) near to 1 mHz which can be considered due to the electrode polarization [33]. The relaxation peak near 0.1Hz can be considered as indicator of oil dielectric characteristics whereas the peak at 0.01Hz can be

considered as marker for paper insulation properties. Considering this fact, an effort has been taken to correlate the peak near 0.01 Hz with condition assessment parameters (like moisture) for paper insulation.

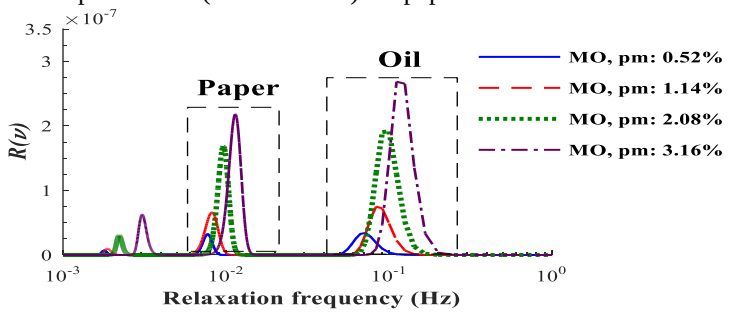


Fig. 7.2. RFD functions for Mineral oil-paper samples at different Moisture content.

From Fig. 7.2, it can also be seen that, the relaxation frequency distribution (RFD) function peak increases for both 0.1Hz ($M_{oil}$) and 0.01Hz ($M_{paper}$) with increase of paper moisture. This is an interesting observation which can be used for predicting the paper moisture. Again, it may be observed from Fig. 7.2 that, with the increment of moisture in the prepared samples, the peaks ($M_{oil}$ and $M_{paper}$) are found to be increased and shifted towards higher frequencies i.e. the peak frequency $f_{p\_paper}$ is shifted. Observing this fact, it can be stated that, the peak frequency $f_{p\_paper}$ is a moisture sensitive parameter. This shifting of $f_{p\_paper}$ is due to the fact that, increment of moisture increases the particle polarizability which decreases the corresponding relaxation time [22].

Fig. 7.3 shows the variation of RFD functions for mineral and vegetable oil-based paper insulation. It may be observed from Fig. 7.3 that, the $M_{oil}$ values for vegetable oil-based insulation is higher than corresponding values of MO based insulation for the similar value of paper moisture. This is due to the fact that, in case of VO based insulation, the vegetable oil has higher affinity towards the moisture in comparison with the MO. Higher amount of the moisture in VO relatively enhances the overall polarization characteristics within it which in turns increases the response current. It is understood from the section 7.2.1 that, the values of $M_{oil}$ is dependent on the magnitude of the response current. Therefore, the $M_{oil}$ for VO is higher than the MO for similar value of paper moisture. On the other hand, as the moisture affinity for VO is higher, therefore, the higher amount of moisture migrates towards it when compared with MO based insulation. So, the amount of moisture in paper for VO based insulation becomes lower in comparison with the MO based insulation. As the moisture content in cellulosic part of VO based insulation

is lower, therefore, $M_{paper}$ for VO based insulation is lower than the corresponding value for MO based insulation.

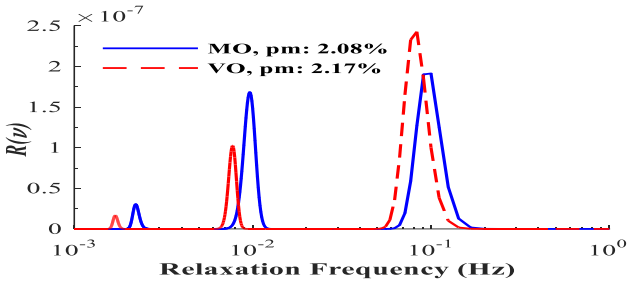


Fig. 7.3. Variation of RFD functions of MO vs VO.

Fig. 7.4(a) and 7(.4b) show the variation of RFD functions for mineral oil based nanofluids impregnated paper samples and vegetable oil based nanofluids impregnated paper samples, respectively. It can be observed from Fig. 7.4(a) and 7.4(b) that, both $M_{oil}$ and $M_{paper}$ decreases for nano-particle based insulation than pure oil-based insulation. This fact illustrates that, addition of nano-particles in MO and VO decreases the corresponding movement of dipoles within oil and paper. The decrement of dipolar movement in turn reduces the dielectric loss which in turn advantageous from practical point of view. Besides, it may also be observed from Fig. 7.4(a) and 7.4(b) that, $M_{oil,}$ $M_{paper}$ and their corresponding peak frequency ($f_{p\_paper}$) are lower for $Al_2O_3$ in comparisons with the $TiO_2$ (for both VO and MO). This phenomenon in turn shows the superiority of $Al_2O_3$ than $TiO_2$ based insulation. Besides, the chemical structures of mineral and vegetable oils are different. Dispersion of different nano-particles with the oils develop bonds with the oil molecules that affect their dipolar relaxation characteristics which is reflected in their corresponding RFD spectra. Hence, the oils (in Table 7.1 & 7.2) used for experimental purpose have different dipolar relaxation characteristics which can be observed from the Fig. 7.4. Various existing dielectric model analyzes the polarization and depolarization current to address these changes of polarization process and based on the results, the moisture distribution of the insulation is predicted [22-24].

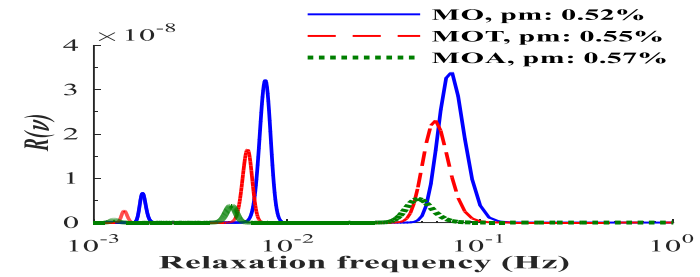


(a)

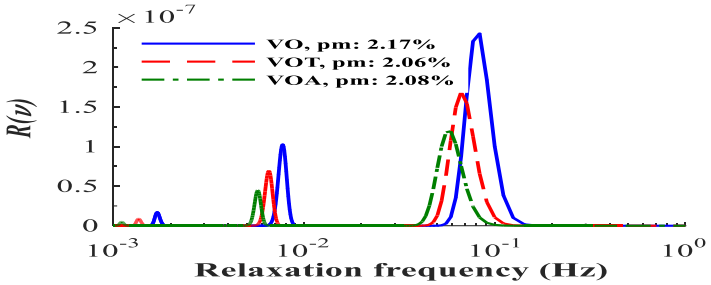


(b)

Fig. 7.4. Variation of Relaxation frequency distribution functions of (a) mineral oil based nanofluids and (b) vegetable oil based nanofluids.

Table 7.1 $f_{p\_paper}$ and $M_{Paper}$ for Mineral Oil and Its Nanofluids Paper Samples

| MO | | | |
|---|---|---|---|
| Paper moisture (%) | Activation energy (*eV*) | Relaxation Frequency, $f_{p\text{-}paper}$ (mHz) | Relaxation Peak $M_{paper}$ |
| 0.52 | 0.65 | 7.692 | 3.21E-08 |
| 1.14 | 0.52 | 8.197 | 6.62E-08 |
| 2.08 | 0.36 | 9.615 | 1.68E-07 |
| 3.16 | 0.28 | 11.363 | 2.18E-07 |
| MOT | | | |
| 0.55 | 0.36 | 6.25 | 1.65E-08 |
| 1.09 | 0.32 | 7.299 | 5.14E-08 |
| 2.07 | 0.29 | 8.772 | 9.81E-08 |
| 3.12 | 0.26 | 10.204 | 1.81E-07 |
| MOA | | | |
| 0.58 | 0.54 | 5.128 | 3.85E-09 |
| 1.11 | 0.48 | 6.452 | 2.82E-08 |
| 2.15 | 0.41 | 8.197 | 6.63E-08 |
| 3.06 | 0.38 | 9.434 | 1.39E-07 |

The aim of the suggested technique is to estimate the overall moisture content (Overall Humidity level) within the transformer insulation by using relaxation frequency distribution technique.

Table 7.2 $f_{p\_paper}$ and $M_{Paper}$ for Vegetable Oil and Its Nanofluids Paper Samples

| VO | | | |
|---|---|---|---|
| Paper moisture (%) | Activation energy ($eV$) | Relaxation Frequency, $f_{p\text{-}paper}$ (mHz) | Relaxation Peak $M_{paper}$ |
| 0.52 | 0.65 | 7.692 | 3.21E-08 |
| 1.14 | 0.52 | 8.197 | 6.62E-08 |
| 2.08 | 0.36 | 9.615 | 1.68E-07 |
| 3.16 | 0.28 | 11.363 | 2.18E-07 |
| VOT | | | |
| 0.65 | 0.47 | 4.464 | 8.02E-09 |
| 0.61 | 0.42 | 4.950 | 2.73E-08 |
| 0.54 | 0.35 | 6.536 | 6.98E-08 |
| 0.41 | 0.32 | 8.130 | 9.32E-08 |
| VOA | | | |
| 0.47 | 0.65 | 4.115 | 3.01E-09 |
| 0.42 | 0.61 | 4.425 | 1.66E-08 |
| 0.37 | 0.49 | 5.714 | 4.50E-08 |
| 0.32 | 0.41 | 7.092 | 8.85E-08 |

## *7.4.3. Effect Of Moisture on Real and Imaginary Part of Complex Capacitance*

Effect of moisture content on the real and imaginary part of the complex capacitance for MO have been presented in Fig. 7.5 and 7.6, respectively. From the Fig. 7.5 and 7.6, it may be observed that, with the increment of moisture, both real and imaginary part of complex capacitance are increased. Increment of moisture in the insulating liquid lead to the increment of charge carriers. This fact leads to the increment of the dielectric losses i.e. C' and C" profiles. Another interesting fact may be observed that moisture effect more in the lower frequency ranges than the higher frequency ranges. From the Fig. 7.5 and 7.6, it can be further concluded that after 100Hz the changes of C' and C" are negligible. This fact again revealed that the dispersion of the C' and C" profiles are below 100Hz i.e. in the low frequency range. So, this Low Frequency Dispersion (LFD) can help in determination of the effect of moisture in the insulating medium.

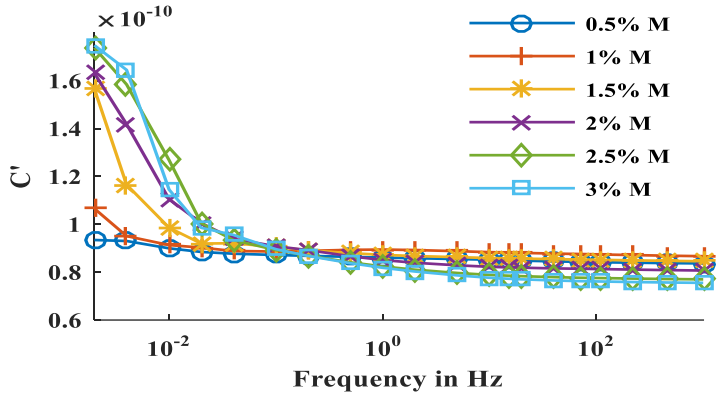


Fig. 7.5. Effect of moisture on real part of complex capacitance.

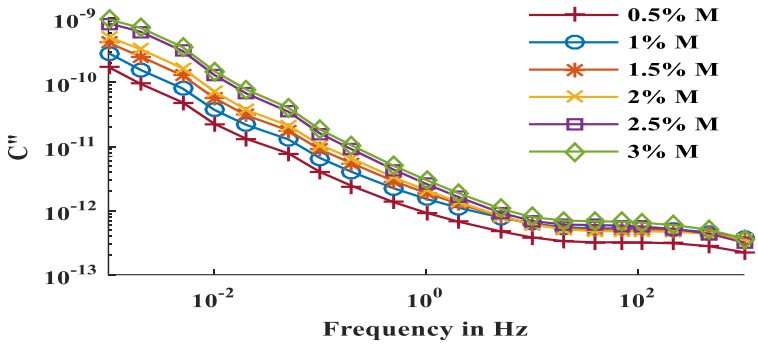


Fig. 7.6. Effect of moisture on imaginary part of complex capacitance.

## *7.4.4. Estimation of Paper Moisture using*

### 7.4.4.1. Peak Frequency of RFD

As discussed in section 7.4.2, $f_{p\_paper}$ can be utilized to estimate the moisture content percentage. The variation of paper moisture with $f_{p\_paper}$ (obtained from Table 7.1 and 7.2) for both MO and VO based insulation have been presented in Fig. 7.7(a) and 7.7(b), respectively. Considering the change of paper moisture with $f_{p\_paper}$, an empirical equation has been established using the least square regression method and has been shown in (7.17).

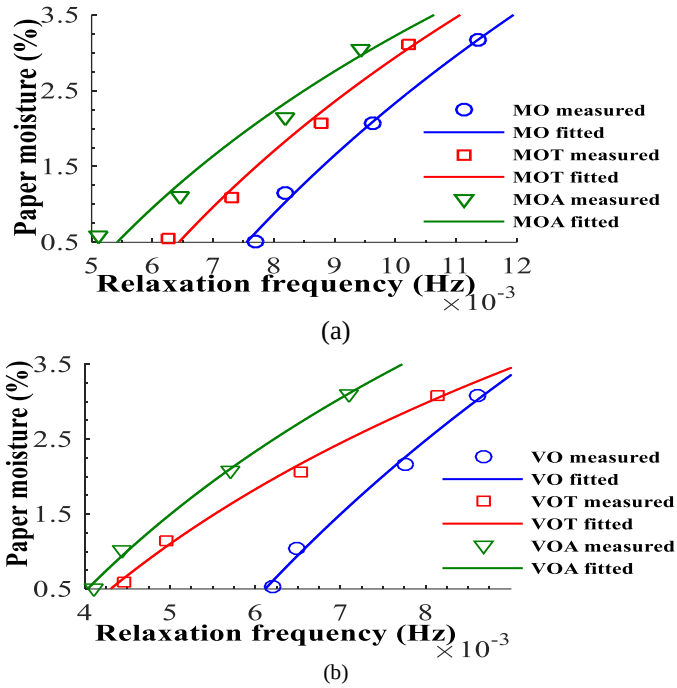


Fig. 7.7. Variation of paper moisture with relaxation frequency for (a) mineral oil based nanofluids-paper samples and (b) vegetable oil based nanofluids-paper samples.

$$Paper\ moisture\ (\%) = \frac{1}{a_2}\ln\left(\frac{f_{p_{paper}}}{a_1}\right) \tag{7.17}$$

In (7.17), $a_1$ and $a_2$, are the fitted coefficients and their values for the different samples are presented by Table 7.3. From Table 7.3, the R square values for each sample can be observed greater than 96% which ensures the effectiveness of the fitting process.

Table 7.3 Fitted Coefficient of (7.17)

| Parameter | $a_1$ | $a_2$ | R square |
|---|---|---|---|
| **MO** | 0.006996 | 0.1529 | 0.9961 |
| **MOT** | 0.005879 | 0.1808 | 0.9836 |
| **MOA** | 0.004843 | 0.2249 | 0.9661 |
| **VO** | 0.005717 | 0.1353 | 0.9937 |
| **VOT** | 0.003796 | 0.2502 | 0.9937 |
| **VOA** | 0.003617 | 0.2169 | 0.9970 |

7.4.4.2. Peak Amplitude of RFD

Similarly, the variation of paper moisture with $M_{paper}$ have been shown in Fig. 7.8. The variation of paper moisture with $M_{paper}$ have been fitted by linear equation (as given in (7.18)). In (7.18), $b_1$ and $b_2$ are the fitting coefficients and their corresponding values for different test samples have been represented in Table 7.4. The R-square values of the fitting equation for the test samples are above 90% which in turn indicates the strong correlation between the paper moisture and $M_{paper.}$

$$Paper\ moisture\ (\%) = b_1 \times M_{paper} + b_2 \tag{7.18}$$

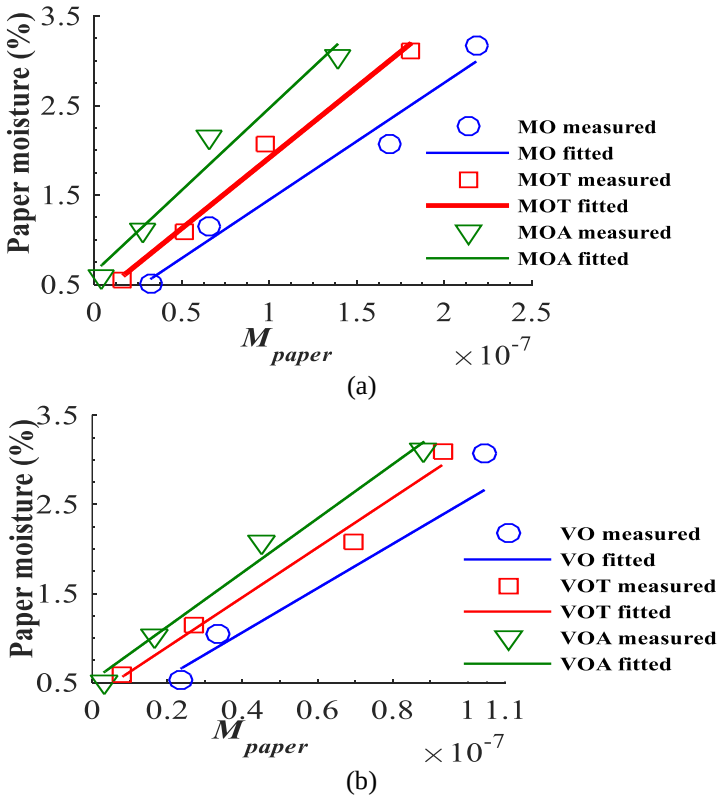


Fig. 7.8. Variation of paper moisture with relaxation peak for (a) mineral oil based nanofluids-paper samples and (b) vegetable oil based nanofluids-paper samples.

Table 7.4 Fitted Coefficient of (7.18)

| Parameter | $b_1$ | $b_2$ | R square |
|---|---|---|---|
| **MO** | 1.31E+07 | 0.1400 | 0.9708 |
| **MOT** | 1.58E+07 | 0.3358 | 0.9881 |
| **MOA** | 1.83E+07 | 0.6359 | 0.9661 |
| **VO** | 2.48E+07 | 0.0719 | 0.8949 |
| **VOT** | 2.79E+07 | 0.3419 | 0.9798 |
| **VOA** | 3.04E+07 | 0.5215 | 0.9856 |

### 7.4.4.3. LFD Parameters

As reported in [14], the dielectric properties of oils rely on the ion conduction and space charge polarisation at lower frequency. Due to space charge polarization, the accumulation of the charge carriers reduces which leads to the increment of capacitance [15]. Again, from Chapter 3, Section 3.3 it can be observed that, peaks of C' and C" are in the low frequency. Low Frequency Dispersion (LFD) can be a good indicator of moisture change. LFD of C' and C" can be determined with the expression (7.19) and (7.20), respectively [11].

$$\Delta C' = C'_{1mHz} - C'_{100Hz} \tag{7.19}$$

$$\Delta C'' = C''_{1mHz} - C''_{100Hz} \tag{7.20}$$

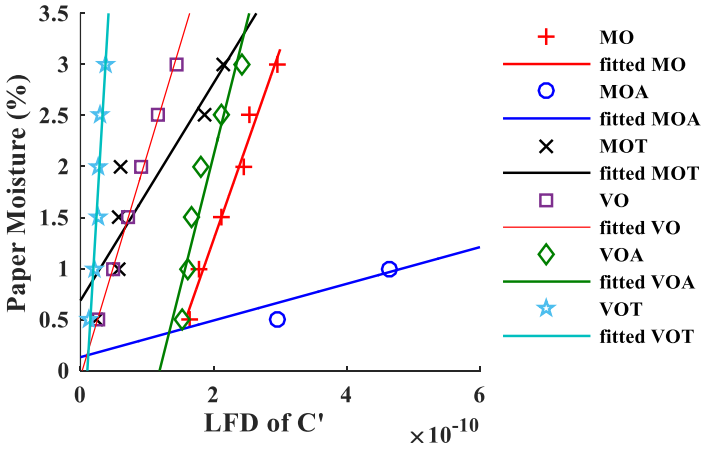


Fig. 7.9. Estimation of paper moisture using LFD of real part of complex capacitance.

For the estimation of the moisture content of the insulating paper samples using LFD of C', the curves between the percentage of moisture content and corresponding LFD of C' are fitted using polynomial regression method as shown in Fig. 7.9. From the regression of every sample, the fitting coefficient ($R^2$) is more than 91% which indicate good fitting. Hence, an empirical relationship can be established between ΔC' and moisture content (%mc) as represented in (7.21) and the fitted coefficients of (7.21) for each prepared samples are given in Table 7.5.

$$Paper\ moisture\ \% = A1\times 10^{10}\times(\Delta C') + A2 \qquad (7.21)$$

Table 7.5. Fitted Coefficient of (7.21)

| | A1 | A2 | $R^2$ |
|---|---|---|---|
| **MO** | 3.72 | -4.88 | 0.98 |
| **MOA** | 3.59 | 0.26 | 0.97 |
| **MOT** | 2.13 | 1.37 | 0.91 |
| **VO** | 3.15 | -0.13 | 0.99 |
| **VOT** | 4.19 | -5.16 | 0.92 |
| **VOA** | 24.06 | -2.28 | 0.95 |

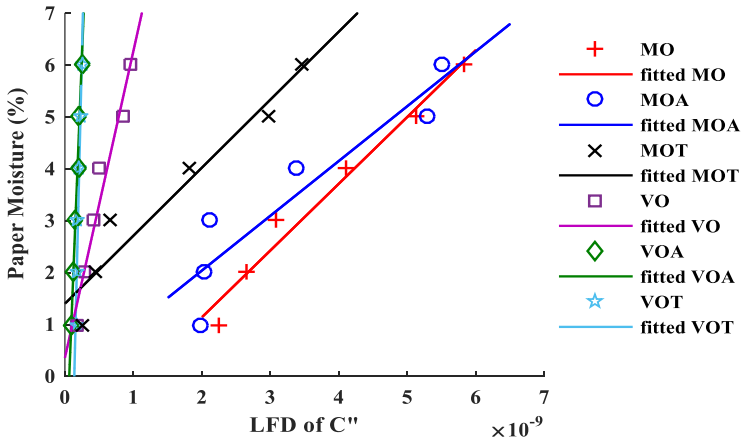


Fig. 7.10. Estimation of paper moisture using LFD of imaginary part of complex capacitance.

Again, for the determination of the moisture content of paper using LFD of C", the curves between the percentage moisture content of the paper and corresponding LFD of C" are fitted using polynomial regression method as

shown in Fig. 7.10. In this fitting method for each sample, the calculated $R^2$ is more than 90% which indicate good fitting. Hence, an empirical relationship can be established between ΔC" and moisture content (%mc) which is represented in (7.22) and the fitted coefficients of (7.22) for each prepared samples are given in Table 7.6.

$$Paper\ moisture\ \% = \mathrm{B1} \times 10^{10} \times \left(\Delta C''\right) + \mathrm{B2} \qquad (7.22)$$

Table 7.6. Fitted Coefficient of (7.22)

| | **B1** | **B2** | **$R^2$** | **RMSE** |
|---|---|---|---|---|
| **MO** | 1.28 | -1.43 | 0.97 | 0.34 |
| **MOA** | 1.05 | -0.07 | 0.96 | 0.76 |
| **MOT** | 1.31 | 1.40 | 0.93 | 0.55 |
| **VO** | 4.62 | 0.37 | 0.97 | 0.43 |
| **VOA** | 38.65 | -2.11 | 0.97 | 0.31 |
| **VOT** | 49.65 | -6.49 | 0.93 | 0.62 |

## *7.4.5. Establishing a correlation between Activation Energy and Peak Amplitude of RFD*

Activation energy of prepared samples has been calculated using (7.15) and has been presented in Table 7.1 (for mineral oil-based samples) and Table 7.2 (for vegetable oil-based samples). The change in activation energy with $M_{paper}$ have been presented in Fig. 7.11 for oil impregnated paper samples. This variation with different paper moisture have been fitted by logarithmic equation (as given in (7.23)). In (7.23), $c_1$ and $c_2$ are the fitting coefficients and their corresponding values for different test samples have been shown in Table 7.7. The R-square values of the fitting equation for the test samples are above 95% which in turn indicates the significant correlation between the activation energy and $M_{paper.}$

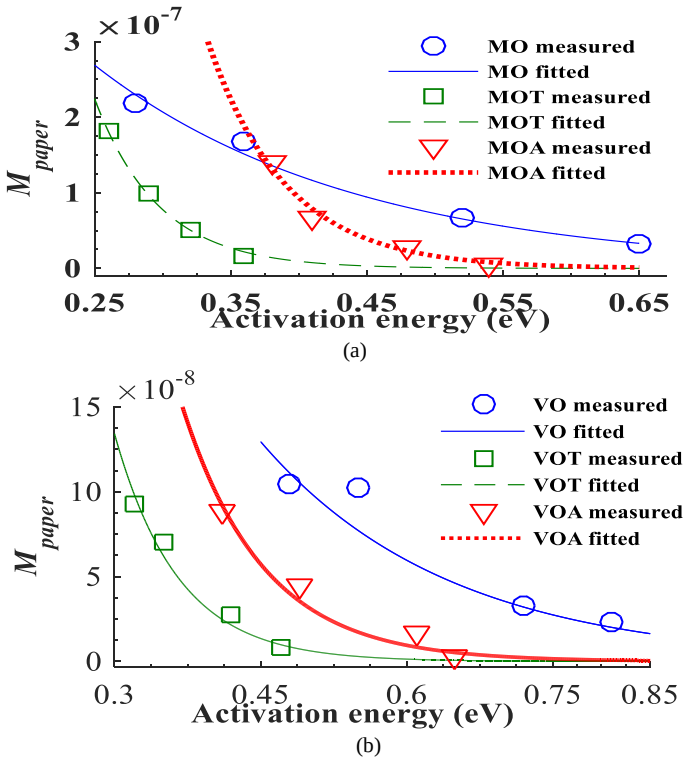


Fig. 7.11. Variation of activation energy with relaxation peak for (a) mineral oil based nanofluids-paper samples and (b) vegetable oil based nanofluids-paper samples.

$$Activation\ energy\ (eV) = \frac{1}{c_2}\ln\left(\frac{M_{paper}}{c_1}\right) \tag{7.23}$$

Table 7.7. Fitted Coefficient of (7.23)

| Parameter | $c_1$ | $c_2$ | R square |
|---|---|---|---|
| **MO** | 9.96E-07 | -5.237 | 0.9808 |
| **MOT** | 4.50E-05 | -21.2 | 0.9979 |
| **MOA** | 10.03E-05 | -17.44 | 0.9772 |
| **VO** | 1.33E-06 | -5.173 | 0.9641 |
| **VOT** | 1.32E-05 | -15.29 | 0.9727 |
| **VOA** | 1.26E-05 | -11.98 | 0.9583 |

## *7.4.6. Validation of Derived Equations for Estimating insulation characteristics*

In order to validate the derived equations (7.17-7.23), the paper moisture and activation energy have been estimated using these equations for the new prepared test samples. It is to be noted that, few test samples having different moisture contents (MO with pm 1.58%, MOT with pm 1.63%, MOA with pm 1.72%, VO with pm 2.59%, VOT with pm 2.54% and VOA with pm 2.39%) have been prepared. The $f_{p\_paper}$ and $M_{paper}$ of the above-mentioned prepared test prototypes have been determined considering the processes as discussed in section 7.2.1. The values of $f_{p\_paper}$, and $M_{paper}$ of the newly prepared test prototypes have been presented in Table 7.8. Using the values of $f_{p\_paper}$ and $M_{paper}$, the paper moisture of the newly prepared test prototypes has been estimated by (7.17) and (7.18), respectively. The predicted paper moisture and the corresponding estimating error of paper moisture have been presented in Table 7.9. It can be seen from Table 7.9 that, the estimating error of paper moisture is less than 10% which shows the effectiveness of (7.17) and (7.18).

Table 7.8 $f_{p\_paper}$ , $M_{Paper}$ , $\Delta C'$ and $\Delta C''$ of the Samples Prepared for Experimental Validation

| | **MO, pm: 1.58%** | **MOT, pm: 1.63%** | **MOA, pm: 1.72%** | **VO, pm: 2.59%** | **VOT, pm: 2.54%** | **VOA, pm: 2.49%** |
|---|---|---|---|---|---|---|
| $f_{p\_paper}$ **(mHz)** | 8.85 | 7.98 | 7.353 | 8.065 | 7.246 | 6.41 |
| $M_{Paper}$ | 1.18E-07 | 7.96E-08 | 5.07E-08 | 1.06E-07 | 8.67E-08 | 7.06E-08 |
| $\Delta C'$ | 2.06E-10 | 1.2E-10 | 6.2E-10 | 1.92E-10 | 0.5E-10 | 2.03E-10 |
| $\Delta C''$ | 2.15E-9 | 0.51E-9 | 1.84E-9 | 3E-9 | 0.21E-9 | 0.19E-9 |

Table 7.9 Estimated Paper Moisture Using $f_{p\_paper}$ AND $M_{paper}$

| **Sample** | **Paper moisture (%)** | **Estimated paper moisture (%) by (17)** | **Estimated paper moisture (%) by (18)** | **Error (%) (17)** | **Error (%) (18)** |
|---|---|---|---|---|---|
| **MO** | 1.58 | 1.54 | 1.68 | 2.7 | 6.3 |
| **MOT** | 1.63 | 1.69 | 1.59 | 3.6 | 2.5 |
| **MOA** | 1.72 | 1.86 | 1.56 | 7.9 | 9.3 |
| **VO** | 2.59 | 2.54 | 2.69 | 1.8 | 3.9 |
| **VOT** | 2.54 | 2.58 | 2.45 | 1.7 | 3.5 |
| **VOA** | 2.41 | 2.64 | 2.19 | 9.5 | 9.1 |

To validate the above two empirical relationship between moisture content and LFD of C' and C", aforementioned test samples have been considered. From the FDS result of that sample, ΔC' and ΔC" have been calculated using (7.16) and (7.20) and given in Table 7.10. The moisture content of that sample is predicted using (7.21) and (7.22). The calculated errors are also given in Table 7.10 which ensure the establishment of those relationship.

Table 7.10. Validation of (7.21) and (7.22)

| Sample | Paper moisture (%) | Estimated paper moisture (%) by (ΔC') | Estimated paper moisture (%) by (ΔC") | Error (%) (ΔC') | Error (%) (ΔC") |
|---|---|---|---|---|---|
| **MO** | 1.58 | 1.62 | 1.49 | 2.5 | 5.7 |
| **MOT** | 1.63 | 1.74 | 1.81 | 6.7 | 11.4 |
| **MOA** | 1.72 | 1.81 | 1.66 | 5.2 | 3.5 |
| **VO** | 2.59 | 3.01 | 2.43 | 16.2 | 6.2 |
| **VOT** | 2.54 | 2.86 | 2.49 | 12.6 | 1.9 |
| **VOA** | 2.41 | 2.28 | 2.37 | 5.4 | 1.6 |

Table 7.11 Estimated Activation Energy using $M_{paper}$

| Sample | $M_{Paper}$ | Activation energy (eV) | Estimated Activation energy (eV) by (19) | Error (%) |
|---|---|---|---|---|
| **MO** | 1.18E-07 | 0.43 | 0.41 | 4.6 |
| **MOT** | 7.96E-08 | 0.31 | 0.30 | 3.3 |
| **MOA** | 5.07E-08 | 0.46 | 0.44 | 4.3 |
| **VO** | 1.06E-07 | 0.52 | 0.49 | 5.8 |
| **VOT** | 8.67E-08 | 0.34 | 0.33 | 2.9 |
| **VOA** | 7.06E-08 | 0.45 | 0.43 | 4.4 |

Besides paper moisture, the activation energy of the newly prepared test prototypes has been estimated by $M_{paper}$ using (7.23) as shown in Table 7.11. The corresponding error for activation energy have been evaluated and presented in Table 7.11. It can be seen from Table 7.11 that, the corresponding estimating error for each sample are less than 6%. This fact indicates that, the proposed method is effective for estimating activation energy.

## 7.5. Inference

In this chapter, an advanced method has been adopted to predict the overall moisture level of paper as well as the activation energy using depolarization current. For this purpose, virgin oils (MO and VO) as well as

nano-fluids impregnated insulation models have been prepared in the laboratory. Based on the dielectric relaxation current, relaxation frequency distribution (RFD) function of the insulation model has been evaluated. It has been observed that, RFD spectra can provide the information relating to the relaxation characteristics of oil (near 0.1 Hz) and paper (0.01Hz). The parameters ($M_{paper}$ and $f_{p\_paper}$) of RFD spectra have been utilized for predicting the overall moisture level in paper. Based on the dependency of paper moisture on $M_{paper}$ and $f_{p\_paper}$, two empirical relationships have been developed. The effectiveness of the empirical relationships has been verified through the newly prepared insulation model. Again, with the increament of moisture, both real and imaginary part of complex capacitance are increased. Furthermore, it can be observed that moisture effect more in the lower frequency ranges than the higher frequency ranges. Therefore, LFD of C' and C'' have been chosen to estimate the moisture content of the paper. For this purpose, two empirical relationships between LFD of C' and C'' and moisture content have been established and have been validated with a newly prepared sample. Similarly, the dependency of activation energy on $M_{paper.}$ has been observed. Considering the variation of activation energy with $M_{paper}$, an empirical relationship between these two parameters have been established which has further been verified on the newly developed insulation models. Thus, the results presented in the paper show that, the suggested method can be suitable for assessing the condition of dielectric model which can further predict the remaining life of the insulation inside the power transformer. Moreover, this assessment can enhance the reliability of the performance of power transformer.

# Chapter 8

# Conclusions & Future Work Recommendation

## 8.1. Conclusions

In this thesis, a comprehensive framework is developed to reduce the research gap towards the applicability of the nanofluids based on mineral and biodegradable oil as a next generation liquid dielectric used for high voltage equipment. This is accomplished by thoroughly investigating the suitability of established electrical-based condition monitoring methods created for the next generation of insulation systems, such as nanofluids based on mineral and biodegradable oil insulation. At first a through literature survey has been conducted which revealed that, the use of nanofluids as an alternative to mineral oil in high voltage equipment still faces profuse challenges. Considering these challenges, in this thesis, researches about the dielectric properties of different nanofluids has been carried and compared with mineral and vegetable oil.

For this purpose, different experimental setup for ac breakdown voltages, viscosity, nano-particle size distribution in prepared samples and dielectric spectroscopic measurements were developed which has thoroughly been discussed in chapter 2. Nanofluids samples containing semi-conducting nanoparticle, $TiO_2$ (titania), and a non-conducting nanoparticle, $Al_2O_3$ (alumina), have been prepared in laboratory for investigation of their dielectric properties. From chapter 3, it can be observed that, the presence of $Al_2O_3$ (alumina) in mineral oil increases corresponding *tanδ* values, whereas dispersion of $TiO_2$ (titania) decreases the corresponding *tanδ* values compared to pure mineral oil. On the other hand, a reverse phenomenon has been observed for vegetable oil. Again, by dispersing this nanoparticle, nonlinearity in conduction current cannot be improved for vegetable oil. However, activation energy of the nanofluids is found to be decreased. Further, there is an increase in viscosity after dispersing nanoparticles which is not desirable. These facts lead to search for another kind of nanofluids as discussed in chapter 4 where nanofluids have been prepared by mixing with a semiconducting type nanoparticle ($TiO_2$) and a non-conducting type nanoparticle ($Al_2O_3$) in a certain ratio. It has been revealed that, hybrid nanofluids can be a better choice than single nanofluids and the base oils (mineral oil or vegetable oil) for their improved dielectric properties. For the concern of environmental issue, vegetable oil is preferred over mineral oil.

However, there are significant issues with vegetable oil, such as its high cost, increased viscosity and increased moisture intrusion. Regarding this problem, mixed oil i.e. a particular percentage of mineral oil substituted with vegetable oil and has been proposed as a base oil for the preparation of nanofluids in chapter 5 which shows enhanced dielectric properties in terms of viscosity, dc conductivity, nonlinearity study, $tan\delta$ and temperature dependency than the mineral and vegetable oil. Then, in chapter 6, two crucial parameters, breakdown voltage and ac conductivity of the different prepared nanofluids have been examined when assessing an insulating oil for use in transformers. Here, the breakdown voltages for each sample with 1%, 10%, and 50% risk probabilities has been estimated using Weibull distribution. From this analysis of breakdown voltage and ac conductivity, mixed oil with titania shows improved result among the prepared nanofluids. Moreover, moisture effect has also been considered in this thesis in chapter 7. Moisture i.e. the aging byproduct of the transformer insulation which can migrates from oil to paper and vice versa and degrades their quality. Therefore, precautionary measurement of moisture can ensure the life of the transformer. In this context, few moistures sensitive parameters from RFD spectra and LFD of complex capacitance obtained from PDC and FDS, respectively have been identified to estimate the moisture content in transformer insulation to avoid premature failure of transformer.

## 8.2. Scope of the Future Works

This investigation provides several suggestions for further studies, which are bestowed below.

- Long term stability of the nanofluids is still a challenge for researchers. In future, the effect of stability of the nanofluids on their dielectric characteristics has been planned to investigate.
- Environmental effect of the nanofluids has been planned to study.
- The electro-thermal aging effect of different nanofluids on their dielectric properties has been planned to study.
- In future, synthetic ester-based hybrid nanofluids and mixed nanofluids have been planned to prepare. Moreover, a comparative study of their dielectric properties with other existing oils has been planned to conduct.
- Effects of another important aging byproduct of the transformer i.e. acids like Acetic acid, Formic acids, Levulinic acid, Naphthenic and Stearic acids etc. on the dielectric properties of the oils can be studied in future. Moreover, use of nanoparticles on the base oil has been planned to investigate for mitigating the adverse effect of acids.

# References

[1] T. O. Rouse, "Mineral insulating oil in transformers," IEEE Electrical Insulation Magazine, Vol. 14, Issue 3, pp. 6-16, 1998.

[2] A. P. Kumar and R. P. Singh, "Biocomposites of cellulose reinforced starch: Improvement of properties by photo-induced crosslinking", Journal of Bioresource Technology, Vol. 99, pp. 8803-8809, 2008.

[3] M.Maharana, N.Baruah, S. K. Nayak, N.Meher, and P. K. Iyer, "Condition Assessment of Aged Ester-Based Nanofluid Through Physicochemical and Spectroscopic Measurement," IEEE Trans. Dielectr. Instrum. Meas., vol. 68, no. 12, pp. 4853-4863, 2019.

[4] S. Choi and J.A. Eastman, "Enhancing thermal conductivity of fluids with nanoparticles," Proceedings of the ASME Int, Mech. Eng. congress and exhibition,1995, pp. 99-105.

[5] C. T. Dervos, J. A. Mergos, P. Skafidas, M. D. Athanassopoulou, and P. Vassiliou, "Effect of water on permittivity of nanodielectrics exposed to the atmosphere", IEEE Trans. Dielectr. Electr. Insul., vol. 16, no. 6, pp. 1558-1565, 2009.

[6] I. Fofana, A. Bouaicha, M. Farzaneh, and J. Sabau, "Ageing Behaviour of Mineral Oil and Ester Liquids: a Comparative Study," in Annual report of IEEE conference on Electrical Insulation and Dielectric Phenomena, pp. 87-90, 26-29 Oct. 2008, Quebec, QC

[7] I. Fofana, A. Bouaicha, M. Farzaneh, J. Sabau, D. Bussieres, and E. B. Robertson, "Decay products in the liquid insulation of power transformers", in IET Electric Power Applications, Vol. 4, pp. 177-184, 2010.

[8] M. J. Heathcote, "Basic Materials", in J and P Transformer Book - A Practical Technology of the Power Transformer (13th Edition),: Elsevier, 2007.

[9] N. J. Fox and G. W. Stachowiak, "Vegetable oil-based lubricants—A review of oxidation" in Tribology International, Vol. 40, pp. 1035-1046, 2007

[10] F. D. Gunstone, "The chemistry of oil and fat". Oxford: Blackwell, 2004.

[11] I. A. Metwally, "Failures, Monitoring and New Trends of Power Transformers", IEEE Potentials Magazine Vol. 30, Issue 3, pp. 36-43, 2011.

[12] V. Sokolov, Z. Berler, and V. Rashkes, "Effective methods of assessment of insulation system conditions in power transformers: a view based on practical experience", in Proceeding of Electrical Insulation and Electrical Manufacturing & Coil Winding Conference, pp. 659-667, 1999, Cincinnati, OH.

[13] L. Yu, L. Jian, and Z. Zhaotao, "Gases dissolved in natural ester fluids under thermal faults in transformers," in IEEE Conference Record of the International Symposium on Electrical Insulation, pp. 223-226, 10-13 June 2012, San Juan, PR

[14] D. Martin, C. Ekanayake T. Saha, Hui Ma, N. Lelekakis, K. Williams, "State of the Art Review On Managing Vegetable Oil Filled Transformers", presented in the Cigre Study Committee B3 & Study Committee D1 colloquium, September 2013, Brisbane , Australia.

[15] T. V. Oommen and T. A. Prevost, "Cellulose insulation in oil-filled power transformers: part II maintaining insulation integrity and life", IEEE Electrical Insulation Magazine, Vol. 22, Issue 1, pp. 5-14, 2006.

[16] M. Koch and T. Prevost, "Analysis of dielectric response measurements for condition assessment of oil-paper transformer insulation", IEEE Transactions on Dielectrics and Electrical Insulation, Vol. 19, pp. 1908-1915, 2012.

[17] Cigre working group. D1.01.09, "Dielectric Response Methods for Diagnostics of Power Transformers", Cigre Brochure 216, 2004.

[18] Cigre working group. D. T. 14, "Dielectric Response Diagnoses For Transformer Windings", Cigre brochure 414, 2010.

[19] M. Koch, S. Raetzke, and M. Krueger, "Moisture diagnostics of power transformers by a fast and reliable dielectric response method", in Conference Record of the IEEE International Symposium on Electrical Insulation, pp. 1-5, 6-9 June 2010, San Diego, CA

[20] https://patents.google.com/patent/US428648A/en

[21] H. R. Sheppard, ‘‘A century of progress in electrical insulation 1886- 1986,’’ IEEE Elect. Insul. Mag., vol. 2, no. 5, pp. 20–30, Sep. 1986.

[22] G. Mercier, ‘‘WEMCOL capacitor fluid development,’’ in Proc. Elect./Electron. Insul. Conf., 1997.

[23] S. Vishal and P. Vikas, ‘‘Transformer’s history and its insulating oil,’’ in Proc. 5th Nat. Conf. (INDIACom), Mar. 2011.

[24] T. V. Oommen, C. C. Claiborne, and J. T. Mullen, ‘‘Biodegradable electrical insulation fluids,’’ in Proc. Elect. Insul. Conf. Elect. Manuf. Coil Winding Conf., Sep. 1997, pp. 465–468.

[25] K. R. Linsley, ‘‘Nonflammable small power transformers,’’ in Proc. Amer. Power Conf., Apr. 1981, pp. 2–7.

[26] I. Fofana, V. Wasserberg, H. Borsi, and E. Gockenbach, ‘‘Challenge of mixed insulating liquids for use in high-voltage transformers.1. Investigation of mixed liquids,’’ IEEE Elect. Insul. Mag., vol. 18, no. 3, pp. 18–31, May 2002.

[27] H. Diana, Alan Watson, “Prebreakdown phenomenon in organic ester transformer fluid,” in Proc. IEEE International Symposium on Electrical Insulation, June 1990, pp. 57-60.

[28] David Sundin, “The service history of ester-based fluids used in railway transformers,” in Proc. IEEE International Symposium on Electrical Insulation, June 1990, pp. 31-34.

[29] T.V. Oommen, C.C. Claiborne, E.J. Walsh, “Introduction of a new fully biodegradable dielectric fluid,” in Proc. IEEE Annual Textile, Fiber and Film Industry Technical Conference, May 1998, pp. 1-4.

[30] C.P. McShane, G. Gauger, J. Luksich, “Fire Resistant Natural Ester Dielectric Fluid and Novel Insulation System for Its Use,” in Proc. IEEE/PES Transmission and Distribution Conference, April 1999, pp. 890- 894.

[31] K.J. Rapp G.A. Gauger J. Luksich, “Behaviour of Ester Dielectric Fluids Near the Pour Point,” in Proc. IEEE international Conference on Electrical Insulation and Dielectric Phenomena, October 1999, pp. 459- 462.

[32] E. Gockenbach, H. Borsi, “Performance and new application of ester liquids,” in Proc. Fourteenth IEEE International Conference on Dielectric Liquids, July 2002, pp. 203-206.

[33] P. Thomas, “Biodegradable dielectric liquids for transformer applications,” International Symposium on Electrical Insulating Materials, June 2005, pp. 135-136.

[34] “IEEE Guide for Acceptance and Maintenance of Natural Ester Fluids in Transformers,” IEEE standard C57.147-2008, 2008-07-11.

[35] S.D. Smith, Barry L. Beaster, “Design and Test Experience with Natural Ester Fluid for Power Transformers –Update,” in Proc. IEEE/ PES General Meeting, July 2009, pp. 1-3.

[36] CIGRE Report 436 “Experiences in service with new insulating liquids,” Study Material of Working Group A2.35, pp. 1-94, Oct. 2010.

[37] D. M. Mehta, P. Kundu, A. Chowdhury, V. K. Lakhiani and A. S. Jhala, "A review on critical evaluation of natural ester vis-a-vis mineral oil insulating liquid for use in transformers: Part 1," in IEEE Transactions on Dielectrics and Electrical Insulation, vol. 23, no. 2, pp. 873-880, April 2016,

[38] D. M. Mehta, P. Kundu, A. Chowdhury, V. K. Lakhiani and A. S. Jhala, "A review of critical evaluation of natural ester vis-a-vis mineral oil insulating liquid for use in transformers: Part II," in *IEEE Transactions on Dielectrics and Electrical Insulation*, vol. 23, no. 3, pp. 1705-1712, June 2016.

[39] S. Okabe, M. Kohtoh, M. Tsuchie, and T. Amimoto: “Influence of Diverse Compounds on Electrostatic Charging Tendency of Mineral Insulating Oil used for Power Transformer Insulation”, IEEE Trans. Dielectr. Electr. Insul., Vol. 16, pp. 900-908, 2009.

[40] S. Okabe, M. Kohtoh, and T. Amimoto: “Investigation of Electrostatic Charging Mechanism in Aged Oil-immersed Transformers”, IEEE Trans. Dielectr. Electr. Insul., Vol. 17, pp. 287-293, 2010.

[41] Gengadevi Kaliappan, Madavan Rengaraj,"Aging assessment of transformer solid insulation: A review", Materials Today: Proceedings, Elsevier, vol. 47, no. 1, Pages 272-277,2021.

[42] IEEE Working Group 09 (Thermal aspects of transformers) of Study Committee 12. Lifetime Evaluation of Transformers. Electra 1993; 150:39–51.

[43] Leijon M, Dahlgren M, Walfridsson L, Ming L, Jaksts A. A recent development in the electrical insulation systems of generators and transformers. IEEE Electrical Insulation Magazine 2001; 17(3):10–15.

[44] Kan H, Miyamoto T. Proposals for an improvement in transformer diagnosis using Dissolved Gas Analysis. IEEE Electrical Insulation Magazine 1995; 11(6):15–21.

[45] Working Group Report. Background information on high voltage temperature insulation for liquid-immersed power transformers. IEEE Transactions on Power Delivery 1994; 9(4):1892–1906.

[46] Fessler WA, Kaufmann GH, Rouse TO. Accelerated aging studies of distribution transformers containing naphthenic and paraffinic mineral oils. 1978 IEEE International Symposium on Electrical Insulation, Philadelphia, PA. IEEE Pub: 78CH1287-2EI, June 12–14, 1978; pp. 279–290.

[47] Emsley AM, Stevens GC. Review of chemical indicators of degradation of cellulosic electrical paper insulation in oil-filled transformers. IEE Proceedings—Science, Measurement and Technology 1994; 141(5):324–335.

[48] Lu¨tke H, Ho¨hlein I, Kachler AJ. Transformer ageing research on furanic compounds dissolved in insulating oil. Cigre 2002 session proceedings, 24 August, 2002 to 30 August 2002. 2002; 15–302.

[49] Scheirs J, Camino G, Tumiatti W, Avidano M. Study of the mechanism of thermal degradation of cellulosic paper insulation in electrical transformer oil. Die Angewandte Makromolekulare Chemie 1998; 259(1):19–25.

[50] Patrick McSC, Rapp KJ, Corkran JL, Gauger GA, Luksich J. Aging of Paper Insulation in Natural Ester Dielectric Fluid. 2001 IEEE/PES Transmission & Distribution Conference & Exposition, October 28–November 02, 2001, Atlanta GA.

[51] Densley RJ, Gupta BK. Effect of temperature on sensitivity of diagnostic tests on oil-impregnated paper insulation. Proceedings of the IEEE Electrical Insulation Conference and Electrical Manufacturing and Coil Winding Conference 2001; 601–604.

[52] Rouse TO. Mineral insulating oil in transformers. IEEE Electrical Insulation Magazine 1998; 14(3):6–16.

[53] Csepes G, Kispal I, Fekete J, Romvari Z, Brooks R, Szebeni M, Bognar A, Uri E, Babos S. Correlation Between Electrical and Chemical Testing Techniques for Assessing Degradation of Oil-paper Insulation. Intern Conf Large HV Electric Systems. CIGRE: Paris, France, Paper No. 15-202, 1998.

[54] Du Y, Zahn M, Lesieutre BC, Mamishev AV, Lindgren SR. Moisture Equilibrium in Transformer paper-oil systems. IEEE Electrical Insulation Magazine, 1999; 15(1):11–20.

[55] Sheiretov Y, Zahn M. Dielectrometry measurements of moisture dynamics in oil-impregnated pressboard. IEEE Transactions on Dielectrics and Electrical Insulation 1995; 2(3):329–351.

[56] Breen G, On the behalf of Study Committee 12. Essential requirements to maintain transformers in service. Cigre session August 30–September 5, 1992; 12–103.

[57] Moser HP, Dahinden V, Schneider E, Brechna H, Zu¨ger F. New results on aging of Aramid and cellulose pressboard under selective conditions. CIGRE Symposium Vienna (Austria) 1987; 500–505.

[58] Fabre J, Pichon A. Deteriorating processes and products of paper in oil. Application to transformers. CIGRE conference on Large High Voltage Electric Systems Paris, 1960; 137.

[59] Peralta-Videa, J.R.; Zhao, L.; Lopez-Moreno, M.L.; Rosa, G.D.L.; Hong, J.; Gardea-Torresdey, J.L. Nanomaterials and the environment: a review for the biennium 2008 - 2010. J. Hazard. Mater., 2011, 186, 1-15.

[60] Al-Mubaddel, F.S.; Haider, S.; Al-Masry, W.A.; Al-Zeghayer, Y.; Imran, M.; Haider, A.; Ullah, Z. Engineered nanostructure: a review of their synthesis, characterization and toxic hazard considerations. AJC., 2012.

[61] Scida, K.; Stege, P.W.; Haby, G.; Messina, G.A.; Garcia, C.D. Recent application of carbon-based nanomaterials in analytical chemistry: critical review. Anal. Chim. Acta, 2011, 691, 6-17.

[62] Dreizin, E.L. Metal-based reactive nanomaterials. Prog. Energ. Combust., 2009, 35, 141-167.

[63] Singh, S.C.; Ram, G. Drop shape zinc oxide quantum dots and their self-assembly into dendritic nanostructure: liquid assisted pulsed lase ablation and characterizations. Appl. Surf. Sci., 2012, 258, 2211-2218.

[64] Gong, S.; Yang, G.; Ban, D.; Fu, J.; Fu, Y. Three-pulsed photon echo induced by the optical transitions of excitonsin core-shell CdSe/ZnS nanocrystal quantum dots. Opt. Mater., 2011, 34, 36-41.

[65] Sebaa, M.; Nguyen, T.Y.; Paul, R.K.; Mulchandani, A.; Liu, H. Graphene and carbon nanotubes-graphene hybrid nanomaterials for human embryonic stem cell culture. Mater. Lett., 2013, 92, 122- 125.

[66] Yuan, J.; Muller, A.H.E. One-dimensional organic-inorganic hybrid nanomaterials. Polymer, 2010, 51, 4015-4036.

[67] H. Akoh, Y.Tsukasaki, S.Yatsuya, and A.Tasaki, ―Magnetic properties of ferromagnetic ultrafine particlesprepared by vacuum evaporation on running oil substrate.‖ Journal of Crystal Growth, 45, 495–500, 1978.

[68] J.A.Eastman, U.S.Choi, S.Li, L.J.Thompson, S.Lee, ―Enhanced thermal conductivity through the development of nanofluids‖, Materials Research Society Symposium-Proceedings, Materials research Society, Pittsburgh, PA, USA, Boston, MA, USA, vol.457:pp.3-11, 1997.

[69] H.T.Zhu, Y.S.Yin, A, ―A novel one-step chemical method preparation of copper nanofluids‖, Journal of Colloid and Interface Science, vol.227, no.1, pp.100-130, 2004.

[70] C–H. Lo, T-T. Tsung, L-C. Chen, C.-H. Su and H.-M.Lin, ―Fabrication of Copper Oxide Nanofluid Using Submerged Arc Nanoparticle Synthesis System (SANSS)‖.Journal of Nanoparticle Research 7: 313–320, 2005.

[71] S. Lee, S. U.S. Choi, S. Li, and J. A. Eastman, ―Measuring thermal conductivity of fluids containing oxide nanoparticles, ‖ Journal of Heat Transfer, vol. 121, no. 2, pp. 280–289, 1999.

[72] X. Wang, X. Xu, and S. U. S. Choi, ―Thermal Conductivity of Nanoparticle-Fluid Mixture, ‖ Journal of Thermophysics and Heat Transfer 13: 474–480, 1999.

[73] S. M. S. Murshed, K. C. Leong, and C. Yang, ―Enhanced Thermal Conductivity of TiO2 ―Water Based Nanofluids‖, International Journal of Thermal Sciences 44: 367–373, 2005.

[74] Y. Xuan and Q. Li, ―Heat transfer enhancement of nanofluids,‖ International Journal of Heat and Fluid Flow, vol. 21, no. 1, pp. 58– 64, 2000.

[75] K.Kwak, C.Kim, Kor.-Austr. Rheol. J., 17, 35, 2005.

[76] J. A. Eastman, S. U. S. Choi, S. Li, W. Yu, and L. J. Thompson, ―Anomalously increased effective thermal conductivities of ethylene glycol-based nanofluids containing copper nanoparticles,‖ Applied Physics Letters, vol. 78, no. 6, pp. 718–720, 2001.

[77] X. Feng, H. Ma, S. Huang *et al.*., Aqueous-organic phase-transfer of highly stable gold, silver, and platinum nanoparticles and new route for fabrication of gold nanofilms at the oil/water interface and on solid supports, Journal of Physical Chemistry B, vol. 110, no. 25, pp. 12311–12317, 2006.

[78] W. Yu, H. Xie, L. Chen, and Y. Li, ―Enhancement of thermal conductivity of kerosene-based Fe3O4 nanofluids prepared via phasetransfer method,‖ Colloids and Surfaces A, vol. 355, no. 1–3, pp. 109–113, 2010.

[79] X. Wei and L.Wang, ―Synthesis and thermal conductivity of microfluidic copper nanofluids,‖ Particuology, vol. 8, no. 3, pp. 262– 271, 2010.

[80] H. T. Zhu, C. Y. Zhang, Y. M. Tang, and J. X. Wang, ―Novel synthesis and thermal conductivity of CuO nanofluid,‖ Journal of Physical Chemistry C, vol. 111, no. 4, pp. 1646–1650, 2007.

[81] D. A. Mansour *et al.*, "Multiple nanoparticles for improvement of thermal and dielectric properties of oil nanofluids," IET Sci. Meas. Technol., vol. 13, no. 7, pp. 968–974, 2019.

[82] Y. Du *et al.*, "Effect of semiconductive nanoparticles on insulating performances of transformer oil," IEEE Trans. Dielectr. Electr. Insul., vol. 19, no. 3, pp. 770–776, 2012.

[83] W. Li *et al.*, "External Dielectric Performance of Various Vacuum Interrupter Envelope Constructions," 5th Int. Conf. Electr. Power Equip. Switching Technol. (ICEPE-ST), 2019, pp. 484–489.

[84] M. Rafiq *et al.*, "Effect of different nanoparticle types on breakdown strength of transformer oil," IEEE Conf. Electr. Insul. Dielectr. Phenom. (CEIDP), 2016, pp. 436–440.

[85] M. M. Alharthi, S. S. Ghoneim and I. B. Taha, "Breakdown voltage of the Transformer oils under certain conditions," Int. J. Appl. Eng. Res., vol. 13, no. 6, pp. 3810–3815, 2018.

[86] E. S. M. El-Refaie *et al.*, "Enhancing flashover strength along oil/ pressboard interface using nanofluids," Alexandria Eng. J., vol. 59, no. 1, pp. 475–483, 2020.

[87] N. S. Suhaimi *et al.*, "Optimum electrical and dielectric performance of multi-walled carbon nanotubes doped disposed transformer oil," Energies, vol. 13, no. 12, 2020.

[88] M. S. Mohamad *et al.*, "AC breakdown voltage and viscosity of palm fatty acid ester (PFAE) oil-based nanofluids," J. Electr. Eng. Technol., vol. 12, no. 6, pp. 2333–2341, 2017.

[89] N. A. Sabiha, S. S. M. Ghoneim and M. M. Hessien, "Breakdown performance of transformer oil in the presence of single-phase nanocrystalline ZnO and nano-partial substitution," IET Sci. Meas. Technol., vol. 13, no. 5, pp. 737–745, 2019.

[90] S. Chandrasekar *et al.*, "Developing eco-friendly nanostructured oil: Partial discharge and breakdown voltage characterization of transformer corn oil," IEEE Trans. Dielectr. Electr. Insul., vol. 27, no. 5, pp. 1611– 1618, 2020.

[91] K. Swati *et al.*, "Understanding Corona discharge activity in titania nanoparticles dispersed in transformer oil under AC and DC voltages," IEEE Trans. Dielectr. Electr. Insul., vol. 24, no. 4, pp. 2325–2336, 2017.

[92] J. Kurimský *et al.*, "Effect of magnetic nanoparticles on partial discharges in transformer oil," J. Magnetism Magn. Mater., vol. 496, 2020, Art no. 165923.

[93] E. G. Atiya, D. E. A. Mansour and M. A. Izzularab, "Partial Discharge Development in Oil-Based Nanofluids: Inception, Propagation and Time Transition," IEEE Acc., vol. 8, pp. 181028–181035, 2020.

[94] S. S. Bamji *et al.*, "Space charge in polypropylene containing synthetic nano particles," IEEE Conf. Electr. Insul. Dielect. Phenom. (CEIDP), 2009, pp. 662–665.

[95] X. Huang, P. Jiang and T. Tanaka, "A review of dielectric polymer composites with high thermal conductivity," IEEE Electr. Insul. Mag., vol. 27, no. 4, pp. 8–16, 2011.

[96] A. Beheshti, M. Shanbedi and S. Z. Heris, "Heat transfer and rheological properties of transformer oil-oxidized MWCNT nanofluid," J. Therm. Anal. Calorimetry, vol. 118, no. 3, pp. 1451–1460, 2014

[97] M. Bakrutheen, R. Karthik and R. Madavan, "Investigation of critical parameters of insulating mineral oil using semiconductive nanoparticles," Int. Conf. Circuits and Power Comput. Technol. (ICCPCT), 2013, pp. 294–299.

[98] R. T. A. R. Prasath *et al.*, "Dielectric and thermal conductivity studies on synthetic ester oil based TiO2 nanofluids," 3rd Int. Conf. Condition Assessment Techn. Electr. Syst. (CATCON), 2017, pp. 289-292.

[99] H. W. Chiam *et al.*, "Numerical study of nanofluid heat transfer for different tube geometries – A comprehensive review on performance," Int. Commun. Heat and Mass Transfer, vol. 86, pp. 60–70, 2017.

[100] S. C. Pugazhendhi, "Experimental evaluation on dielectric and thermal characteristics of nano filler added transformer oil," Int. Conf. High Voltage Eng. Appl. (ICHVE), 2012, pp. 207–210.

[101] T. S. Ramu, B. K. Keshavan and K. N. B. Murthy, "Application of a class of nano fluids to improve the loadability of power transformers," EEE 10th Int. Conf. Propert. Appl. Dielectr. Mater. (ICPADM), 2012, pp. 1–6.

[102] R. T. A. R. Prasath *et al.*, "Mineral oil based high permittivity CaCu3Ti4O12 (CCTO) nanofluids for power transformer application," IEEE Trans. Dielectr. Electr. Insul., vol. 24, no. 4, pp. 2344–2353, 2017.

[103] A. Asadi and K. Kalaitzidou, "2 – Process-Structure-Property Relationship in Polymer Nanocomposites," in Experimental Characterization, Predictive Mechanical and Thermal Modeling of Nanostructures and their Polymer Composites: Elsevier, 2018, pp. 25–100.

[104] D. A. Mansour *et al.*, "Multiple nanoparticles for enhancing breakdown strength and heat transfer coefficient of oil nanofluids," 2017 Nineteenth International Middle East Power Systems Conference (MEPCON), 19–21 Dec. 2017, pp. 1406–1410.

[105] M. Maharana *et al.*, "Nanofluid-based transformer oil: effect of ageing on thermal, electrical and physicochemical properties," IET Sci. Meas. Technol., vol. 12, no. 7, pp. 878–885, 2018.

[106] B. X. Du, X. L. Li and M. Xiao, "High thermal conductivity transformer oil filled with BN nanoparticles," IEEE Trans. Dielectr. Electr. Insul., vol. 22, no. 2, pp. 851–858, 2015.

[107] B. X. Du, X. L. Li and J. Li, "Thermal conductivity and dielectric characteristics of transformer oil filled with bn and Fe3O4 nanoparticles," IEEE Trans. Dielectr. Electr. Insul., vol. 22, no. 5, pp. 2530–2536, 2015.

[108] S. N. Suhaimi *et al.*, "A Review on Oil-Based Nanofluid as NextGeneration Insulation for Transformer Application," J. Nanomater., 2020.

[109] A. A. Hussien *et al.*, "A brief survey of preparation and heat transfer enhancement of hybrid nanofluids," J. Mech. Eng., vol. 65, no. 7-8, pp. 441–453, 2019.

[110] D. S. Saidina, M. Z. Abdullah and M. Hussin, "Metal oxide nanofluids in electronic cooling: a review," J. Mater. Sci., vol. 31, no. 6, pp. 4381– 4398, 2020.

[111] D. H. Fontes, G. Ribatski and E. P. Bandarra Filho, “Experimental evaluation of thermal conductivity, viscosity and breakdown voltage AC of nanofluids of carbon nanotubes and diamond in transformer oil,” Diamond and Related Mater., vol. 58, pp. 115–121, 2015.

[112] M. Maharana *et al.*, “Comparative study of mechanical and electrical strength of kraft paper in nanofluid based Transformer oil and mineral oil,” Proc. Int. Symp. Electr. Insul. Mater. (ISEIM), 2017, vol. 2, pp. 646–649.

[113] J. Huang *et al.*., “Enhancement of mechanical and electrical performances of insulating presspaper by introduction of nanocellulose,” Composites Sci. Technol., vol. 138, pp. 40–48, 2017.

[114] M. Maharana *et al.*, “Electro-Mechanical and Chemical Strength Analysis of Thermally Aged Nanofluid Impregnated Kraft Paper,” IEEE Conf. Electr. Insul. Dielectr. Phenom. (CEIDP), 2018, pp. 121–124.

[115] A. A. Hussien *et al.*, “A brief survey of preparation and heat transfer enhancement of hybrid nanofluids,” J. Mech. Eng., vol. 65, no. 7-8, pp. 441–453, 2019.

[116] N. Ali, J. A. Teixeira and A. Addali, “A Review on Nanofluids: Fabrication, Stability, and Thermophysical Properties,” J. Nanomater., 2018.

[117] S. Umar *et al.*, “Investigation of the effect of pH adjustment on the stability of nanofluid,” AIP Conf. Proc., 2018, vol. 2031.

[118] A. Banisharif *et al.*, “Thermophysical properties of water ethylene glycol (WEG) mixture-based Fe3O4 nanofluids at low concentration and temperature,” J. Mol. Liquids, vol. 302, p. 112606, 2020.

[119] Y. Mohammadfam, S. Zeinali Heris and L. Khazini, “Experimental Investigation of Fe3O4/hydraulic oil magnetic nanofluids rheological properties and performance in the presence of magnetic field,” Tribol. Int., vol. 142, p. 105995, 2020.

[120] D. E. A. Mansour, R. F. Emara and M. K. El-Nemr, “Heat transport characteristics of oil-based nanofluids with different types of nanoparticles,” 19th IEEE Int. Conf. Dielectr. Liquids, (ICDL), 2017, pp. 1–4.

[121] A. Beheshti, M. Shanbedi and S. Z. Heris, “Heat transfer and rheological properties of transformer oil-oxidized MWCNT nanofluid,” J. Therm. Anal. Calorimetry, vol. 118, no. 3, pp. 1451–1460, 2014.

[122] V. A. Primo *et al.*, “AC breakdown voltage of Fe3O4 based nanodielectric fluids. Part 1: Analysis of dry fluids,” IEEE Trans. Dielectr. Electr. Insul., vol. 27, no. 2, pp. 352–359, 2020.

[123] Y. Zhou *et al.*, “Statistical analysis of moisture's effect on AC breakdown strength of TiO2 nanofluids,” J. Mol. Liquids, vol. 249, pp. 420–428, 2018.

[124] Q. Han *et al.*, “The Application of Polyhedral Oligomeric Silsesquioxanes on Vegetable Insulating Oil Modification,” 20th IEEE Int. Conf. Dielectr. Liquids (ICDL), 2019, pp. 1–4.

[125] A. Raymon and R. Karthik, “Reclaiming aged transformer oil with activated bentonite and enhancing reclaimed and fresh transformer oils with antioxidants,” IEEE Trans. Dielectr. Electr. Insul., vol. 22, pp. 548– 555, 2015.

[126] R. Liu, “The Challenges and Opportunities of Nanofluids,” 2nd Int. Conf. Electr. Mater. and Power Equip. (ICEMPE), 2019, pp. 110–114.

[127] R. T. A. R. Prasath *et al.*, "Mineral oil based high permittivity CaCu3Ti4O12 (CCTO) nanofluids for power transformer application," IEEE Trans. Dielectr. Electr. Insul., vol. 24, no. 4, pp. 2344–2353, 2017.

[128] V. A. Primo *et al.*, "Analysing the impact of Moisture on the AC Breakdown Voltage of Fe3O4 Based Nanodielectric Fluids," 2nd IEEE Int. Conf. Dielect. (ICD), 1-5 July 2018, pp. 1–4.

[129] S. Mesdaghi *et al.*, "Effect of Sn4+–Zn2+–Co2+ Doping on Structural and Magnetic Properties of M-Type Barium Hexaferrites," IEEE Trans. Magn., vol. 55, no. 1, pp. 1V6, 2019.

[130] M. R. Hussain *et al*., "Dielectric Performance of Magneto-Nanofluids for Advancing Oil-Immersed Power Transformer," IEEE Acc., vol. 8, pp. 163316–163328, 2020.

[131] G. Ababei *et al*., "Influence of the chemically synthesis conditions on the microstructure and magnetic properties of the Co-Fe-B nanoparticles," J. Magnetism Magn. Mater., vol. 451, pp. 565–571, 2018.

[132] Y. Veli *et al*., "The Design of the Secondary Electrical Circuit of a Flyback Transformer with Hybrid Magnetic Core," 11th Int. Symp. Adv. Topics Electr. Eng. (ATEE), 2019, pp. 1–6.

[133] M. Abbas *et al.*, "Hierarchical porous spinel MFe2O4 (M=Fe, Zn, Ni and Co) nanoparticles: Facile synthesis approach and their superb stability and catalytic performance in Fischer-Tropsch synthesis," Int. J. Hydrogen Energy, vol. 45, pp. 10754–10763, 2020.

[134] J. Kurimský *et al*., "Effect of magnetic nanoparticles on partial discharges in transformer oil," J. Magnetism Magn. Mater., vol. 496, 2020, Art no. 165923.

[135] V. A. Primo *et al.*, "Investigation of the Lightning Impulse Breakdown Voltage of Mineral Oil based Fe3O4 Nanofluids," Coatings, vol. 9, no. 12, p. 799, 2019.

[136] H. J. Kim, I. C. Bang, and J. Onoe, ―Characteristic stability of bare Au-water nanofluids fabricated by pulsed laser ablation in liquids,‖ Optics and Lasers in Engineering, vol. 47, no. 5, pp. 532–538, 2009.

[137] D. Zhu, X. Li, N. Wang, X. Wang, J. Gao, and H. Li, ―Dispersion behavior and thermal conductivity characteristics of Al2O3-H2O nanofluids,‖ Current Applied Physics, vol. 9, no. 1, pp. 131–139, 2009.

[138] X. Wei and L.Wang, ―Synthesis and thermal conductivity of microfluidic copper nanofluids,‖ Particuology, vol. 8, no. 3, pp. 262– 271, 2010.

[139] H. Zhu, C. Zhang, Y. Tang, J. Wang, B. Ren, and Y. Yin, ―Preparation and thermal conductivity of suspensions of graphit e nanoparticles,‖ Carbon, vol. 45, no. 1, pp. 226–228, 2007.

[140] X. Wei, H. Zhu, T. Kong, L. Wang, ―Synthesis and thermal conductivity of Cu2O nanofluids,‖ International Journal of Heat and Mass Transfer, vol. 52, no.19-20, pp.4371-4374, 2009.

[141] Y. Fovet, J. Y. Gal, and F. Toumelin-Chemla, ―Influence of pH and fluoride concentration on titanium passivating layer: stability of titanium dioxide,‖ Talanta, vol. 53, no. 5, pp. 1053–1063, 2001.

[142] A. K. Singh and V. S. Raykar, ―Microwave synthesis of silver nanofluids with polyvinylpyrrolidone (PVP) and their transport properties,‖ Colloid and Polymer Science, vol. 286, no. 14-15, pp. 1667–1673, 2008.

[143] Y. Hwang, J. K. Lee, C. H. Lee *et al*.., ―Stability and thermal conductivity characteristics of nanofluids,‖ Thermochimica Acta, vol. 455, no. 1-2, pp. 70–74, 2007.

[144] X. Li, D. Zhu, and X. Wang, ―Evaluation on dispersion behavior of the aqueous copper nanosuspensions,‖ Journal of Colloid and Interface Science, vol. 310, no. 2, pp. 456–463, 2007.

[145] B.R. Munson, D.F. Young, T.H. Okiishi, Fundamentals of Fluid Mechanics, John Wiley & Sons Inc., 1998.

[146] D. W. Oh, A. Jain, J. K. Eaton, K. E. Goodson and J. S. Lee, ―Thermal Conductivity Measurement and Sedimentation Detection of Aluminum Oxide Nanofluids by Using the3ωMethod,‖ International Journal of Heat and Fluid Flow, ISSN: 0142-727X, vol. 29, no. 5, pp. 1456-1461, 2008.

[147] H. Zhu, D. Han, Z. Meng, D. Wu, C. Zhang, ―Preparation and thermal conductivity of CuO nanofluid via a wet chemical method.‖ Nanoscale Research Letters, vol.6, no.1, p.181, 2011

[148] P. Razi, M.A. Akhavan-Behabadi, M. Saeedinia,―Pressure drop and thermal characteristics of CuO–base oil nanofluid laminar flow in flattened tubes under constant heat flux,‖ International Communications in Heat and Mass Transfer,vol.38,pp.964-971,2011.

[149] D. Wu, H. Zhu, L. Wang, L. Liua, Curr. NanoSci, vol.5, pp.103-112, 2009.

[150] I. Madni, C.-Y. Hwang, S.-D. Park, Y.-H. Choa, H.-T. Kim, Mixed surfactant system for stable suspension of multiwalled carbon nanotubes, Colloids Surface A: Physicochem. Eng. Aspects358 (1-3), pp.101-107, 2010.

[151] W. Yu, H. Xie, L. Chen, and Y. Li, ―Enhancement of thermal conductivity of kerosene-based Fe3O4 nanofluids prepared via phasetransfer method,‖ Colloids and Surfaces A, vol. 355, no. 1–3, pp. 109–113, 2010.

[152] M. Chandrasekar, S. Suresh, A. Chandra Bose, ―Experimental investigations and theoretical determination of thermal conductivity and viscosity of Al2O3/water nanofluid,‖ Exp. Therm. Fluid Sci. 34 (2), pp.210-216, 2010.

[153] Y. Hwang, J-K. Lee, J-K. Lee, Y-M. Jeong, S-i.Cheong, Y-C. Ahn, S.H. Kim, ―Production and dispersion stability of nanoparticles in nanofluids,‖ PowderTechnol. 186 (2), pp.145-153, 2008.

[154] X.F. Li, D.S. Zhu, X.J. Wang, N. Wang, J.W. Gao, H. Li, Thermal conductivity enhancement dependent pH and chemical surfactant for Cu-H2O nanofluids, Thermochim.Acta 469 (1-2),pp. 98-103,2008.

[155] M.N. Pantzali, A.A. Mouza, S.V. Paras, ―Investigating the efficiency of nanofluids as coolants in plate heat exchangers (PHE),‖ Chem. Eng. Sci. 64 (14), pp.3290-3300, 2009.

[156] W. Yu, H. Xie, ―A Review on Nanofluids: Preparation, Stability Mechanisms, and Applications,‖ Journal of Nanomaterials, vol2012, pp.1-17, 2012.

[157] X. Yang and Z. H. Liu, ―A kind of nanofluid consisting of surface-functionalized nanoparticles, ―Nanoscale Research Letters, vol. 5, no. 8, pp. 1324–1328, 2010.

[158] L. Chen and H. Xie, ―Surfactant-free nanofluids containing double- and single-walled carbon nanotubes functionalized by a wet mechanochemical reaction,‖ Thermochimica Acta, vol. 497, no. 1-2, pp. 67–71, 2010.

[159] H. Xie, H. Lee, W. Youn, M. Choi, ―Nanofluids containing multiwalled carbon nanotubes and their enhanced thermal conductivities,‖ J. Appl. Phys. 94 (8), pp.4967–4971, 2003.

[160] D. Wen, G. Lin, S. Vafaei, and K. Zhang, ―Review of nanofluids for heat transfer applications, ‖Particuology, vol. 7, no. 2, pp. 141– 150, 2009.

[161] X. J. Wang and X. F. Li, ―Influence of pH on nanofluids‘ viscosity and thermal conductivity,‖ Chinese Physics Letters, vol. 26, no. 5, Article ID 056601, 2009.

[162] Ali, A.R.I., Salam, B. A review on nanofluid: preparation, stability, thermophysical properties, heat transfer characteristics and application. *SN Appl. Sci.* vol. **2**, no. 1636, pp. 1-17, 2020.

[163] P. Krajnik, F. Pusavec, and A. Rashid, "Nanofluids: properties, applications and sustainability aspects in materials processing technologies", in Advances in Sustainable Manufacturing: Proceedings of the 8th Global Conference on Sustainable Manufacturing, pp. 107–113, Springer, Berlin, Germany, 2011.

[164] J. W. Sutherland, V. N. Kulur, and N. C. King, "An experimental investigation of air quality in wet and dry turning", CIRP Annals-Manufacturing Technology, vol. 49, no. 1, pp. 61–64, 2000.

[165] H. A. Jeng and J. Swanson, "Toxicity of metal oxide nanoparticles in mammalian cells", Journal of Environmental Science and Health, vol. 41, no. 12, pp. 2699–2711, 2006.

[166] E. Rial-Gonzalez, S. Copsey, P. Paoli, and E. Schneider, "Priorities for Occupational Safety and Health Research in the EU-25", European Agency for Safety and Health at Work, Strassen, Luxembourg, 2005.

[167] Muhammad Awais, Najeeb Ullah, Javaid Ahmad, Faizan Sikandar, Mohammad Monjurul Ehsan, Sayedus Salehin, Arafat A. Bhuiyan, "Heat transfer and pressure drop performance of Nanofluid: A state-of- the-art review", International Journal of Thermofluids,Elsevier, vol. 9, no. 100065, pp. 1-21, 2021.

[168] Saidur R, Leong KY, Mohammad HA. A review on applications and challenges of nanofluids. Renew Sustain Energy Rev 2011;15(3):1646–68.

[169] Hosokawa M, Nogi K, Naito M, Yokoyama T, Nanoparticle. Technology handbook. Amsterdam, The Netherlands: Elsevier; 2007.

[170] Hwang Y, Lee JK, Lee CH, Jung YM, Cheong SI, Lee CG. Stability and thermal conductivity characteristics of nanofluids. Thermochim Acta 2007;455(1– 2):70–4.

[171] Kwak K, Kim C. Viscosity and thermal conductivity of copper oxide nanofluid dispersed in ethylene glycol. Korea-Austr Rheol J 2005;17:35–40.

[172] Joohyun Lee Kisoo, Han Junemo Koo. A novel method to evaluate dispersion stability of nanofluids. Int J Heat Mass Transf 2014;70:421–9.

[173] Prevost, T.A., Oommen, T.V.: Cellulose insulation in oil-filled power transformers: Part I - history and development. *IEEE Electr. Insul. Mag.* **22**(1), 28–35 (2006)

[174] Chen, S.: *Analysis of transformer common accidents and anti-accident measures*. Master's thesis, School of Electrical and Electronics Engineering, China (2012)

[175] Morsalin, S., *et al*..: Diagnostic challenges in dielectric loss assessment and interpretation: a review. *IET Sci. Meas. Technol*. **13**(6), 767–782 (2019)

[176] Tanaka, T., Yongming, C.: Technical level of oil impregnated insulation in Japan. *Insul. Mater*. **6**(12), 42–46 (1985)

[177] 5Lv, J., Zhan, H., Jin, H.: Power transformer insulation paper: its properties and insulation aging. *China Pulp Pap*. **27**(05), 54–58 (2008)

[178] 6Kohman, G.T.: Cellulose as an insulating material. *Ind. Eng*. **31**(7), 807–817 (1939)

[179] Rahul Soni, Bhinal Mehta,"A review on transformer condition monitoring with critical investigation of mineral oil and alternate dielectric fluids",Electric Power Systems Research, Elsevier, vol. 214, no. B,pp. 1-23, 2023.

[180] S. S. Botha, P. Ndungu, and B. J. Bladergroen, "Physicochemical properties of oil-based nanofluids containing hybrid structures of silver nanoparticles supported on silica," Industrial and Engineering Chemistry Research, vol. 50, no. 6, pp. 3071–3077, 2011.

[181] M. Singh and L. Kundan, "Experimental study on thermal conductivity and viscosity of Al2O3-nanotransformer oil," International Journal on Theoretical and Applied Research in Mechanical Engineering (IJTARME), vol. 2, no. 3, pp. 125–130, 2013.

[182] H. Jin, Dielectric strength and thermal conductivity of mineral oil based nanofluids [M.S. thesis], Delft University of Technology, Delft, The Netherlands, April 2015.

**[183]** R. Karthik, T. S. R. Raja, and R. Madavan, "Enhancement of critical characteristics of transformer oil using nanomaterials," Arabian Journal for Science and Engineering, vol. 38, no. 10, pp. 2725–2733, 2013.

[184] T. K. Saha, M. Darveniza, D. J. T. Hill, and T. T. Le, "Electrical and chemical diagnostics of transformers insulation. B. Accelerated aged insulation samples", in IEEE Transactions on Power Delivery, Vol. 12, pp. 1555-1561, 1997.

[185] T. K. Saha, M. Darveniza, D. J. T. Hill, and T. T. Le, "Electrical and chemical diagnostics of transformers insulation. A. Aged transformer samples", in IEEE Transactions on Power Delivery, Vol. 12, pp. 1547-1554, 1997.

[186] M. Koch, M. Krueger, and M. Puetter, "Advanced insulation diagnostic by dielectric spectroscopy," in Asia Pacific Technical conference, 2009, Sydney, Australia.

[187] J. H. Yew, M. K. Pradhan, and T. K. Saha, "Effects of moisture and temperature on the frequency domain spectroscopy analysis of power transformer insulation", in IEEE Power and Energy Society General Meeting - Conversion and Delivery of Electrical Energy in the 21st Century, pp. 1-8, 20-24 July 2008, Pittsburgh, PA .

[188] IEEE Std. C57.147-2008, "IEEE Guide for Acceptance and Maintenance of Natural Ester Fluids in Transformers".

[189] IEEE Std. C57.152-2013,"IEEE Guide for Diagnostic Field Testing of Fluid-Filled Power Transformers, Regulators, and Reactors"

[190] EEE Std. 62-1995,"IEEE Guide for Diagnostic Field Testing of Electric Power Apparatus - Part 1: Oil Filled Power Transformers, Regulators, and Reactors".

[191] British Std. EN 61203:1995, "Synthetic organic esters for electrical purposes. Guide for maintenance of transformer esters in equipment".

[192] A. Helgeson, "Analysis of Dielectric Response Measurement Methods and Dielectric Properties of Resin-Rich Insulation During Processing", PhD Thesis Electric Power Engineering, Kungl Tekniska Hogskolan, Stockholm, 2000.

[193] S. Chakravorti, D. Dey, B. Chatterjee: Recent Trends in the Condition Monitoring of Transformers. Power Systems. Springer, London (2013).

[194] S. A. Bhumiwat, "Advanced Applications of Polarisation / Depolarisation Current Analysis on Power Transformers," in confrence Records of IEEE International Symposium on Electrical Insulation, pp. 474-477, 9-12 June 2008, Vancouver, BC

[195] S. Sarkar, T. Sharma, A. Baral, B. Chatterjee, D. Dey, and S. Chakravorti, "An expert system approach for transformer insulation diagnosis combining conventional diagnostic tests and PDC, RVM data", in IEEE Transactions on Dielectrics and Electrical Insulation, Vol. 21, pp. 882-891, 2014.

[196] V. Der Houhanessian and W. S. Zaengl, "Application of relaxation current measurements to on-site diagnosis of power transformers" , in IEEE Annual Report of the confrence on Electrical Insulation and Dielectric Phenomena, Vol.1, pp. 45-51, 19-22, Oct 1997, Minneapolis, MN.

[197] A. Baral and S. Chakravorti, "Assessment of non-uniform aging of solid dielectric using system poles of a modified debye model for oil-paper insulation of transformers", in IEEE Transactions on Dielectrics and Electrical Insulation, Vol. 20, pp. 1922-1933, 2013.

[198] T. K. Saha, P. Purkait, and F. Muller, "Deriving an equivalent circuit of transformers insulation for understanding the dielectric response measurements", IEEE Transactions on Power Delivery, Vol. 20, pp. 149-157, 2005.

[199] I. Fofana, H. Hemmatjou, and F. Meghnefi, "Effect of thermal transient on the polarization and depolarization current measurements", in IEEE Transactions on Dielectrics and Electrical Insulation, Vol. 18, pp. 513-520, 2011.

[200] T. K. Saha and P. Purkait, "Impact of the condition of oil on the polarisation based diagnostics for assessing the condition of transformers insulation," in IEEE Power Engineering Society General Meeting, Vol.2, 1881-1886, 12-16 June 2005.

[201] T. Leibfried and A. J. Kachler, "Insulation diagnostics on power transformers using the polarisation and depolarisation current (PDC) analysis", in Conference Record of the IEEE International Symposium on Electrical Insulation pp. 170-173, 7-10 Apr 2002, Boston, MA.

[202] T. K. Saha and P. Purkait, "Investigation of polarization and depolarization current measurements for the assessment of oil-paper insulation of aged transformers", in IEEE Transactions on Dielectrics and Electrical Insulation, Vol. 11, pp. 144-154, 2004.

[203] S. Sarkar, T. Sharma, A. Baral, B. Chatterjee, D. Dey, and S. Chakravorti, "An expert system approach for transformer insulation diagnosis combining conventional diagnostic tests and PDC, RVM data", in IEEE Transactions on Dielectrics and Electrical Insulation, Vol. 21, pp. 882-891, 2014.

[204] V. Der Houhanessian and W. S. Zaengl, "Application of relaxation current measurements to on-site diagnosis of power transformers" , in IEEE Annual Report of the confrence on Electrical Insulation and Dielectric Phenomena, Vol.1, pp. 45-51, 19-22, Oct 1997, Minneapolis, MN.

[205] T. K. Saha, P. Purkait, and F. Muller, "Deriving an equivalent circuit of transformers insulation for understanding the dielectric response measurements", IEEE Transactions on Power Delivery, Vol. 20, pp. 149-157, 2005.

[206] T. K. Saha and P. Purkait, "Impact of the condition of oil on the polarisation based diagnostics for assessing the condition of transformers insulation," in IEEE Power Engineering Society General Meeting, Vol.2, 1881-1886, 12-16 June 2005.

[207] T. Leibfried and A. J. Kachler, "Insulation diagnostics on power transformers using the polarisation and depolarisation current (PDC) analysis", in Conference Record of the IEEE International Symposium on Electrical Insulation pp. 170-173, 7-10 Apr 2002, Boston, MA.

[208] V. Der Houhanessian and W. S. Zaengl, "Time domain measurements of dielectric response in oil-paper insulation systems", in Conference Record of the IEEE International Symposium on Electrical Insulation, Vol.1, pp. 47-52, 16-19 Jun 1996, Montreal, Que.

[209] M. Koch and T. Prevost, "Analysis of dielectric response measurements for condition assessment of oil-paper transformer insulation", IEEE Transactions on Dielectrics and Electrical Insulation, Vol. 19, pp. 1908-1915, 2012.

[210] C. Ekanayake, S. M. Gubanski, A. Graczkowski, and K. Walczak, "Frequency response of oil impregnated pressboard and paper samples for estimating moisture in transformer insulation", in IEEE Transactions on Power Delivery, Vol. 21, pp. 1309-1317, 2006.

[211] "User Manual for Insulation Diagnostic System IDAX 350", 2012.

[212] M. Ohlen and P. Werelius, "Dielectric Frequency Response and temperature dependence of power factor", in Conference Record of the IEEE International Symposium on Electrical Insulation, pp. 1-7, 6-9 June 2010, San Diego, CA.

[213] W. Guo and T. K. Saha, "Study on Moisture in Oil-Paper Insulation by Frequency Domain Spectroscopy", in Asia-Pacific,Power and Energy Engineering Conference, pp. 1-4, 25-28 March 2011, Wuhan.

[214] S.M. Gubanski (chair) , G. Csépes, V. Der, Houhanessian, J. Filippini, P. Guuinic, U. Gäfvert, V., Karius, J. Lapworth, G. Urbani, P. Werelius, W.Zaengl, "Dielectric response methods for diagnostics of power transformers", IEEE Electrical Insulation Magazine, Vol. 19, Issue 3, pp. 12-18, 2003.

[215] Y. F. Du, Y.Z. Lv, J. Q. Zhou, X. X. Li, and C. R. Li, “Breakdown properties of transformer oil-based TiO2 nanofluid,” in Proceedings of the Annual Report Conference on Electrical Insulation and Dielectric Phenomena (CEIDP ’10), pp. 1–4, West Lafayette, Ind, USA, October 2010.

[216] Y. Du, Y. Lv, C. Li *et al.*., “Effect of semiconductive nanoparticles on insulating performances of transformer oil,” IEEE Transactions on Dielectrics and Electrical Insulation, vol. 19, no. 3, pp. 770–776, 2012.

[217] Z. Zhang, J. Li, P. Zou, and S. Grzybowski, “Electrical properties of nano-modified insulating vegetable oil,” in 2010 Annual Report Conference on Electrical Insulation and Dielectric Phenomena, West Lafayette, IN, pp. 1–4, Oct, 2010.

[218] J. G. Hwang, M. Zahn, F. M. O’Sullivan, L. A. A. Pettersson,O. Hjortstam, and R. S. Liu, “Effects of nanoparticle charging on streamer development in transformer oil-based nanofluids,” Journal of Applied Physics, vol. 107, no. 1, Article ID 014310, 2010.

[219] "Insulating liquids - Determination of the breakdown voltage at power frequency - Test method," *IS 6792*, pp. 1-13, 2017.

[220] D. Amin, R. Walvekar, M. Khalid, M. Vaka, N. M. Mubarak and T. C. S. M. Gupta, "Recent Progress and Challenges in Transformer Oil Nanofluid Development: A Review on Thermal and Electrical Properties," IEEE Access, vol. 7, pp. 151422-151438, 2019.

[221] M.H. Ahmadi, A. Mirlohi, M.A. Nazari and R. Ghasempour, "A review of thermal conductivity of various nanofluids", J. of Molecular Liquids, vol. 265, pp 181-188, 2018.

[222] W. S. Zaengl, “Dielectric Spectroscopy in time and frequency domain for HV Power Equipment. I. Theoretical considerations,” IEEE Electr. Insul. Mag., vol. 19, no. 5, pp. 5-19, 2003.

[223] A. Ghaderi , A. Mingotti, F. Lama, L. Peretto, and R. Tinarelli, " Effects of Temperature on MV Cable Joints Tan Delta Measurements," IEEE Trans. Dielectr. Instrum. Meas., vol. 68, no. 10, pp. 3892-3898, 2019.

[224] A. K. Pradhan, C. Koley, B. Chatterjee and S. Chakravorti, “Determination of Optimized Slope of Triangular Excitation for Condition Assessment of Oil-paper Insulation by Frequency Domain Spectroscopy,” IEEE Trans. Dielectr. Electr. Insul., vol. 23, no. 3, pp. 1303-1312, 2016.

[225] D. A. Mansour and A. M. Elsaeed, “Heat transfer properties of transformer oil-based nanofluids filled with $Al_2O_3$ nanoparticles,” *IEEE Int. Conf. Power and Energy (PECON)*, 2014, pp. 123-127.

[226] D. Zhu, X. Li, N. Wang, X. Wang, J. Gao and H. Li,“Dispersion behavior and thermal conductivity characteristics of $Al_2O_3$-$H_20$ nanofluids,” Current Applied Physics, vol. 9, no. 1, pp. 131-139, 2009.

[227] A. A. S. Akmal, H. Borsi, E. Gockenbach, V. Wasserberg, and H. Mohseni, "Dielectric behavior of insulating liquids at very low frequency," IEEE Trans. Dielectr. Electr. Insul., Vol. 13, pp. 532-538, 2006.

[228] Z. Yuan, H. Miao, G. Chen, G. Wilson, and P. Jarman, "Frequency dependence of conductivity of new mineral oil studied by dielectric spectroscopy," Int'l. Conf. High Voltage Eng. Application (ICHVE), pp. 634-637, 2012.

[229] K. Bandara, C. Ekanayake and T. K. Saha, “Modelling the Dielectric Response Measurements of Transformer oil,” IEEE Trans. Dielectr. Electr. Insul., vol. 22, no. 2, pp. 1282-1291, 2015.

[230] E. Frau and S.Schintke, “Modulated 3D Cross-Correlation Dynamic Light Scattering of Magnetic Nanoparticle Inks”, Proceedings of the *20th International Conference on Transparent Optical Networks (ICTON)*, pp. 1-4, 2018.

[231] J. Jacob, P. Preetha and T. K. Sindhu, "Stability analysis and characterization of natural ester nanofluids for transformers," *IEEE Transactions on Dielectrics and Electrical Insulation*, vol. 27, no. 5, pp. 1715-1723, 2020.

[232] R. Saidur, K. Y. Leong, and H. A. Mohammad, "A review on applications and challenges of nanofluids," *Renew. Sustain. Energy Rev.*, vol. 15, no. 3, pp. 1646–1668, Apr. 2011.

[233] P. Sun, W. Sima, X. Jiang, D. Zhang, J. He and Q.Chen,"Failure of Nano-modified Oil Impregnated Paper Under Repeated Impulse Voltage: Effects of TiO2 Nanoparticles on Space Charge Characteristics," IEEE Trans. Dielectr. Electr. Insul., vol. 25, no. 6, pp. 2103-2111, 2018.

[234] D. Mansour, A. Elsaeed and M. Lzzularab, "The Role of Interfacial Zone in Dielectric Properties of Transformer Oil-based Nanofluids," IEEE Trans. Dielectr. Electr. Insul., vol. 23, no. 6, pp. 3364-3372, 2016.

[235] T. Tanaka, "Dielectric Nanocomposites with Insulating Properties," IEEE Trans. Dielectr. Electr. Insul., vol. 12, no. 5, pp. 914-928, 2005.

[236] C. R. Daubert and B. E. Farkas, "Food Analysis Laboratory Manual (Second edition)", Springer science, 2003.

[237] J. Li, Z. Zhang, P. Zou, S. Grzybowski and M. Zahn, "Preparation of a Vegetable Oil-Based Nanofluid and Investigation of Its Breakdown and Dielectric Properties," IEEE Electr. Insul. Mag., vol. 28, no. 5, pp. 43-50, 2012.

[238] A. Setayeshmehr, I. Fofana, C. Eichler, A. Akbari, H. Borsiand E. Gockenbach, "Dielectric Spectroscopic Measurements on Transformer Oil-Paper Insulation under Controlled Laboratory Conditions," IEEE Trans. Dielectr. Electr. Insul., vol. 15, No. 4, pp. 1100-1111, 2008.

[239] Y. Du, Y. Lv, C. Li, M. Chen, J. Zhou, X. Li, Y. Zhou and Y. Tu, "Effect of electron shallow trap on breakdown performance of transformer oil-based nanofluids", J. of Applied Physics, Vol. 110, pp. 104104(1) – 104104(4), 2011.

[240] S. Mukherjee, P. C. Mishra, S. K. S. Parashar and P. Chaudhuri, "Role of temperature on thermal conductivity of nanofluids: a brief literature review", Heat Mass Transfer, Vol. 52, pp. 2575-2585, 2016.

[241] M. K. Moraveji, F. Talebkeikhah and M. Arjmanda, "On evaluation of thermophysical properties of transformer oil-based nanofluids: A comprehensive modeling and experimental study", J. of Molecular Liquids, vol. 300, No. 112249, 2020.

[242] J. Jacob et al, , "Review on natural ester and nanofluids as an environmental friendly alternative to transformer mineral oil" IET Nanodielectrics, vol. 3, no. 2, pp. 33-43, 2020.

[243] N. Baruah, S. K. Nayak and S. K. Pratihar, "Quantitative Effect of Aging Duration on Dielectric Parameters Based on Frequency Response," in IEEE Trans. Instrum. Meas., vol. 71, Art no. 6000909, pp. 1-9, 2022.

[244] B. Barbes et al, "Thermal conductivity and specific heat capacity measurements of $Al_2O_3$ nanofluids," J. Thermal Analysis and Calorimetry, vol. 111, no. 2, pp. 1615-1625, 2013.

[245] Minea, and A. Adriana, "Hybrid nanofluids based on $Al_2O_3$, $TiO_2$ and $SiO_2$: Numerical evaluation of different approaches," Int. Jour. of Heat and Mass Trans., vol. 104, pp. 852-860, 2017.

[246] P. Kanti *et al*, “Thermophysical properties of fly ash–Cu hybrid nanofluid for heat transfer applications” Heat Transfer, vol. 49, no. 8, pp. 4491-4510, 2020.

[247] P. Kanti et al, “Experimental determination of thermophysical properties of Indonesian fly-ash nanofluid for heat transfer applications,” Particulate Science and Technology, Taylor & Francis, vol. 39, no. 5, pp. 1-10, 2021.

[248] Y. Zhong *et al*, “Insulating properties and charge characteristics of natural ester fluid modified by $TiO_2$ semiconductive nanoparticles,” IEEE Trans. Dielectr. Electr. Insul., vol. 20, no. 1, pp. 135-140, 2013.

[249] Fofana *et al*, “Challenge of mixed insulating liquids for use in high-voltage transformers. 1. Investigation of mixed liquids,” *IEEE Electr. Insul. Mag.*, vol. 18, no. 3, pp. 18–31, 2002.

[250] C. Perrier, A. Beroual, and J. L. Bessede, “Improvement of Power Transformers by using Mixtures of Mineral Oil with Synthetic Esters,” *IEEE Trans. Dielectr. Electr. Insul.*, vol. 13, no. 3, pp. 556–564, 2006.

[251] K. Takahashi, K. Miyagi, and R. Hanaoka, “Negative discharge response of blend oil (ester-based insulation oil with aging mineral oil) in a nonuniform field,” *IEEE Int. Conf. Dielectr. Liquids (ICDL)*, 2017.

[252] J. Liu *et al*, “A novel curve database for moisture evaluation of transformer oil-immersed cellulose insulation using FDS and exponential decay model,” *IEEE Access*, vol. 8, pp. 180728–180737, 2020.

[253] A. K. Jonscher, Dielectric Relaxation in Solids: Chelsea Dielectric Press, 1983.

[254] Y. M. Wi, S. K. Joo, and K. B. Song, “Holiday load forecasting using fuzzy polynomial regression with weather feature selection and adjustment,” *IEEE Trans. Power Syst.*, vol. 27, no. 2, pp. 596–603, 2012.

[255] U. Khaled and A. Beroual, "AC dielectric strength of synthetic ester-based $Fe_3O_4$, $Al_2O_3$ and $SiO_2$ nanofluids — conformity with normal and weibull distributions," *IEEE Trans. Dielectr. Electr. Insul.*, vol. 26, no. 2, pp. 625-633, 2019.

[256] S. F. M. Nor *et al.*, "Investigation on the electrical properties of palm oil and coconut oil based $TiO_2$ nanofluids," *IEEE Trans. Dielectr. Electr. Insul.*, vol. 24, no. 6, pp. 3432-3442, 2017.

[257] Y. Hou *et al.*, "Experimental investigations into the enhanced dielectric breakdown performances of propylene carbonate modified by $TiO_2$ nano-particles," *IEEE Trans. Dielectr. Electr. Insul.*, vol. 23, no. 5, pp. 2816-2821, 2016.

[258] T. Kiyan *et al.*, "Weibull Statistical Analysis of Pulsed Breakdown Voltages in High-Pressure Carbon Dioxide Including Supercritical Phase," *IEEE Trans. on Plasma Sci.*, vol. 39, no. 8, pp. 1729-1735, 2011.

[259] T. W. Anderson and D. A. Darling, “Asymptotic theory of certain ‘‘goodness-of-fit’’ criteria based on stochastic processes,” *Annals of Mathe. Statis.*, vol. 23, no. 2, pp. 193–212, 1952.

[260] K. Bandara, C. Ekanayake and T. K. Saha, “Modelling the Dielectric Response Measurements of Transformer oil,” *IEEE Trans. Dielectr. Electr. Insul.*, vol. 22, no. 2, pp. 1282-1291, 2015.

[261] J. Hao *et al.*, "Physical Mechanism Analysis of Conductivity and Relaxation Polarization Behavior of Oil-Paper Insulation Based on Broadband Frequency Domain Spectroscopy," *IEEE Trans. Dielectr. Electr. Insul.*, vol. 28, no. 5, pp. 1571-1578, 2021.

[262] X. Zhao *et al*., "High temperature ac conductivity relaxations in dielectric ceramics: grain boundary/intergranular phase effects*," J Mater. Sci-Mater. E.*, vol. 27, no. 4, pp. 1–11, 2020.

[263] U. Khaled and A. Beroual,"DC breakdown voltage of natural ester oil-based $Fe_3O_4$, $Al_2O_3$, and $SiO_2$ nanofluids", Alexan. Engi. Jour., Elsevier, vol. 59, no. 6, pages 4611-4620, 2020.

[264] T. Takada *et al.*, "Space charge trapping in electrical potential well caused by permanent and induceddipoles for LDPE/MgO nanocomposite," *IEEE Trans. Dielectr. Electr. Insul.*, vol. 15, no. 1, pp. 152–160, 2008.

[265] Y. Lv *et al.*, "$TiO_2$ nanoparticleinduced space charge decay in thermal aged transformer oil," *Appl. Phys. Lett.*, vol. 102, no. 13, p. 132902(1-3) , 2013.

[266] B. Xu *et al.*, "Experimental Study on Microsecond Pulse Breakdown Characteristics of Propylene Carbonate Modified by Al Nanoparticles," *IEEE Trans. on Plasma Sci.*, vol. 45, no. 10, pp. 2691-2695, 2017.

[267] I. Fofana, "50 years in the development of insulating liquids," *IEEE Electr. Insul. Mag.*, vol.29, no. 5, pp. 13-25, 2013.

[268] E. Tuncer and S. M. Gubanski, "On dielectric data analysis using the monte carlo method to obtain relaxation time distribution and comparing non-linear spectral function fits," *IEEE Trans. Dielectr. Electr. Insul.*, vol. 8, No. 3, pp. 310-320, 2001.

[269] N. Farag *et al*, "Numerical transformations of wide-range time- and frequency-domain relaxational spectra," *IEE Proc.-Sci. Mea. Technol., Szarbmcckea. Gemany*, vol. 150, no. 2, 2003, pp. 65-74.

[270] S. K. Ojha *et al*, "Application of Cole–Cole model to transformer oil-paper insulation considering distributed dielectric relaxation," *IET High Volt.*, vol. 4, no. 1, pp. 72–79, 2019.

[271] B. Barbes *et. al*, "Thermal conductivity and specific heat capacity measurements of $Al_2O_3$nanofluids," *J. Thermal Analysis and Calorimetry*, vol. 111, no. 2, pp. 1615-1625, 2013.

[272] Y, Du *et. al*, "Effect of semiconductive nanoparticles on insulating performances of transformer oil," *IEEE Trans. Dielectr. Electr. Insul.*, vol. 19, no. 3, pp. 770-776, 2012.

[273] X. Yang, S. Nielsen and G. Ledwich, "Frequency domain spectroscopy measurements of oil-paper insulation for energized transformers," *IEEE Trans. Dielectr. Electr. Insul.*, vol. 24, no. 3, pp. 1657-1664, 2017.

[274] S. Chowdhury, N. Haque, S. Chatterjee, A. K. Pradhan and S. Chakravorti, "Temperature Compensation of Frequency Domain Spectroscopy Measurement for Condition Assessment of Oil-Paper Insulation," *IEEE Trans. Dielectr. Electr. Insul.*, vol. 29, no. 1, pp. 255-263, 2022.

[275] P. V. Notingher, L. M. Dumitran, S. Busoi, G. Tanasescu, L. V. Badicu and R. Setnescu, "Determination of the remaining lifetime of power transformers liquid insulations based on the absorption/resorption currents," in proceedings of 10th International Symposium on Advanced Topics in Electrical Engineering (ATEE), Bucharest, Romania, pp. 428-433, 2017.

[276] A. K. Pradhan, B. Chatterjee and S. Chakravorti, "Estimation of paper moisture content based on dielectric dissipation factor of oil-paper insulation under non-sinusoidal excitations,"

*IEEE Trans. Dielectr. Electr. Insul.*, vol. 22, no. 2, pp. 822-830, 2015.

[277] A. García, R. Villarroel and D. García, "A Multiphysical Model to Study Moisture Dynamics in Transformers," *IEEE Trans. Power Del.*, vol. 34, no. 4, pp. 1365-1373, 2019.

[278] J. Cheng, "Broadband Dielectric Properties of Impregnated Transformer Paper Insulation at Various Moisture Contents", Master of Science thesis in Electromagnetic Engineering, KTH, Stockholm, Sweden 2011.

[279] H. Kliem, P. Fuhrmann and G. Ark, "A numerical method for the determination of first-order kinetics relaxation time spectra," *IEEE Trans. Dielectr. Electr. Insul.*, vol. 23, no. 6, pp. 919-927, 1988.

[280] P. Debye, Polar Molecules, Dover publication, New York, USA, 1945.

[281] E. Tuncer, Y. V. Serdyuk and S. M. Gubanski, "Dielectric Mixtures: Electrical Properties and Modeling", *IEEE Trans. Dielectr. Electr. Insul.*, vol. 9, no. 5, pp. 809-828, 2002.

Biswajit Chakraborty
09/12/2024